

A SYSTEM FOR AUTOMATIC POSITIONING AND ALIGNMENT OF
FIBER-TIP INTERFEROMETERS

A Thesis

by

MAHESH JALAN

Submitted to the Office of Graduate Studies of
Texas A&M University
in partial fulfillment of the requirements for the degree of

MASTER OF SCIENCE

August 2004

Major Subject: Mechanical Engineering

A SYSTEM FOR AUTOMATIC POSITIONING AND ALIGNMENT OF
FIBER-TIP INTERFEROMETERS

A Thesis

by

MAHESH JALAN

Submitted to Texas A&M University
in partial fulfillment of the requirements
for the degree of

MASTER OF SCIENCE

Approved as to style and content by:

Ravinder Chona
(Chair of Committee)

Chii-Der S. Suh
(Member)

Norris Stubbs
(Member)

Chin B. Su
(Member)

Dennis L. O'Neal
(Head of Department)

August 2004

Major Subject: Mechanical Engineering

ABSTRACT

A System for Automatic Positioning and Alignment of Fiber-Tip Interferometers.

(August 2004)

Mahesh Jalan, B.E., Karnataka Regional Engineering College, Surathkal, India

Chair of Advisory Committee: Dr. Ravinder Chona

The research described in this thesis involves the design, development, and implementation of an automated positioning system for fiber-optic interferometric sensors. The Fiber-Tip Interferometer (FTI) is an essential component in the proven Thermo-Acousto-Photonic NDE technique for characterizing a wide range of engineering materials including polymers, semiconductors and composites. The need to adapt the fiber-optic interferometric system to an industrial environment and to achieve precision control for optimizing interferometric contrast motivated the development of an automated, self-aligning FTI system design. The design enables high-resolution positioning and alignment by eliminating manual subjectivity and allows significantly improved repeatability and accuracy to be attained. Opto-electronic and electromechanical devices including a GRIN lens, 2x2 fused bi-conical taper couplers, photodiodes, motor-controlled tip/tilt stages, oscilloscopes, and a PCI card, constitute a closed-loop system with a feedback controller. The system is controlled by and communicates with a computer console using LabVIEW, a graphical language developed by National Instruments. Specifically, alignment is quantified by scanning the voltage readings at various orientations of the GRIN lens. The experimental setup specific to achieving maximum interferometric contrast intensity when interrogating silicon wafers with various surface depositions is discussed. Results corresponding to the interferometric contrast data obtained at several different standoff distances (Fizeau Cavity magnitudes) demonstrate the robustness of the novel design.

ACKNOWLEDGMENTS

First of all, I thank Dr. Ravinder Chona, my thesis advisor. I was honored to be one of his graduate students. His continuous support, technical guidance and encouragement bolster my confidence and helped me to achieve my research goal. I highly admire his practical knowledge, analytical approach and skill at anticipating problems. His design talents and management skills are equally impressive.

I would also like to thank Dr. Suh for serving on my thesis committee. In my first semester at Texas A&M University, I took Advanced Computer-Aided Engineering Design under him. Under his able guidance, I learned about design methodology and successfully completed a project for Ford Motor Company. I am also thankful to Dr. Norris Stubbs and Dr. Chin B. Su for serving on my thesis committee.

I am also thankful to Dr. Christian P. Burger for his insight into the fiber-tip interferometer system and for sharing his ideas and suggestions to improve upon my research work.

I am especially thankful to Mr. Andrew Rabroker, a graduate student at Texas A&M University for his valuable ideas, numerous suggestions, technical insight and understanding of the fiber-tip interferometer system. His vast knowledge in the theoretical and practical applications of these systems encouraged me to learn all I could to have a more complete understanding and systems approach to problem solving.

I would also like to thank Dr. Martin E. Baltazar, who finished his Ph.D. at Texas A&M University, for his kind assistance in carrying out regular work in the Photomechanics Laboratory. I would also like to thank all my past and present lab-mates who have helped me whenever I had a problem. Finally, I am thankful to the Texas Advanced Research program and to NSF for research funding.

To my parents, Mr. Trilok and Mrs. Bimla Jalan, I give the utmost appreciation. I am truly blessed to have a father who showed me how to be everything I wanted to be and a mother who taught me the meaning of unselfish love. I am also grateful to my three elder brothers who not only helped me with my studies in high school but have also guided me throughout my career and life.

TABLE OF CONTENTS

	Page
ABSTRACT.....	iii
ACKNOWLEDGMENTS.....	iv
TABLE OF CONTENTS.....	v
LIST OF TABLES.....	vii
LIST OF FIGURES.....	viii
 CHAPTER	
I INTRODUCTION.....	1
Interferometry Background.....	1
TAP-NDE Technology	4
Tip/Tilt Angles of GRIN Lens.....	6
Need for an Automated FTI System	8
Thesis Objective.....	8
Thesis Overview	11
Contributions of Thesis.....	12
II FEASIBILITY SCRUTINY.....	13
Mathematical Modeling.....	13
Prior Experiment.....	15
Preliminary Setup Configuration	17
Preliminary Experimental Results and Inferences.....	18
III AUTOMATED FIBER TIP INTERFEROMETER ALIGNMENT SYSTEM DESIGN	21
Automated Fiber Tip Interferometer Alignment System.....	21
Alignment System Design and Instrumentation	21
Automated Alignment Working Principle and Procedure	27
Conclusions of Chapter III.....	41

CHAPTER	Page
IV DESCRIPTION OF THE PHYSICAL CONFIGURATION OF THE DESIGN	42
Assembly Design for Holding the GRIN Lens and the PSD	42
Detection System Configuration.....	44
Conclusions of Chapter IV.....	46
V EXPERIMENTAL VERIFICATION AND RESULTS	47
Experimental Analysis of Coupling of GRIN Lens	47
Target Position for Coarse Alignment	49
Relationship Between GRIN Lens Angles and Fizeau Cavity	49
Coarse Alignment Results.....	51
Fine Alignment Results - Initial Method	55
Results for Fine Alignment - Improved Method.....	62
Conclusions of Chapter V.....	84
VI CONCLUSIONS AND RECOMMENDATIONS FOR FUTURE WORK	85
Conclusions.....	85
Impact	87
Future Work	88
REFERENCES	89
APPENDIX A CIRCUIT DIAGRAM FOR PSD.....	92
APPENDIX B FLOW DIAGRAM FOR LABVIEW PROGRAM USED IN FINE ALIGNMENT SYSTEM	93
VITA.....	102

LIST OF TABLES

	Page
Table 1: Coupling of GRIN Lens.....	48
Table 2: Relation between Fizeau Cavity and Motor Count.....	50
Table 3: Coarse Alignment at 45mm Standoff Distance	51
Table 4: Coarse Alignment at 65mm Standoff Distance	53
Table 5: Coarse Alignment at 100mm Standoff Distance	54
Table 6 : Wiring Connections of 2D-PSD and C4674.....	92

LIST OF FIGURES

	Page
Figure 1: Fizeau-Type Interferometer.....	3
Figure 2: Thermo-Acoustic-Photonic Non-Destructive Evaluation	6
Figure 3: GRIN Lens Tip/Tilt Angles.....	7
Figure 4: View of Fizeau Cavity in FTI System.....	9
Figure 5: Graph of Intensity Versus Fizeau Cavity	10
Figure 6: Spherical Coordinate System	14
Figure 7: Picture of Photocell with Its Amplifier	15
Figure 8: Picture of Tilt/Tip Stage	16
Figure 9: Block Diagram of Positioning System	17
Figure 10: GRIN Lens and Photocell Holder Assembly	18
Figure 11: Electronic Connection for 2D-PSD.....	22
Figure 12: Graph of Voltage Versus Light Spot Position.....	23
Figure 13: DC–Servomotor Driven Tilt/Tip Stage	25
Figure 14: Electronic Connection for Tip/Tilt Stage	25
Figure 15: Schematic Diagram of the Automated Coarse Alignment	28
Figure 16: Working Principle of the Automated Coarse Alignment	29
Figure 17: Ideal Model for Automated Coarse Alignment System	30
Figure 18: Worst Alignment Case before Automated Coarse Alignment System	33
Figure 19: Working Principle of Fine Alignment Procedure for the GRIN Lens	34
Figure 20: Scanning Voltage at Different Reflected Angles	35
Figure 21: New Algorithm for Fine Alignment.....	37

	Page
Figure 22: Opti-Claw Mount Drawing	43
Figure 23: Assembly for Holding the GRIN Lens and the PSD.....	44
Figure 24: Picture of Design Set-up.....	45
Figure 25: Surface Plot at 45mm Fizeau Cavity	56
Figure 26: 2D Plot at 45mm Fizeau Cavity	57
Figure 27: Surface Plot at 65mm Fizeau Cavity	58
Figure 28: 2D Plot at 65mm Fizeau Cavity	59
Figure 29: Surface Plot at 100mm Fizeau Cavity.....	60
Figure 30: 2D Plot at 100mm Fizeau Cavity	61
Figure 31: 3D Waterfall Plot at 45mm Standoff.....	63
Figure 32: Top View Plot at 45mm Standoff.....	63
Figure 33: 3D Waterfall Plot at 65mm Standoff.....	64
Figure 34: Top View Plot at 65mm Standoff.....	64
Figure 35: 3D Waterfall Plot at 90mm Standoff.....	65
Figure 36: Top View Plot at 90mm Standoff.....	65
Figure 37: 3D Waterfall Plot at 110mm Standoff.....	66
Figure 38: Top View Plot at 110mm Standoff.....	66
Figure 39: 3D Waterfall Plot at 130mm Standoff.....	67
Figure 40: Top View Plot at 130mm Standoff.....	67
Figure 41: 3D Waterfall Plot at 140mm Standoff.....	68
Figure 42: Top View Plot at 140mm Standoff.....	68
Figure 43: 3D Waterfall Plot at 160mm Standoff.....	69

	Page
Figure 44: Top View Plot at 160mm Standoff.....	69
Figure 45: 3D Waterfall Plot at 180mm Standoff.....	70
Figure 46: Top View Plot at 180mm Standoff.....	70
Figure 47: 3D Waterfall Plot at 200mm Standoff.....	71
Figure 48: Top View Plot at 200mm Standoff.....	71
Figure 49: Graph of Fizeau Cavity Versus Maximum Voltage Output in the Photo-Detector	72
Figure 50: Data Plots for Trial 1; 45mm Fizeau Cavity	73
Figure 51: Data Plots for Trial 2; 45mm Fizeau Cavity	74
Figure 52: Data Plots for Trial 3; 45mm Fizeau Cavity	75
Figure 53: Data Plots for Trial 4; 45mm Fizeau Cavity	76
Figure 54: Data Plots for Trial 5; 45mm Fizeau Cavity	77
Figure 55: Data Plots for Trial 6; 45mm Fizeau Cavity	78
Figure 56: Data Plots for Trial 7; 45mm Fizeau Cavity	79
Figure 57: Data Plots for Trial 8; 45mm Fizeau Cavity	80
Figure 58: Graph of Maximum Voltage Output Read at the Photo-Detector Versus Trial Number	81
Figure 59: 3D Waterfall and Infringe Plots for Steel Material	83

CHAPTER I

INTRODUCTION

Linear interferometers are widely used instruments that split a light source into two or more beams, which are later recombined to form an interference pattern [1]. The use of optical interferometry as a tool for acquiring the highly transient surface displacements associated with ultrasonic inspection procedures has been successfully demonstrated by a number of researchers. As an alternative to traditional ultrasonic transducers, the Fiber-Tip Interferometer (FTI) is an NDE tool for the measurement of small displacements at the nanometer scale. FTI systems have been widely applied as an essential sensing component in the proven Thermo-Acousto-Photonic Nondestructive (TAP-NDE) technology for the detection of out-of-plane displacements [2]. The fiber based FTI system has significant advantages over conventional methods. The use of fiber optics and optical couplers enables the alignment of object and reference beams inside the fibers and thus renders the system robust and mobile. The only alignment required is to attain normality between the laser beam that is projected out from the Gradient Index (GRIN) lens and the surface being inspected, so as to enable maximum reflection and thus the maximum intensity of the reflected (object) beam. Manual alignment procedures are time consuming and inaccurate. The need for automating the FTI to¹ achieve precise alignment and interferometry of satisfactory resolution motivates the work. This research results in automating and improving the previously reported FTI system by using optical position sensors and control mechanisms for the alignment of the GRIN lens with respect to the specimen under observation.

Interferometry Background

A basic interferometry apparatus consists of two coherent beams of light: an object beam and a reference beam. The object beam passes through or is reflected by the

This thesis follows the style of *IEEE Journal of Solid-State Circuits*.

specimen under observation and the reference beam is the one which is unaffected by the specimen. Since the two beams of light are coherent, they interfere when superimposed. The resulting intensity distributions yield an interferometric fringe pattern that is a contour map of constant optical path, or optical phase, difference. In 1805, Thomas Young succeeded in producing a system of alternating bright and dark fringes in the so-called Young's experiment. Over a period of time, different types of interferometers like the Michelson and Mach-Zehnder, among others, were built. A classical or holo-interferometric arrangement has been utilized by researchers [3-12] to obtain the necessary sensitivity at high frequencies for ultrasonic evaluation of materials. These system instruments achieved sufficient resolution but were designed for laboratory use and thus, were difficult to adapt to field applications [13]. Extremely small displacements encountered in quasi-static and low-to-intermediate frequency vibrations were studied by using fiber optic-based sensors [14-18]. With the advances in technology, many researchers [19-25] have demonstrated that fiber based interferometric systems are well-suited for the ultrasonic evaluation of materials.

Fiber Tip Interferometry (FTI) is an extension of a standard Fizeau type interferometer [22] whose basic configuration is shown in Figure 1. A collimated beam of light is generated from the source and is transmitted through a beam splitter to the surface under observation. The light through the beam splitter first passes through a partially reflecting mirror before reaching the surface. This mirror allows a certain percentage of the light to pass through and reflects the remaining back along the incident path, which acts as a reference beam. The portion of the light passing through the mirror then travels through an open cavity, referred to as the Fizeau cavity, to a reflecting surface. The light reflects from this surface, passes back through the Fizeau cavity and acts as the object beam of the interferometer. The reference and object beams then recombine to form interference. The object beam is shifted in phase from the reference beam by an amount proportional to two times the length of the Fizeau cavity.

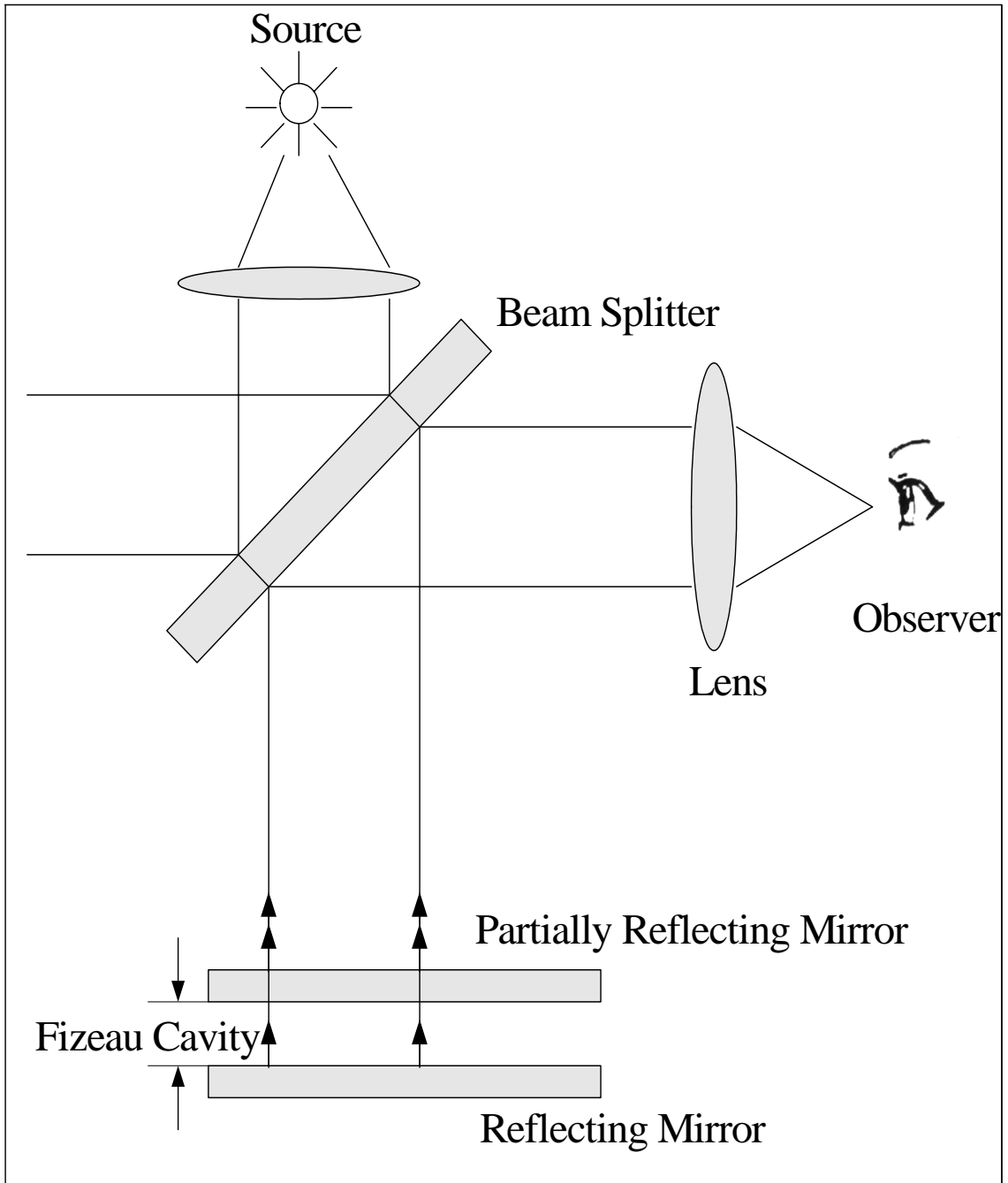


Figure 1: Fizeau-Type Interferometer

TAP-NDE Technology

Photo-acoustic methods have been successfully utilized for non-destructive evaluation for the past few decades. Ultrasonic testing employs ultrasound to examine materials for flaws and other pertinent information by initiating elastic waves from the surface and then capturing the resulting, highly localized, out-of-plane, transient displacement at another location in the material. In [18], the non-contact, non-invasive laser-optic technique developed for inducing and sensing surface acoustic waves is referred to as Thermo-Acousto-Photonic Nondestructive Evaluation (TAP-NDE). The TAP-NDE technique has been found very useful for extracting the properties of metallic, non-metallic and composite materials [19]. It does not have the drawbacks that are inherent to transducer-based techniques and is of better accuracy and resolution in applications involving adverse environments and complicated geometrical surfaces [20]. The method is capable of detecting surface cracks, fractures and geometric variations. TAP-NDE can be broadly classified into three integrated systems as shown in Figure 2.

Wave Generation

A high power Nd: YAG (1.5 J per 8 ns) laser pulse is incident on the specimen surface that is intense enough to create a sharp localized thermal gradient in the surface layer. The thermal gradient induces transient stress waves on the surface of the material. Various material properties, the presence of surface-breaking and near-surface defects, and certain geometric details such as thickness variations, can all be characterized through the changes that these produce in propagating ultrasonic waves.

Wave Detection: Fiber Tip Interferometry Technique

The wave detection system utilizes a continuous He-Ne laser beam operated at a wavelength of 633 nm (red light) to sense out-of-plane displacement. The He-Ne laser is connected to a Fused Bi-Conical Tapered (FBT) Coupler that plays the same role as a beam splitter. A portion of the light is disposed of into an optically absorbing indexing matching fluid (IMF). The remaining portion of light travels to the tip of the fiber optic where the GRIN lens is located for receiving a collimated beam of light with small diameter. About 4% of the light gets reflected back from the tip of the fiber, which acts as the reference beam. The remainder of the laser beam is transmitted to the specimen where a portion of light is reflected back into the GRIN lens. This acts as an object beam. The ultrasonic wave propagating through the specimen carries information pertaining to the material and delivers it to the object beam. Interference results due to the combination of the object beam and the reference beam. The device is called a Fiber-Tip-Interferometer (FTI) [21]. It should be noted that both beams travel in the same fiber except for the Fizeau cavity region that is the gap between the GRIN lens and the specimen surface. The combined beam now travels back through the FBT Coupler to the semi-conductor type photo-diode in which the interference pattern is registered and converted into an electrical voltage output.

Wave Analysis

The photodiode is connected to an oscilloscope that displays the waveforms. The requirement to study and analyze waves both spatially and temporally results in the utilization of a number of signal processing techniques. Each of them has advantages and disadvantages over the other. Depending on the characteristic waves, Fast Fourier Transforms (FFT), Short-Time Fourier Transform (STFT), Wavelet Transform (WT) [22], Gabor Wavelet Transform (GWT), Hilbert Transform (HT) and other mathematical tools are used [23].

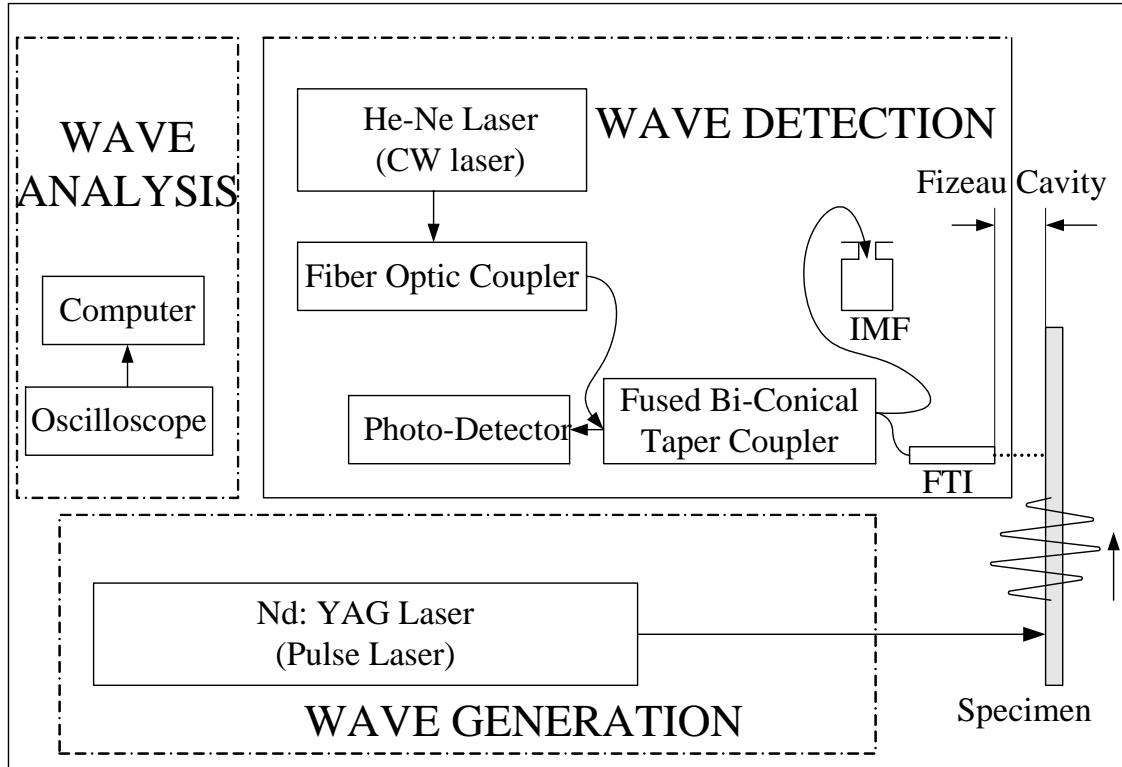


Figure 2: Thermo-Acoustic-Photonic Non-Destructive Evaluation

Tip/Tilt Angles of GRIN Lens

In static alignment, any mechanical component can have a maximum of six degrees of freedom, i.e., three rotational and three translational. The GRIN lens is mounted on a stage capable of all the three mutually perpendicular translational motions and two orthogonal rotational motions, θ_X and θ_Y , as shown in Figure 3. For the perfect alignment of the GRIN lens, the angles θ_X and θ_Y are critical. The third rotational angle, θ_Z , is not useful for alignment purposes. The focus of this thesis is on automating the alignment of the GRIN lens with respect to θ_X and θ_Y to quickly maximize contrast and

position the FTI for optimal performance. The nomenclature for the two angles (θ_X and θ_Y) is defined in Figure 3 and the same is used throughout this report.

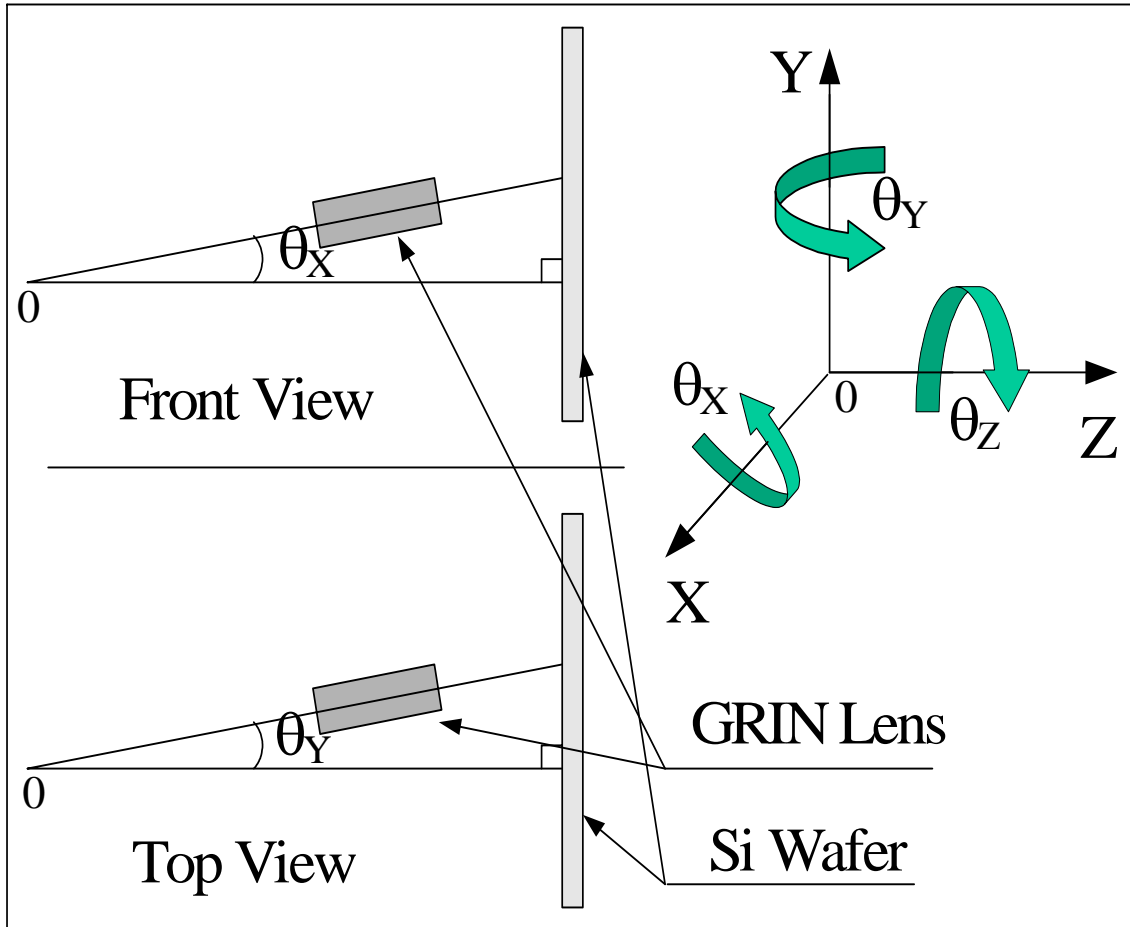


Figure 3: GRIN Lens Tip/Tilt Angles

Need for an Automated FTI System

The FTI detection system developed at Texas A&M University for acquiring transient out-of-plane displacement pulses requires manual positioning of the GRIN lens to achieve optimal interferometry, this has the following drawbacks:

- Hand operated FTI cannot achieve optimal contrast level for interference.
- The alignment procedure is time consuming and inaccurate.
- Large standoff distances between the GRIN lens and the specimen cannot be accomplished.
- The system depends highly on the skills of the operator and thus is tremendously subjective.
- The life of the TAP-NDE system shortens, as the whole system needs a dirt free environment.
- It is difficult to maintain repeatability and precision with manual systems.
- It hinders the capability and feasibility of TAP-NDE for industrial use.

Thesis Objective

The main objective of the research work is to improve upon the previously reported FTI system and optimize the level of contrast in interference pattern by automating the positioning and normal alignment of the GRIN lens and the specimen under observation. This is achieved by upgrading the components of the system. A single mode fiber [21] is shown in Figure 4 where I_R is the intensity of the reference light from the fiber tip; I_o is the intensity of the reflected light from the specimen. I_R is about 3- 4% the total intensity of the light that enters the GRIN lens. This value stays constant for a specific set of laser beam source, FBT coupler, and GRIN lens. The value of I_o , however, is dependent on the Fizeau cavity and the reflectivity of the specimen.

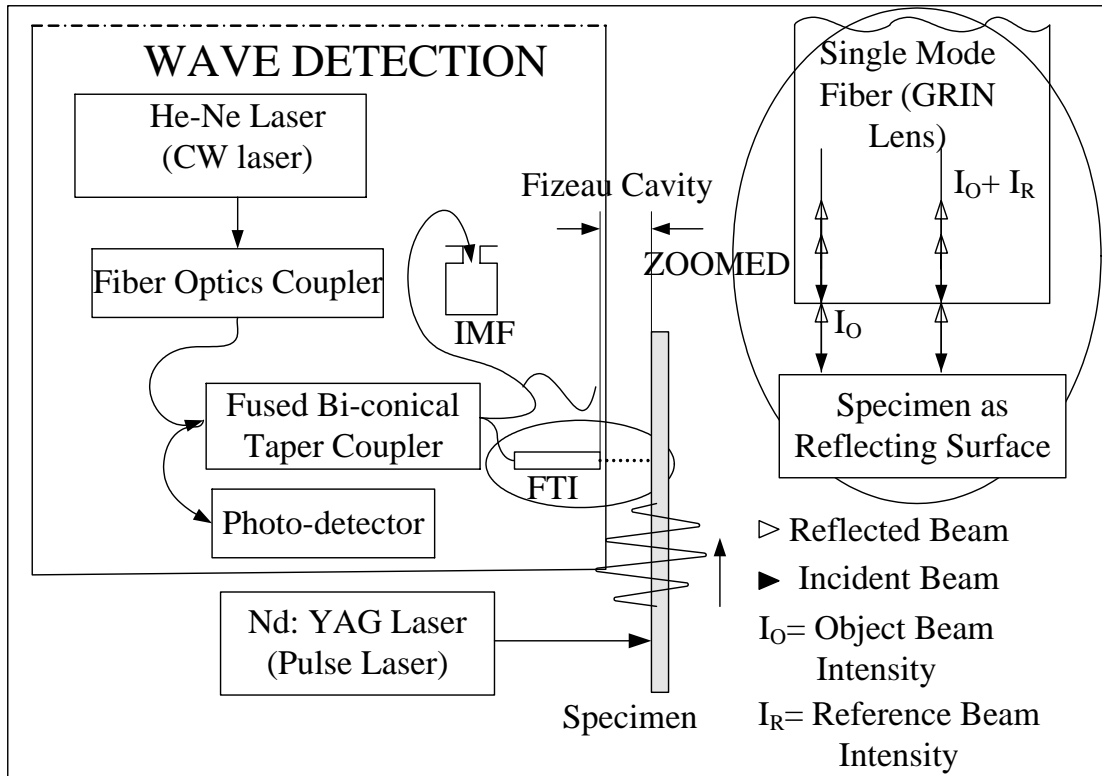


Figure 4: View of Fizeau Cavity in FTI System

Figure 5 pictorially shows the variation of intensity of the reference and object beams with respect to the changes in the Fizeau cavity. To obtain maximum contrast from the interference pattern and to ensure the best output signal at the oscilloscope, a precise and accurate alignment of the GRIN lens with respect to the specimen is required for the GRIN lens to capture the maximum scattered reflection from the specimen surface.

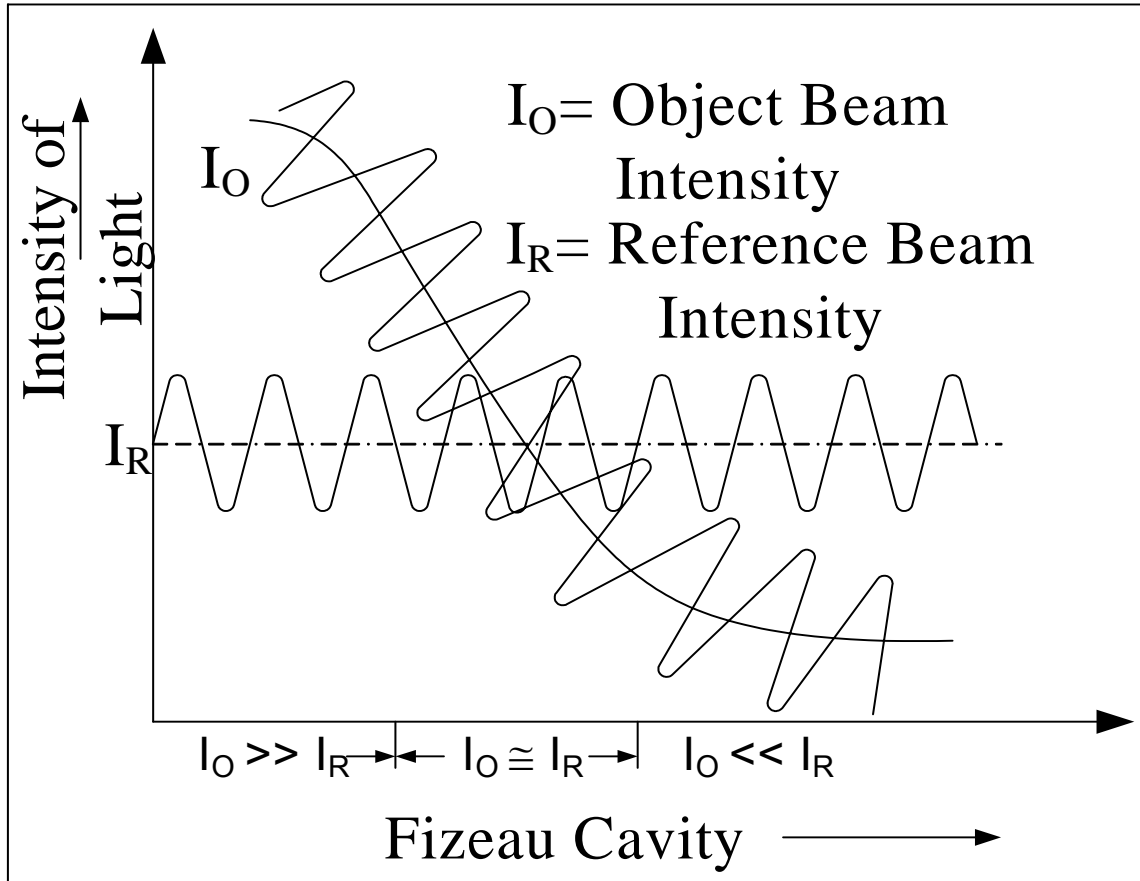


Figure 5: Graph of Intensity Versus Fizeau Cavity

Thus, the objectives of this thesis are to:

- Study the TAP-NDE technology with a special focuses on components utilized in the FTI detection system.
- Analyze the relation between the position of the light spot on the specimen with the two angles of the GRIN lens and the Fizeau cavity.
- New devices are to be explored that can provide a mechanism to locate and control the position of the light spot. These devices should be compatible with the existing non-contacting technique.
- Use various electro-mechanicals, optical, and control systems; design techniques; and analytical studies to conceptualize and embody an automated system that is capable

of achieving the very fine alignment that is necessary for optimal operation of an FTI system.

- Improve the design from an open loop system to closed loop to minimize any system errors.
- Check the new detection system for accuracy, repeatability, and precision at various standoff distances.
- Use flat materials other than a silicon wafer as a specimen to further validate the capability of the design for materials whose surfaces are not as reflective.

Thesis Overview

This thesis addresses on automating the positioning of the fiber tip interferometer. In the course of the project, modifications were made to the controller and the system in an effort to achieve the best possible performance. There are many areas in which these modifications took concurrently. This thesis presents the evolution of the project to its current state and illustrates the performance of the system before and after modifications were implemented, in order to validate the changes.

The thesis consists of six chapters. The present chapter, Chapter I, is the Introduction. Chapter II presents a feasibility study on understanding the capabilities and improvements required in the instrumentation used during wave detection. In Chapter III, various system components and their applications are discussed, along with the design and working principle of all physical components adopted in the automated fiber tip interferometer system. The whole alignment procedure is also explained therein. The algorithm used for attaining precise alignments using LABVIEW software is also discussed in the chapter. The system design configuration can be found in Chapter IV and extensive test results are discussed in Chapter V. Conclusions, recommendations for future work, and applications for which the automated FTI system is suitable are discussed in Chapter VI. The appendix includes the block diagram of the PSD and the flow diagram of the LABVIEW program used for fine alignment.

Contributions of Thesis

The contributions of the thesis are the design and construction of an automated, high-precision, FTI positioning system, and the experimental validation of the proposed design. This novel design is shown to significantly enhance and improve the capability and feasibility of the TAP-NDE technology. Using the automated system, ultrasonic wave detection in flat specimens is highly optimized. Additionally, the overall instrumentation is robust, compact, and easily integrated with the TAP-NDE system which also makes the FTI more easily transportable outside the laboratory.

CHAPTER II

FEASIBILITY SCRUTINY

The detection system in the TAP-NDE technology was studied systematically and carefully. The GRIN lens was mounted in a stage having five degrees of freedom as discussed in Chapter I. A mathematical study was required to understand the kinematics involved in the alignment of the GRIN lens and the effect on the other four of changing one particular parameter. This permitted evaluation of the relationship between all the variables required for the alignment of the GRIN lens with respect to the specimen and to study the feasibility of decoupling any of the variables from the others. This chapter also discusses a preliminary FTI alignment design using an opto-electronic sensor. Experimental study of the GRIN lens alignment system was conducted to understand the various benefits and pitfalls of the preliminary design setup and its components.

Mathematical Modeling

When the GRIN lens is at an angle to the specimen, the reflected light from the specimen falls on the PSD. With the change in the angle of the GRIN lens due to changes of θ_x , θ_y or both, there is a change in the position of the reflection light spot on the PSD. This phenomenon can best be explained using a spherical coordinate system

Let R represents the absolute distance between O and P and Z_0 is the projection of distance R in the Z axis as shown in

Figure 6.

The coordinates of point P are uniquely defined using the followings:

$$X = R * \cos\theta_x * \sin\theta_y \quad \text{-----} \quad (1)$$

$$Y = R * \sin\theta_x \quad \text{-----} \quad (2)$$

$$Z = R * \cos\theta_X * \cos\theta_Y = Z_0 \quad \text{-----} \quad (3)$$

$$R = Z_0 / \{ \cos\theta_X * \cos\theta_Y \} \quad \text{-----} \quad (4)$$

$$Y = Z_0 \sin\theta_X / \{ \cos\theta_X * \cos\theta_Y \} = Z_0 * \tan\theta_X / \cos\theta_Y \quad \text{-----} \quad (5)$$

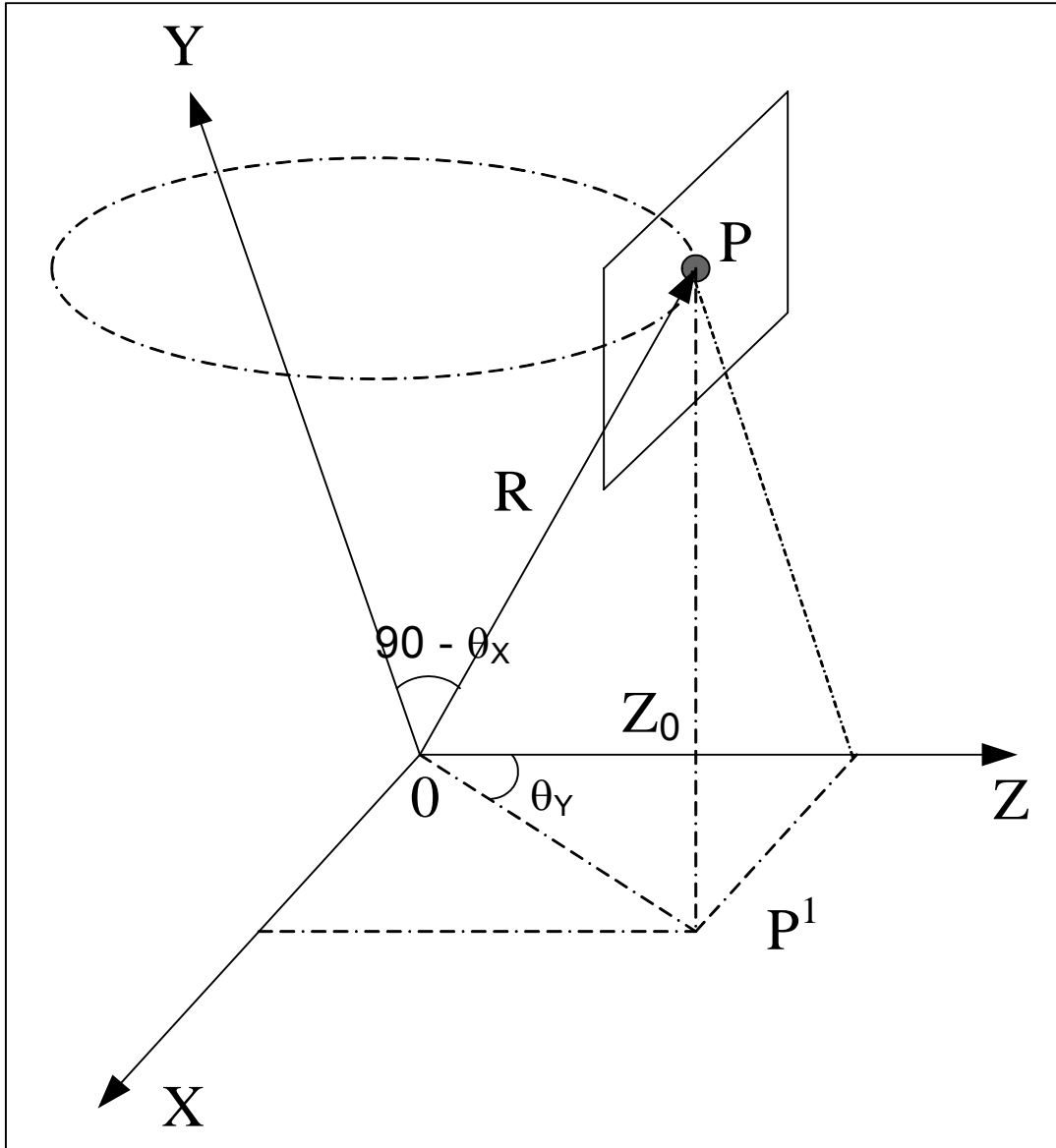


Figure 6: Spherical Coordinate System

Thus, there exists a coupling between θ_X and θ_Y for both X- and Y-coordinate that cannot be separated. For any changes of θ_X , θ_Y or Z_0 , there are also changes in both X- and Y-coordinate, thus is a very critical design constraint.

Prior Experiment

An initial experiment was performed to investigate the various components utilized in the TAP-NDE system and to identify the inherent limitation of the current sensing configuration. In the initial experiment, the concept of using a photocell was explored to automate the alignment of the FTI system. This analysis would determine the plausibility and feasibility of the system design for future work.

Photocell and tip/tilt stages are the two most vital components used for alignment. The following sections give the description of these components.

Photocell

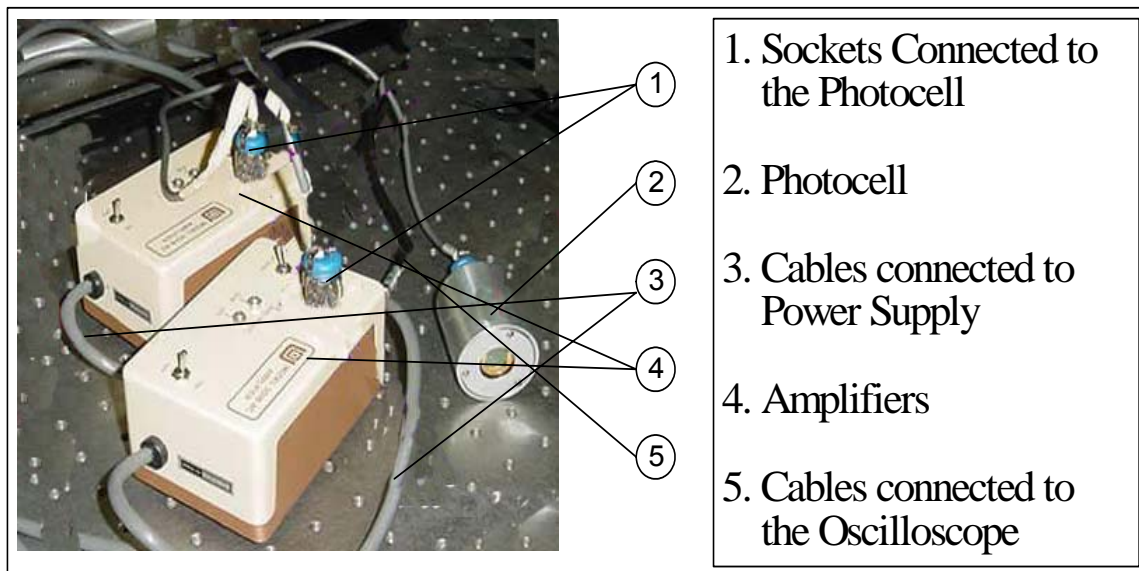


Figure 7: Picture of Photocell with Its Amplifier

Utilizing a photocell in the TAP-NDE detection system was the first step for automating the alignment of the GRIN lens. The photocell is an opto-electronic sensor which utilizes a photosensitive area to keep track of the angle of the GRIN lens. As shown in Figure 7, the photocell is connected to two amplifiers, which in turn are connected to two end connectors that can be connected to the two channels of the oscilloscope. The position of the light spot incident on the photocell can be mapped to a voltage output from the two channels of the oscilloscope, in which the output coordinate readings corresponding to a light spot at the center of the photocell are zeros.

Tilt/Tip Stage

Figure 8 shows a tilt/tip stage that provides two independent tilt adjustments. These adjustments allow optical components such as the GRIN lens to be oriented at desired angles with respect to the specimen. The two axes are spring-loaded to eliminate backlash. The tilt range for each of the axes is $\pm 5^\circ$ and the corresponding resolution is 15 arc-seconds. Standard adjustment screws were used to drive the stage angles.



Figure 8: Picture of Tilt/Tip Stage

Preliminary Setup Configuration

The block diagram for the preliminary design setup is shown in Figure 9. A silicon wafer specimen was mounted in front of the photocell. A holder was designed to hold both the photocell and the GRIN lens as shown in Figure 10. Angles of the GRIN lens were changed with reference to the specimen so that the laser beam passing through the GRIN lens could strike the silicon wafer [18] and its reflection from the wafer surface could be captured at the photocell. The photocell was connected to the oscilloscope where the position of the beam spot on the photocell was measured as a voltage. A mapping was then made between the change of x-y coordinates on the oscilloscope with respect to every small change in the angular tilts (θ_x and θ_y , angular displacement about x- and y- axis, respectively). This procedure allowed proper positioning and alignment to be established.

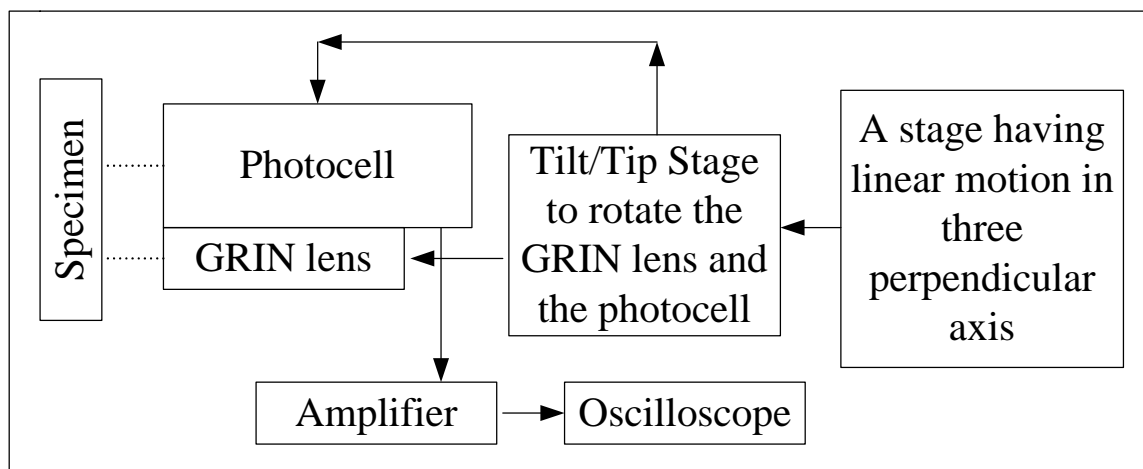


Figure 9: Block Diagram of Positioning System

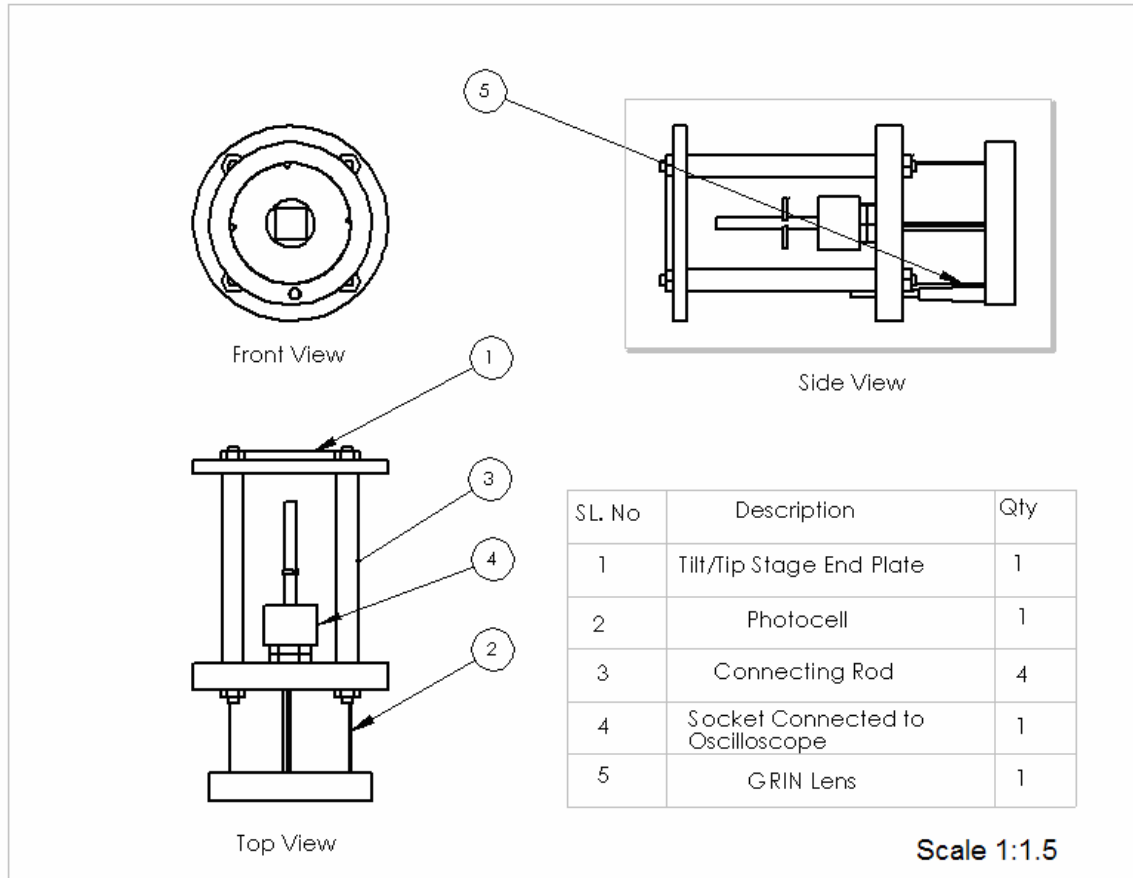


Figure 10: GRIN Lens and Photocell Holder Assembly

Preliminary Experimental Results and Inferences

Preliminary work performed to date has conceptually established that an automated FTI alignment system can be designed by attaching a photocell behind the GRIN lens that can act as a feedback system for monitoring the angular orientation of the GRIN lens with respect to the silicon wafer. The concept of using the photocell was found to be highly advantageous and appropriate for non-contact measurement of any small angle changes. Any angle changes in μrad are amplified and mapped in terms of

voltage reading. It was also found that there is one and only one voltage reading for any particular combination of the two angles of the GRIN lens, which is essential for alignment purposes. The photocell was also found to be highly compatible with the TAP-NDE technology. Being an opto-electronics component, the device fits well with the non-contact method and thus can significantly improve its capability.

Thus, the preliminary experimental study has helped understand how the mechanism of automating the GRIN lens alignment can be realized. However, the initial study also exposed certain limitations and highlighted where improvement is needed. The followings are the limitations found with the configuration and its components:

- Angle changes in the GRIN lens cannot be explicitly measured or determined as the present Newport tilt/tip stage does not have a micrometer or any other measuring device in the lead screw of the angular motion adjustment. Therefore, it is not possible to count the precise angular turns during angular adjustment.
- The photosensitive area of the photocell is too small to be practical. Thus, the GRIN lens cannot be mounted in front of the photocell. This makes the configuration design complicated.
- The photocell is bulky.
- The mapping between the position of the reflected beam spot on the photocell and its position output in the oscilloscope in volts was found to be nonlinear.
- A variation in the GRIN lens tip/tilt angle is registered by the oscilloscope as a bright spot in a voltage grid, thus the exact voltage reading along either x- or y-direction cannot be readily extracted.
- Precise measurement of the distance between the photocell and the silicon wafer is required.
- The whole alignment system is an open loop system that renders the system unreliable and incapable of self-adjustment for better accuracy.

To overcome the above limitations, the followings were identified as action items:

- Use of an angular tilt stage that can be driven by either a motor or a micrometer. Accurate measurement of the angle changes and fine adjustment is necessary to attain fine alignment.
- Use of a position-sensing detector (PSD) having a larger active sensing area than current PSD is available, i.e., from $12 \times 12 \text{ mm}^2$ to $22 \times 22 \text{ mm}^2$. To enable a robust design, the PSD also needs to be compact.
- A PSD that provides continuous position data with desired high resolution, accuracy and reliability.
- With the linear change in the angles of the GRIN lens, the PSD should provide linear variation in the voltage output in the oscilloscope.
- A new design/concept that can accommodate a wide range of standoff distances is needed.
- Design of a close-loop control system, which is essential for achieving accurate and automatic angular measurement and adjustment.

CHAPTER III

AUTOMATED FIBER TIP INTERFEROMETER ALIGNMENT SYSTEM DESIGN

Automated Fiber Tip Interferometer Alignment System

It has been established that fiber-based interferometry as the sensing element in the proven TAP-NDE technology is adequate for material characterization [24-27]. The need for adapting the FTI system in industrial settings to achieve precise control for optimizing interferometric contrast at large standoff distances motivated the development of an automated FTI system. New developments in the fields of photo-electronics like PSDs and micro-positioning devices enable the building of an automatic positioning system for the alignment of the GRIN lens in the FTI arrangement.

Alignment System Design and Instrumentation

The various components used in the automated alignment system design are discussed in the following sections.

Position Sensing Detector (PSD)

The PSD from Hamamatsu Corporation² is an opto-electronic sensor that provides continuous position data of a light spot traveling over a photosensitive surface. There are two types of PSDs: segmented PSDs and lateral effect PSDs. Segmented PSDs consist of two or four segments of a common substrate photo-diode separated by a gap or dead region; whereas lateral effect PSDs are continuous single element planar diffused

² Hamamatsu Corporation, 360 Foothill Road, Bridgewater, NJ 08807

photodiodes with no gaps. Applications such as robotics, mechatronics, medical equipment, precision part assembly and vibration analysis all require position sensors having characteristics including non-contacting, compact, sub-micron resolution, and the ability to access difficult to reach locations. When used in conjunction with lasers, they can be used for alignment, calibration and analysis of machinery.

PSDs have many advantages compared to the discrete-element detectors such as the charged-coupled device (CCD). PSDs have high position resolution, high-speed response and simple operating circuits. The centroid position of a given light distribution incident on the surface of the detector is determined from the amplitude [28] and the phase [29] of the current at the metal electrode. When a light spot falls on a PSD, an electric charge proportional to the light energy is generated at the incident position. This electric charge is driven through the resistive layer and collected by the electrodes. The PSD is thus connected to the electronic driving board that in turn is connected to the power supply and oscilloscope as illustrated in Figure 11.

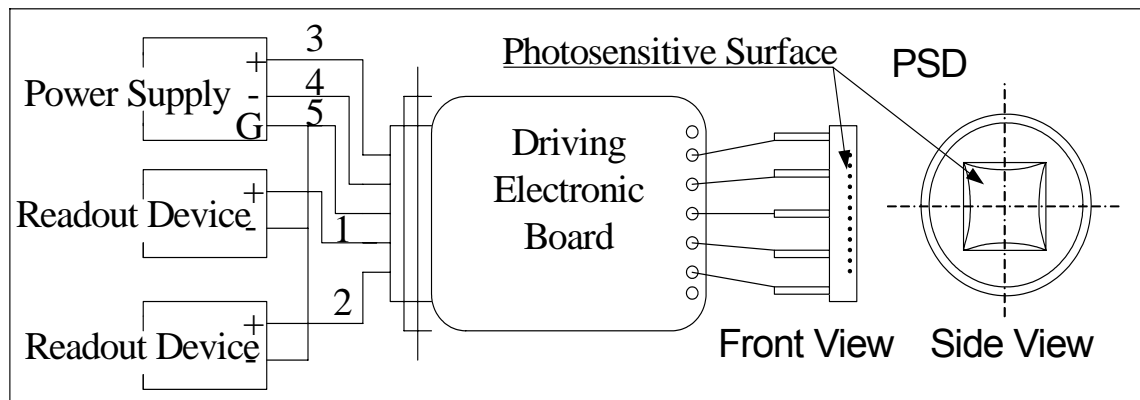


Figure 11: Electronic Connection for 2D-PSD

The wiring connection between the electronic driving board and pin of PSD are detailed in Appendix A. The driving board is designed to provide position data in terms of volts/mm with respect to the center of the 2D-PSD regarded as the origin point, in both

the X- and Y-directions. So, there is a one-to-one mapping between the light spot position and the voltage output. Also the relationship between the position of the beam spot on the PSD and its position output in the oscilloscope in volts is linear, as shown in Figure 12.

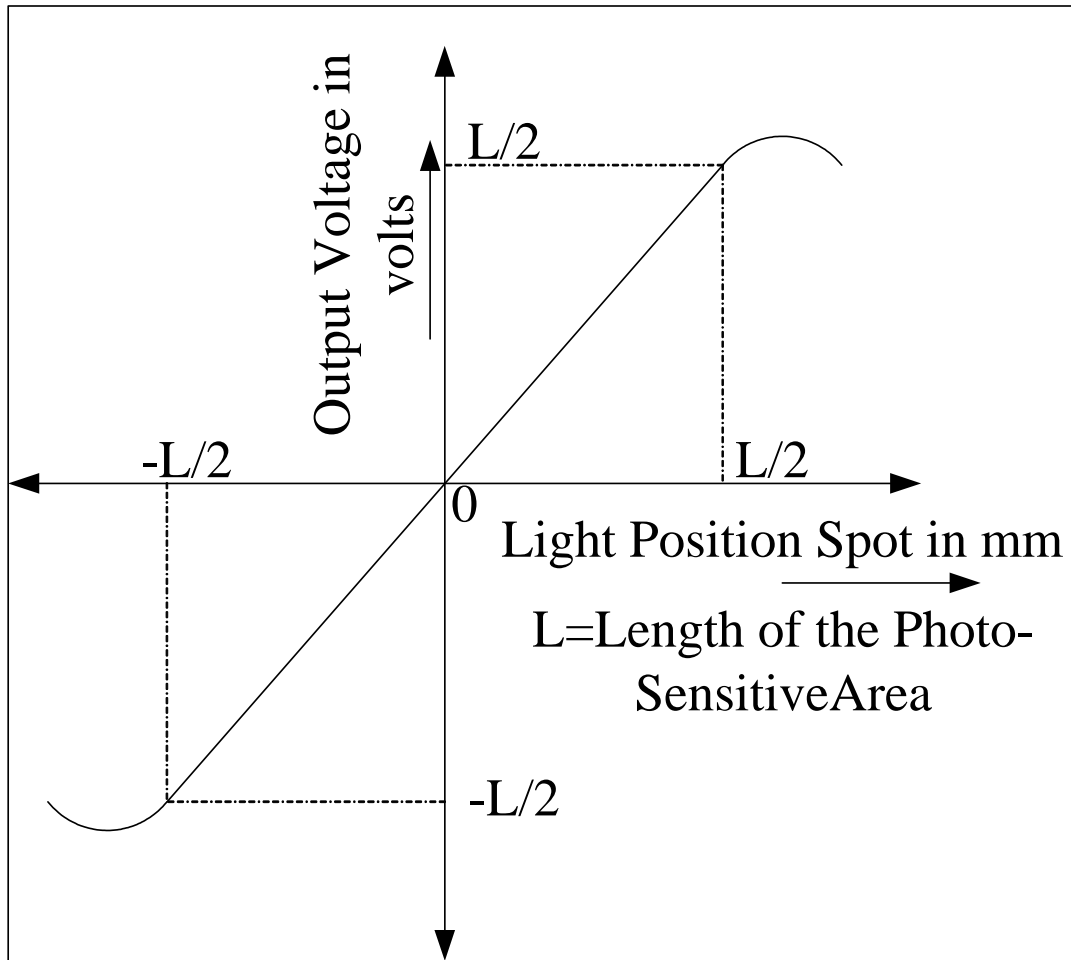
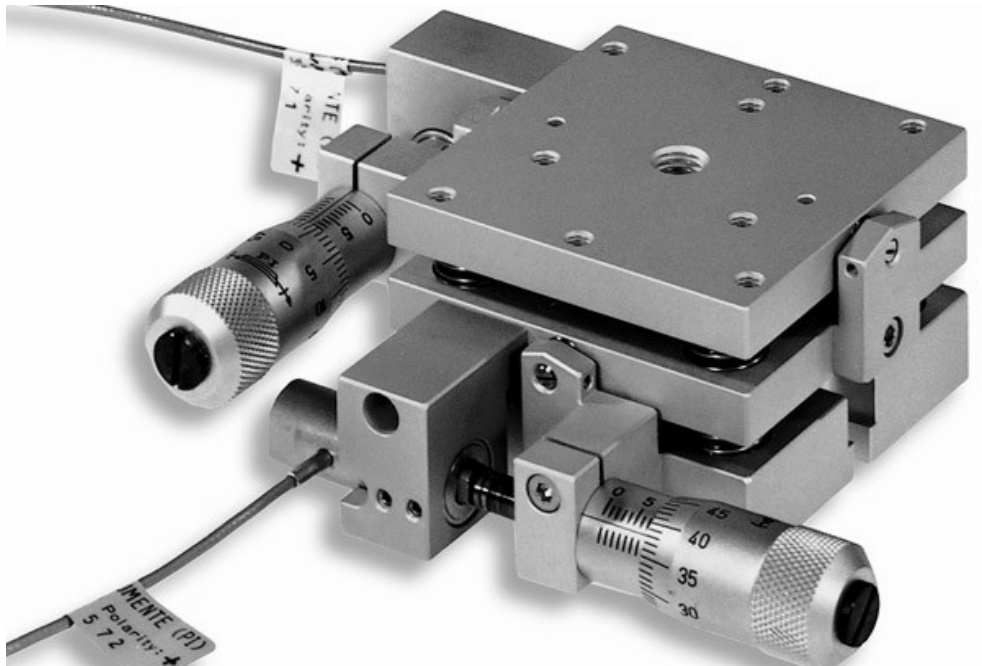


Figure 12: Graph of Voltage Versus Light Spot Position

Micro-Positioning Tilt/Tip Stage

Micro-positioning refers to mechanical movement with positioning accuracy and resolution in the micron or high sub-micron range. Polytec PI³ model M042.D01 as shown in Figure 13 provides two independent orthogonal angular adjustments that feature excellent resolution and repeatability. The two tip/tilt axes (θ_X and θ_Y) of the stage are spring-preloaded for the elimination of backlash. Such a stage is suitable for taking small loads only. As illustrated in Figure 14, the stage is equipped with closed loop DC-servo-motor drives that provide a $0.28 \mu\text{rad}$ resolution. The tilt range in both axes is ± 9 degree. Sets of limit switches eliminate the possibility of overtravel. The dc motor controllers are connected to the computer from which the stage is driven and controlled by user-friendly software LABVIEW and NetMove. The feedback on the position is obtained from the rotary encoder mounted to the DC micrometers via the controller.



³ Polytec PI, Inc, 1342 Bell Avenue Suite 3-A, Tustin, California 92780

Figure 13: DC- Servomotor Driven Tilt/Tip Stage

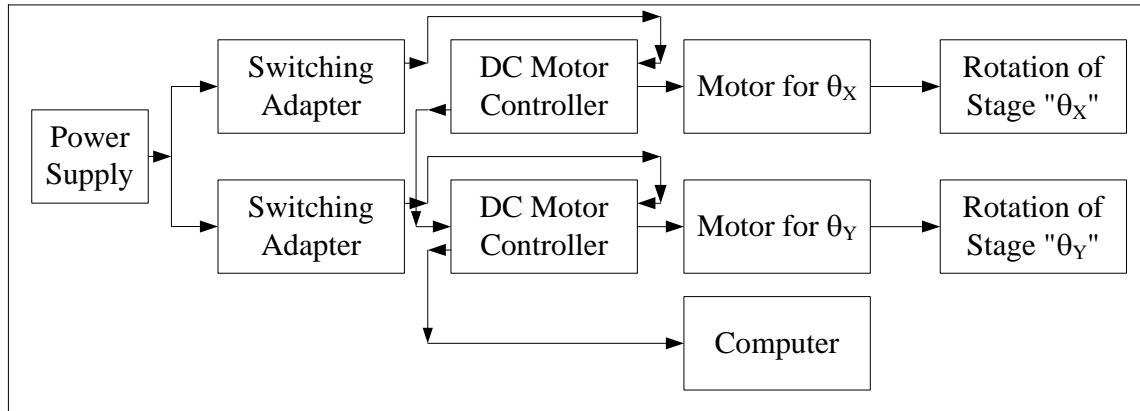


Figure 14: Electronic Connection for Tip/Tilt Stage

GRIN Lens

A GRADIENT INDEX (GRIN) lens is an oxide glass lens whose material refractive index varies continuously as a function of spatial coordinates in the medium. This lens is used to focus and collimate a laser beam resulting in a desired beam diameter or spot size. Pigtail style collimators designed by OZ Optics⁴ have previously been used in the TAP-NDE system. The specification of the collimator is LPC-01-663-4/125-S-.4-1.81GR-40-3S-3-0.3. This collimator has angles designed to attain very low back reflection. It had been experimentally found that the back reflection for the collimator is less than 0.1% of the light entering the GRIN lens. Therefore, this type of collimator is not very suitable for attaining an optimal level of contrast in the interference pattern, especially for silicon wafer specimens of high reflectivity. Pigtail style collimators of specification LPC-01-663-4/125-S-.4-1.81GR-40-3S-3-0.5-SP have the same properties but with their

⁴ OZ Optics Limited, 219 Westbrook Road, Carp, Ontario K0A 1L0, Canada

flats polished. These collimators are found to reflect approximately 4% of the total light back inside the fused bi-conical tapered coupler and thus significantly improve the contrast in the resulting interference pattern.

Photo Detectors

Photodetectors manufactured by EOT⁵ utilize the photovoltaic effect to convert light energy into an electrical current. The photodetectors contain their own BNC connector that facilitates its connection with other devices including oscilloscopes by using a shielded cable with male BNC connectors on both ends. EOT's photodiode can be connected to face contact (FC) fiber optic connectors for use with fiber pigtailed light sources. Output from the photodetectors can be amplified or non-amplified. The amplified photodiodes are used in applications such as measuring the pulse width of Q-switched lasers. The non-amplified photodiodes are very useful in measuring the changes of laser power intensity in terms of average voltage output.

NI-PCI Card and BNC Connector Block

National Instruments⁶ PCI -6013 delivers economical, reliable data acquisition capability. The board features 16 analog inputs at 200 kS/s, 16-bit resolution. It also features a highly precise voltage reference used during self-calibration. A simple software call initiates self-calibration, which minimizes errors caused by temperature drift and time. NI-DAQ is robust driver software used with National Instruments data acquisition and signal conditioning product. This easy-to-use software tightly integrates the full functionality of DAQ hardware to LABVIEW and other software. The BNC connector block has easy connectivity for analog input and output.

⁵ Electro-Optics Technology , Inc , 1030 Hasting Streets, Ste 140, Traverse City, MI 49686.

⁶ National Instruments, 11500 N Mopac Expwy, Austin, TX -78757-3504

Automated Alignment Working Principle and Procedure

It is necessary to automate the precise alignment of the GRIN lens with respect to the specimen (silicon wafer) for achieving the automation of the best interferometric output. The whole alignment procedure can be broadly classified into two steps: Automated Coarse Alignment and Automated Fine Alignment. The coarse alignment is followed by high precision, fine alignment to achieve sub-micron accuracy.

Working Principle for Automated Coarse Alignment

A method of coarse alignment is used for the initial alignment of the GRIN lens. The block diagram of the coarse alignment is illustrated in Figure 15. Both the GRIN lens and the PSD are mounted in the micro-positioning tip/tilt stage that is capable of two angular rotations (θ_x & θ_y). These angles are controlled and driven by the computer through NetMOVE or LABVIEW software. The PSD is mounted behind the GRIN lens to keep track of the angle of the reflected light from the specimen. The PSD is designed to provide position data of the incident laser beam spot in terms of V/mm with respect to the center of the 2D-PSD regarded as the origin point in both the X- and Y- directions. The oscilloscope captures the voltage output from the PSD.

First, the voltage reading of the PSD at a position approximately behind the center of the GRIN lens is noted. This point is called the target point as shown in Figure 16. The target point is independent of the distance between the GRIN lens and the specimen and therefore always remains fixed. Any misalignment between the specimen and the GRIN lens would result in the reflection of the laser beam from the wafer surface onto the photosensitive surface of the PSD. This point is called as the initial point. The voltage at this location is also noted. A small angle (θ_x & θ_y) change of the GRIN lens is achieved via computer to move the back reflection spot towards the target position. This procedure is repeated four to five times until the back reflection is almost close to the

target position. At this point, the back reflection of light beam from the silicon wafer will hit the GRIN lens.

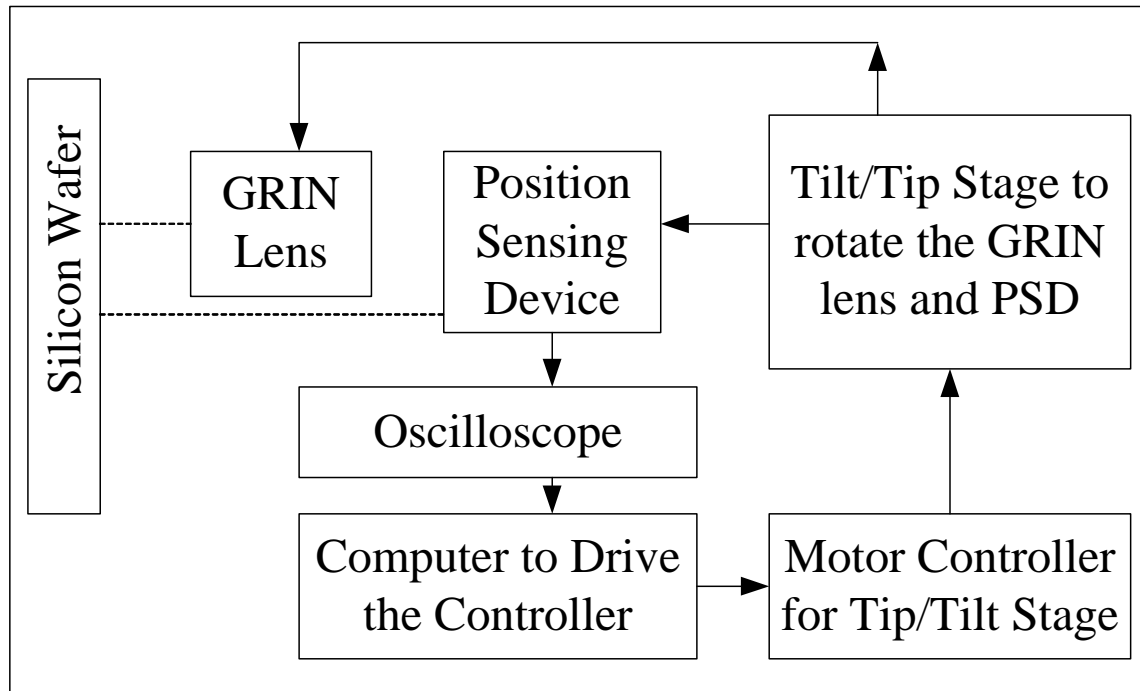


Figure 15: Schematic Diagram of the Automated Coarse Alignment

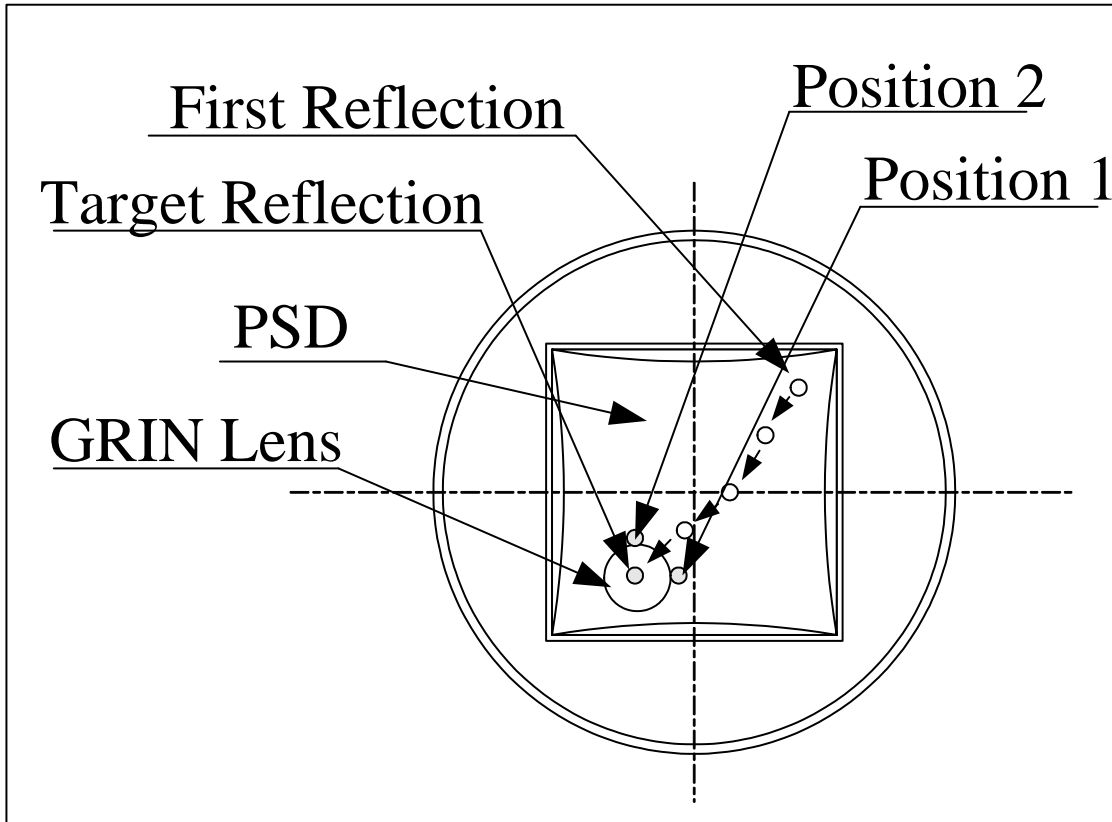


Figure 16: Working Principle of the Automated Coarse Alignment

The perfect and ideal model for this application will be the case where the center of the GRIN lens and the PSD coincide. With this arrangement, the target position will be at zero voltage output for both θ_x & θ_y angles of the GRIN lens. The model can be further idealized by creating a hole in the center of the PSD. The diameter of the hole and the outer diameter of the GRIN lens should be a close fit, thus resulting in a much more compact alignment system as shown in Figure 17. Also the alignment time is reduced because of simple design and photosensitive area all around the GRIN lens.

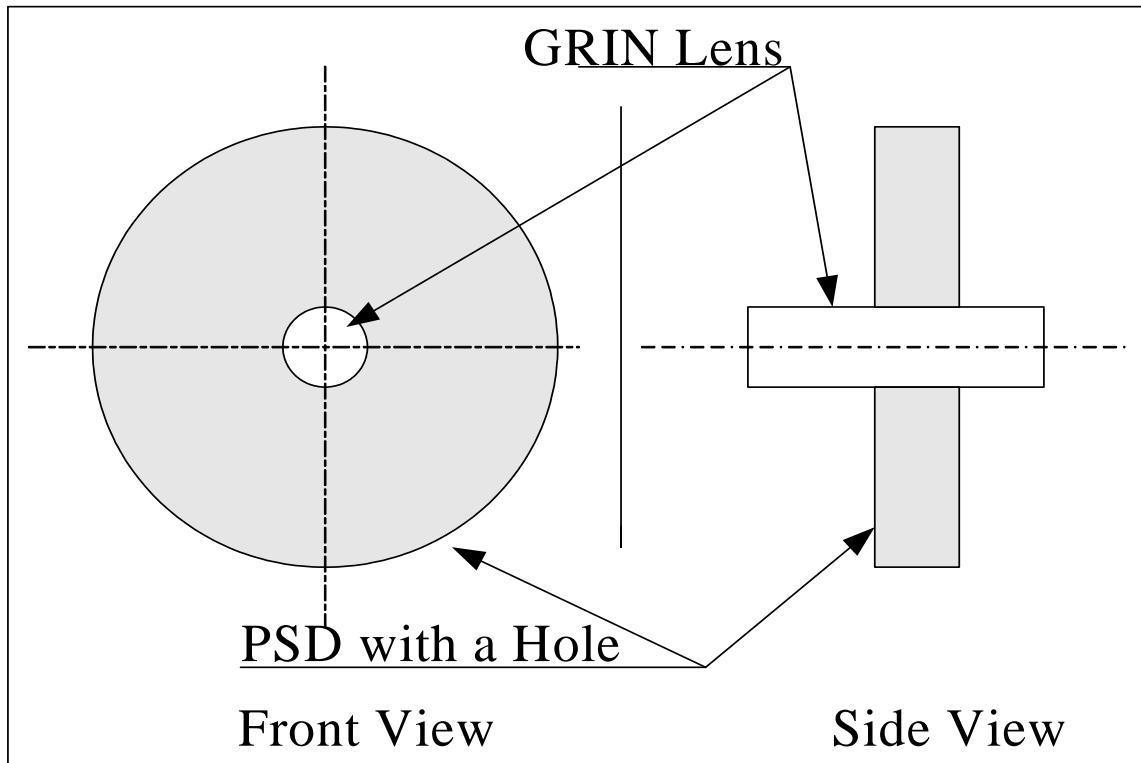


Figure 17: Ideal Model for Automated Coarse Alignment System

Automated Coarse Alignment Procedure

The following steps are followed for the coarse alignment of the GRIN lens.

- Step 1: Start the He-Ne laser beam. Wait for about 30 minutes for laser beam to become stabilized.
- Step 2: Mount the silicon wafer onto a manual tip/tilt stage in front of the GRIN lens.
- Step 3: Adjusted the silicon wafer angles so that the laser beam from the GRIN lens is orthogonal to the flat silicon wafer surface. This is a coarse alignment procedure and is done by checking the light intensity out from the Fused Bi-Conical Tapered (FBT) Coupler leg connected to the photo detector.

- Step 4: The first goal is to find the output voltage reading of the PSD if the beam spot is incident on the photosensitive area exactly behind the center of the GRIN lens. This point is called the target point for the coarse alignment. As the GRIN lens is mounted in front of the PSD, the light beam cannot strike the PSD at perfectly aligned position.
- Step 5: In order to determine the output voltage at the target point, the silicon wafer is purposely misaligned from the aligned position by keeping the angle θ_X constant and changing the angle θ_Y . As angle θ_Y changes, the back reflection from the silicon wafer moves away from the center along the Y-axis. The first back reflection that hits the PSD is recorded and the output voltage values for the X and Y position of the incident laser beam on PSD are registered. This point is shown as Position 1 in Figure 14. Similarly, the back reflection in the PSD at Position 2 is obtained by keeping angle θ_Y constant and changing angle θ_X and the voltage output in the oscilloscope is registered.
- Step 6: The position of the target point in term of voltage is found from the voltage readings of Position 1 and Position 2. This voltage reading is called VT_X and VT_Y . This target position is constant at all times as both the GRIN lens and the PSD are mounted on the same tip/tilt stage. Thus, target position is independent of the length of the Fizeau cavity. In future experiments this value remains unchanged and requires no recalculation.
- Step 7: The tip/tilt angle of GRIN lens is disturbed and an approximate distance between the GRIN lens and the silicon wafer is measured.
- Step 8: The voltage reading corresponding to the initial incident light on the PSD is obtained from the oscilloscope. This voltage corresponds to the x and y position of the PSD with origin at the center of the PSD.
- Step 9: Small angle changes are made in the GRIN lens so that the incident light moves towards the target point.
- Step 10: The micrometer motor count for angles $\Delta\theta_X$ and $\Delta\theta_Y$ is noted along with the two voltage readings V_X and V_Y in the oscilloscope.
- Step 11: The difference in the previous and present voltage readings ΔV_X and ΔV_Y is calculated.

- Step 12: The change in voltage reading for every 10,000 motor counts is measured for both θ_X and θ_Y .
- Step 13: Steps 9 and 12 are repeated a few times and average values for $(\Delta V_X / \Delta \theta_X) * 10000$ and $(\Delta V_Y / \Delta \theta_Y) * 10000$ are determined.
- Step 14: The desired voltage change in X-direction = $VD_X = VT_X - \text{last voltage reading corresponding to X-coordinate}$ and the desired voltage change in y-direction = $VD_Y = VT_Y - \text{last voltage reading corresponding to Y-coordinate}$ are computed.
- Step 15: The required micrometer motor counts for θ_X direction = $10000 * VD_X / (\Delta V_X / \Delta \theta_X)$ and the required micrometer motor counts for θ_Y direction = $10000 * VD_Y / (\Delta V_Y / \Delta \theta_Y)$.
- Step 16: The tip/tilt stage angles are adjusted by moving angles θ_X and θ_Y using the micrometer motor counts as obtained in Step 15.
- Step 17: Coarse alignment is completed and fine alignment begins.

Working Principle for Automated Fine Alignment

After performing the coarse alignment, fine alignment steps begin. The worst scenario in the coarse alignment procedure would be the case where the reflection from the silicon wafer strikes at the position just outside the periphery of the GRIN lens diameter as shown in Figure 18.

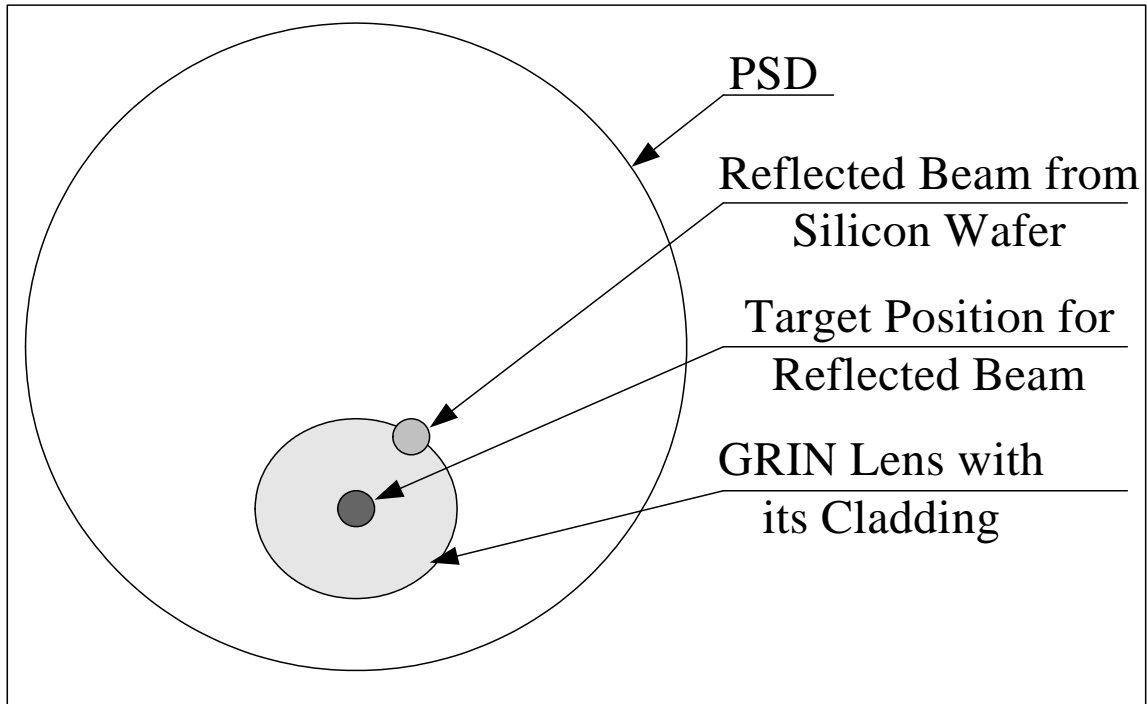


Figure 18: Worst Alignment Case before Automated Coarse Alignment System

The GRIN lens is mounted on the dc servomotor driven tilt/tip stage, whose angles are controlled by and communicated with LABVIEW as shown in Figure 19. Modification is made in the FTI detection system by capturing the non-amplified voltage-time output from the photodetector. The average voltage is captured in the NI PCI card attached to the computer.

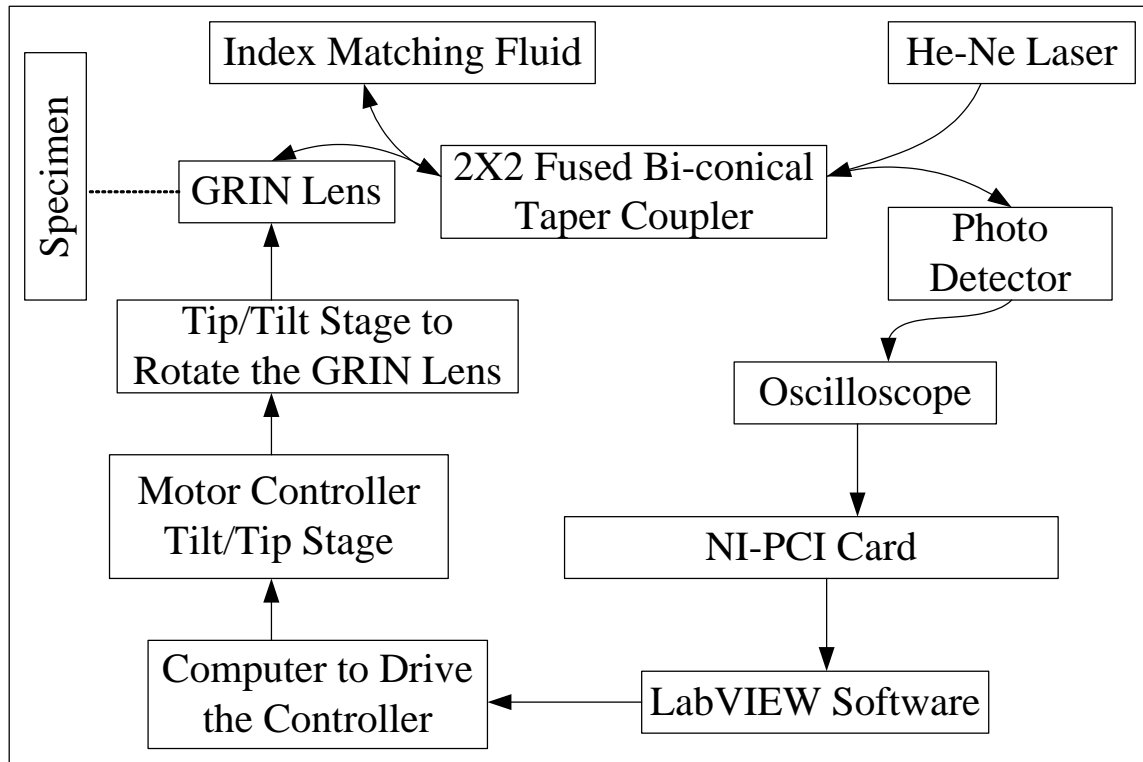


Figure 19: Working Principle of Fine Alignment Procedure for the GRIN lens

This voltage-time sample is utilized in the LABVIEW program to capture the voltage average for certain data samples. At every small increment in positioning the GRIN lens, the LABVIEW program captures the GRIN lens angles θ_X & θ_Y (measured with respect to a home position to be defined later) and the average voltages for some data samples. The angles θ_X & θ_Y are defined in terms of the number of counts of motor rotation of the servo motor controlled tip/tilt stage.

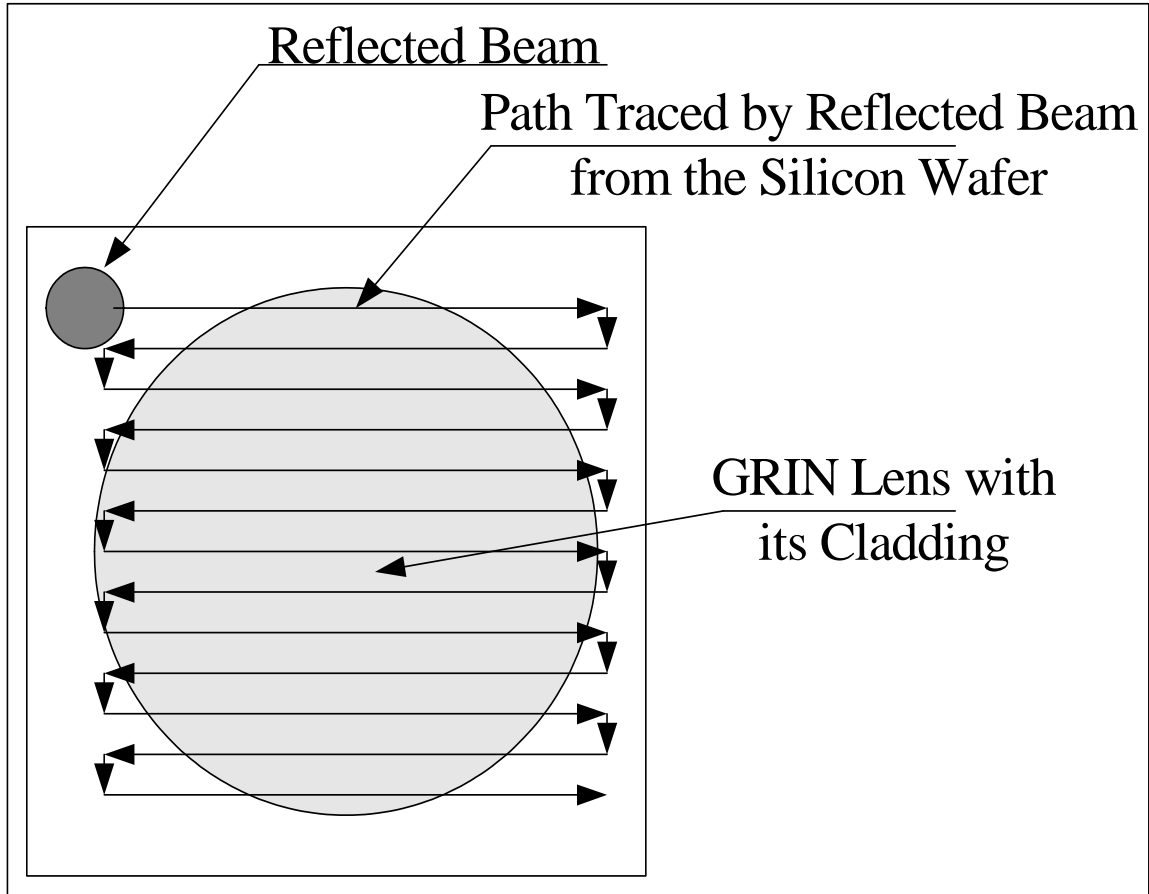


Figure 20: Scanning Voltage at Different Reflected Angles

A LABVIEW program was developed to change the angle of the GRIN lens at μrad level, which traces the path of the reflected beam to cover the whole GRIN lens area as shown in Figure 20. At the beginning position, angles θ_x & θ_y are defined at the home position as zero. Any angle change of the GRIN lens is measured with reference to this home position. At every micro angle change, angles θ_x & θ_y and voltage average for some data samples are generated in a spreadsheet by LABVIEW. The optimal level of contrast in the interference of the reference beam with the object beam is the location where maximum average voltage output is achieved. Thus, LABVIEW reads the

maximum average voltage and its corresponding angle readings from the spreadsheet and moves the GRIN lens to the desired location. It also generates a 3D-waterfall plot with photo-detector voltage as a function of the two GRIN lens angles.

Improved Working Principle for Automated Fine Alignment

The working principle described earlier for scanning the interference intensity was found to have one major pitfall. As the scan area is large, most of the output voltage readings are less than 1.7mV, signifying that much time was wasted on capturing unwanted angles of the GRIN lens and the voltage output. It takes about 6 minutes to run the whole LABVIEW program. Thus, improvement is required for the algorithm to find a better method to attain the maximum level of contrast in the interferometer.

Recognizing the need, an improved algorithm dividing the LABVIEW scanning program into two steps is developed. First, the reflected beam from the specimen is reflected so that the angle increment of the GRIN lens is increased by twice from the previous method. The controller stops at the position where the PCI card captures a voltage higher than 2.5 mV. In the second step, the angles of the GRIN lens are changed slightly such that the reflection from the specimen is moved slightly backward as well as upward. This change is done to accommodate any error that might occur in case the voltage output surpasses the maximum value. The new voltage scan loop would thus reduce to a very small area as shown in Figure 21.

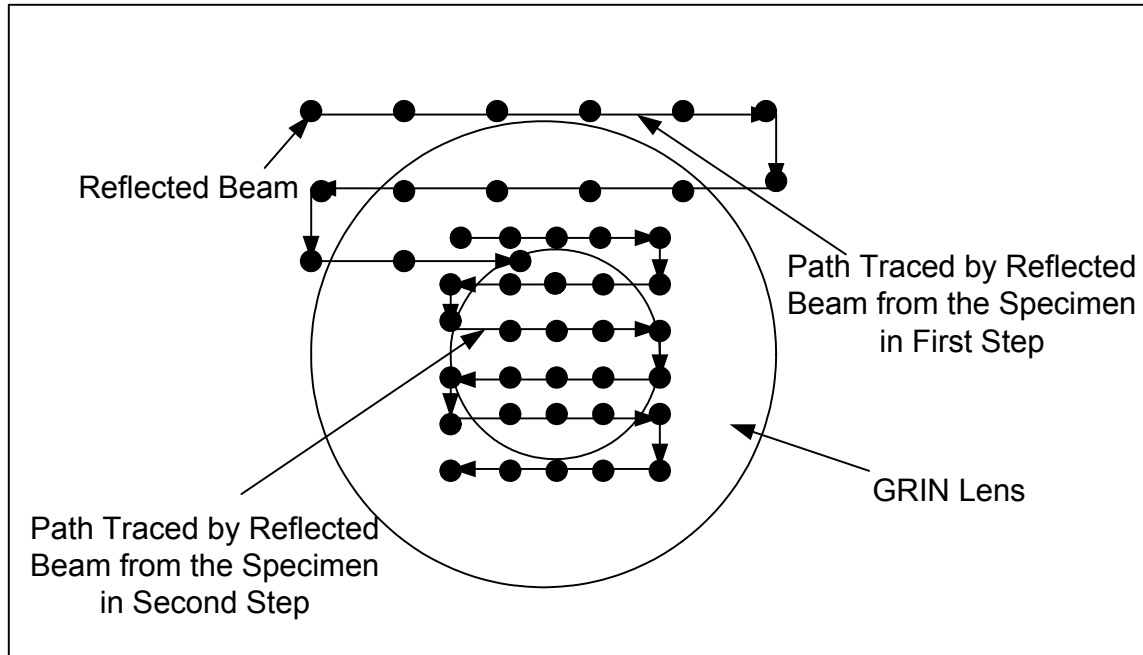


Figure 21: New Algorithm for Fine Alignment

Increment of the angular motor is then made smaller, thus better precision and accuracy and significant reduction in scanning time. A flow chart for the computation of maximum contrast in the interference pattern can be found in Appendix B.

Steps in the LABVIEW Program for Automated Fine Alignment

The LABVIEW program for fine alignment of the GRIN lens with reference to the specimen consists of following steps. These steps are useful for understanding the logic behind the flow chart found in Appendix B and the execution of the program.

- Step 1: Opens and configures a COM port for controller specific data transfer. COM port 1 or 2 can be selected as per connection.
- Step 2: Initializes networking between the two independent tip/tilt motion devices. L, I, J, K, P, Q and R are integer variable used in the program.
- Step 3: Device 1 is selected.

- Step 4: Define $L = 0$.
- Step 5: Send the MN command. MN is defined as motor on. It turns the red LED lights in the controller to green. This gives the signal that the device is now on-line and ready for motion.
- Step 6: Send the command DP90,DI120,DD300,SV400000. The DP (define proportional gain) command sets the slope of the proportional relationship between the position error and the motor voltage. The higher the gain value set, the greater the stiffness of the position coupling, which means a small error value causes a proportionally larger motor current. The DI (defined integral gain) command function is to overcome friction-induced static errors. The DD (define derivative gain purpose is to increase damping and reduce overshoot at the end of motion. DP, DI and DD can be set from 0 to 32,767 values. The SVn command causes the motor to accelerate up to a speed of n counts/s for subsequent motion commands. The value is given in encoder counts per second. The range for setting velocity is from 0 to 500,000 counts per seconds.
- Step 7: If the device is 1, move the motor in the positive direction else move it in the negative direction. The motor counts depend on the rough measurement of Fizeau cavity.
- Step 8: Get the current position of the file and write it in an output file "start position.txt".
- Step 9: Define this position as home position for the device and write the current position in the start position.txt. The current position should read zero in the output file.
- Step 10: Device 2 is selected.
- Step 11: If $L > 0$, go to step 12, else $L = L+1$ and go back to step 5. L is defined in step 4.
- Step 12: Define $I = 0$.
- Step 13: Device 1 is selected.
- Step 14: Send command such that the reflection from the specimen makes a small increment (in micrometers) downward.

- Step 15: Get the current position of device 1 and write it on the first column of the output file “First Large Voltage.txt”.
- Step 16: Device 2 is selected.
- Step 17: I, a variable, is divided by 2. If remainder is zero, go to step 18 else go to Step 24.
- Step 18: Define $J = 0$.
- Step 19: Send command such that the reflection from the specimen makes a small increment (in micrometer) in the right-hand side as looked from the specimen side.
- Step 20: Obtain the current position of device 2 and write it on the second column of the output file “First Large Voltage.txt”.
- Step 21: Get the average voltage value from the NI- PCI card and write it on the third column of the output file “First Large Voltage.txt”.
- Step 22: If the voltage value is greater than 2.5mV, go to step 30 else go to step 23.
- Step 23: If $J < 21$, $J = J + 1$ and repeat steps 19 – 22, else go to step 29.
- Step 24: Define $K = 0$
- Step 25: Send command such that the reflection from the specimen makes a small increment (in micrometer) in the left-hand side.
- Step 26: Obtain the current position of device 2 and write it on the second column of the output file “First Large Voltage.txt”.
- Step 27: Capture the average voltage value from NI- PCI card and write it on the third column of the output file “First Large Voltage.txt”.
- Step 28: If $K < 21$, $K = K + 1$ and repeat steps 25 – 27, else go to step 29.
- Step 29: Set $I = I + 1$. If $I > 20$ go to step 30 else go to step 13.
- Step 30: Set the device 1 motor such that the back reflection moves slightly upwards (few micrometers) and define it as home position and set the device 2 motor such that the back reflection moves slightly on the left-hand side (few micrometers) and define it also as home position.
- Step 31: Define $P = 0$
- Step 32: Device 1 is selected.

- Step 33: Send command such that the reflection from the specimen makes a small increment (in sub-micron) downward.
- Step 34: Get the current position of device 1 and write it on the first column of the output file "small scan.txt".
- Step 35: Device 2 is selected.
- Step 36: P is divided by 2. If remainder is zero, go to step 37 else go to step 42.
- Step 37: Define $Q = 0$
- Step 38: Send command such that the reflection from the specimen makes a small increment (in sub-micron) in the right-hand side.
- Step 39: Obtain the current position of device 2 and write it on the second column of the output file "small scan.txt".
- Step 40: Get the voltage value from the NI-PCI card and write it on the third column of the output file "small scan.txt".
- Step 41: If $Q < 26$, $Q = Q + 1$ and repeat steps 38 - 40, else go to step 47.
- Step 42: Define $R = 0$
- Step 43: Send command such that the reflection from the specimen makes a small increment (in sub-micron) in the left-hand side.
- Step 44: Obtain the current position of device 2 and write it on the second column of the output file "small scan.txt".
- Step 45: Capture the average voltage value from the NI-PCI card and write on the third column of the output file "small scan.txt".
- Step 46: If $R < 26$, $R = R + 1$ and repeat steps 43 – 45, else go to step 47.
- Step 47: Set $P = P + 1$. If $P > 25$ go to step 48 else go to step 32.
- Step 48: Get the maximum voltage output from the file "small scan.txt" file and get its corresponding motor position (say X and Y) of two devices.
- Step 49: Select device 1 and move it to position X.
- Step 50: Select device 2 and move it to position Y and alignment is completed.
- Step 51: Generate a 3D plot by using the output file "small scan.txt" with motor counts of device 1 and 2 as x-axis and y-axis respectively and average voltage at that position as z-axis.
- Step 52: Close the COM port.

Conclusions of Chapter III

This chapter begins with describing the instrumentation employed to achieve the objective defined in Chapter I and to overcome the limitations found with the preliminary FTI setup design as illustrated in Chapter II. These instrumentation electronics and accompanying mechanisms have been extensively illustrated and the application and appropriateness of the automated FTI system has been demonstrated. These devices have sufficient resolution to satisfy the requirements for both the coarse and fine alignment procedures. The automated working principle for the alignment of the GRIN lens is delineated. The combination of coarse and fine positioning techniques has been explained that result in an accurate and fast alignment of the GRIN lens.

A step-by-step procedure designed for the coarse alignment of the GRIN lens is described. A LABVIEW program is constructed using the working principle and programming logic developed for the research. The program results in automating the fine alignment and, through which, an output text file is then created with three columns; namely, the angle θ_x in terms of device 1 motor counts, the angle θ_y in terms of device 2 motor counts and the voltage output from the oscilloscope. The GRIN lens angles are then moved to the position where the maximum voltage output is found. The precision and accuracy depends on the number of loops for making small incremental changes. Larger numbers of loops would result in smaller angular increment and thus, more precise and accurate alignment.

CHAPTER IV

DESCRIPTION OF THE PHYSICAL CONFIGURATION OF THE DESIGN

The working principles and procedures for both coarse and fine alignment establish the foundation for the configuration design of the novel automated FTI system. The design setup utilizes the various instruments described in the previous chapters. The coarse design alignment utilizes an extra component, namely a PSD. After an in-depth study of alternatives, a setup design was fabricated for holding both the GRIN lens and PSD to utilize the maximum photosensitive area for the coarse alignment system. The various components of the detection system of the TAP-NDE technology were rearranged and reassembled with various wiring, cables and connectors. The complete assembly renders the coarse and fine alignment system closed-loop so that it is more efficient and reliable.

Assembly Design for Holding the GRIN Lens and the PSD

A Target Point as defined earlier is the coordinate in the PSD exactly behind the center of the GRIN lens. The coarse alignment system requires the target point to be fixed and not varying with the changes in the tip/tilt angle of the GRIN lens. This can be achieved by designing a holder for holding both the GRIN lens and the PSD in the same tip/tilt stage.

The shape and configuration of the PSD plays a vital role in designing the holder assembly. It is circular in shape with a 52-mm diameter. It does not have any mounting holes and is very delicate, thus needing a very special holder for stabilized mounting. The opti-claw manufactured by New Focus⁷ as shown in Figure 22 can be used to hold such circular shaped objects. It automatically centers any optic with a diameter from

0.10" (2.5 mm) to 2.0" (52 mm) to within 0.005". A PSD can be easily mounted by simply slipping it into the spring-loaded arms and tightening the set-screws. It locks the jaws solidly by pushing them against the mounting plate, locking as solidly as a fixed-diameter mount. An L-shaped rectangular frame is attached with the opti-claw arms. The rectangular frame has two M4 holes on it to facilitate mounting with other parts.

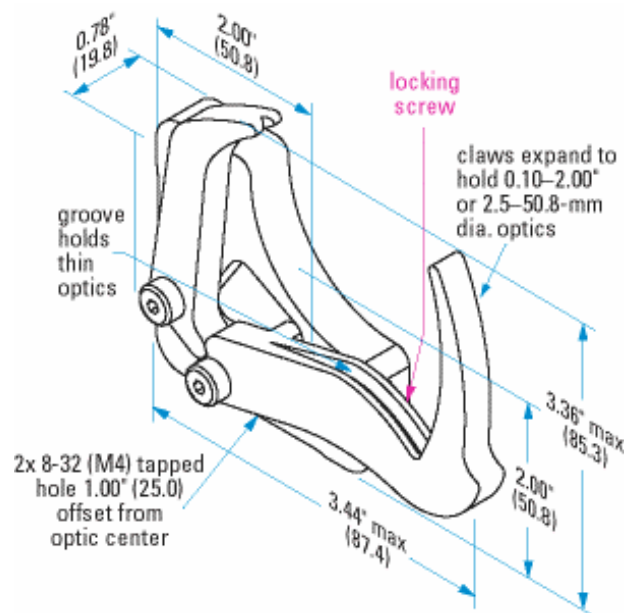


Figure 22: Opti-Claw Mount Drawing

The assembly model of the holder is given in Figure 23. A holder is designed such that it gets attached with the tip/tilt stage and provides a stable base to hold the L-shaped rectangular frame of the Opti-Claw mount and a connecting arm that grips the GRIN lens. As per the proposed coarse alignment model, the GRIN lens is mounted in front of the PSD. Some of the photosensitive area of the PSD is blocked by the GRIN lens and the arm holding the GRIN lens. Thus, in order to utilize the maximum active area of the PSD for the coarse alignment of the GRIN lens, the holder arm was designed to hold the GRIN lens in front of the bottom left of the PSD. A notch is also made in the

⁷ New Focus, Inc, 2584 Junction Avenue, San Jose, CA 95134

holder arm to optimize the active area available for beam reflection from the specimen. Material is removed from unwanted places to minimize the holder assembly weight on the PI tip/tilt stage.

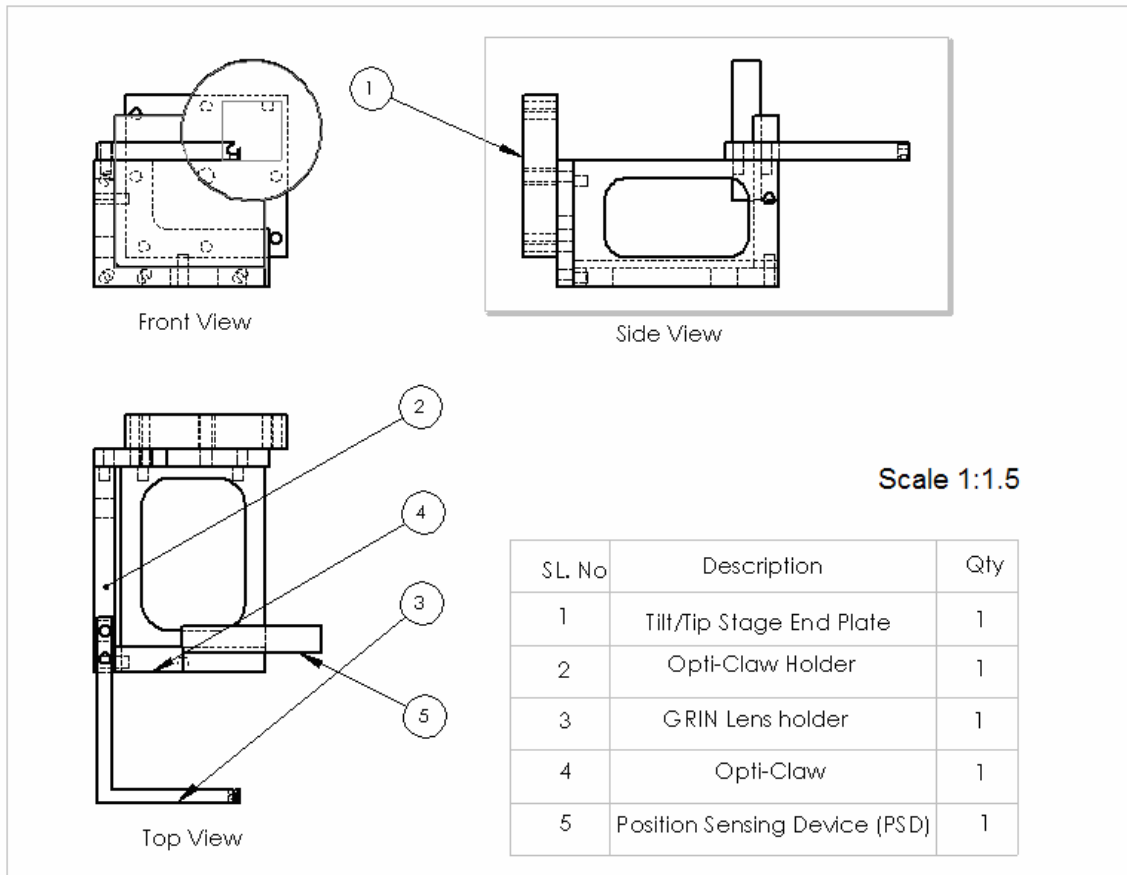


Figure 23: Assembly for Holding the GRIN Lens and the PSD

Detection System Configuration

The physical setup shown in Figure 24 is an assembly of a He-Ne laser, a fused bi-conical tapered coupler, a pigtail style collimator (GRIN lens) with an FC connector at

one end, a photodiode, a PSD, a tilt/tip stage, a dc-servo motor controller, a $\pm 15V$ dc power supply, a PSD driving board, an oscilloscope and a computer. Both the GRIN lens and PSD are mounted on a stage having five d.o.f; namely, 3 orthogonal linear motions along the X-, Y- and Z-direction and 2 angular rotations (θ_X & θ_Y). Rotation in the Z-direction is not required for GRIN lens alignment. The tip/tilt stage angles θ_X & θ_Y are communicated with and controlled by LABVIEW software via the dc servo motor controller. The specimen is mounted in front of the GRIN lens on the same optical table.

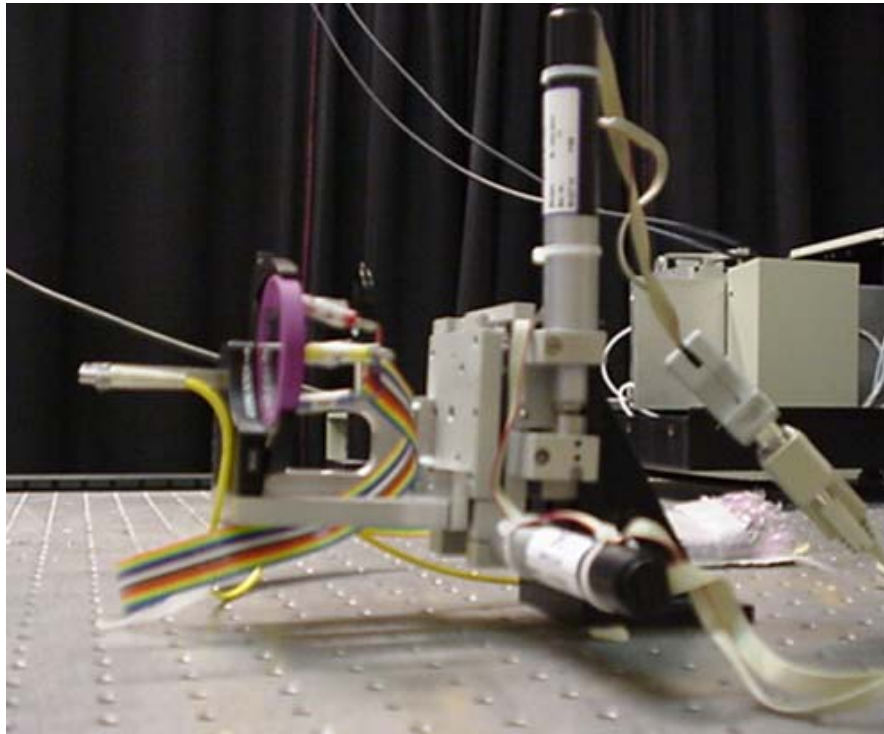


Figure 24: Picture of Design Set-up

As per the coarse alignment procedure described previously, the PSD is mounted behind the GRIN lens such that the maximum active area of the PSD is available for back reflection. The PSD is connected to an electronic driving board. By using wiring, the driving board is connected to a power supply and an oscilloscope as the readout device.

The power supply is set at a constant $\pm 15\text{V}$ output. From the voltage output, four-to-five iterations are made to rotate the tip/tilt stage such that the back reflection would land very close to the target/desired point. The fine alignment system uses the same physical set up as that of the coarse alignment except that the PSD and oscilloscope are not used for the alignment procedure. A LABVIEW program is used for precise alignment of the GRIN lens with the silicon wafer specimen.

Conclusions of Chapter IV

The components and their assembly into an automated FTI alignment system were established as per the design plan. In Section 4.1, the complete holder assembly was described. The holder was designed and manufactured for holding both the PSD and the GRIN lens in the dc servomotor driven tilt/tip stage. With any changes in tip/tilt stage angles, the relative angles between the PSD and GRIN lens do not vary, thus fix the target/desired position. As the target position for the back reflection is independent of the distance between the GRIN lens and the silicon wafer, this feature renders flexibility to the alignment system. Section 4.2 describes the whole design setup. This setup is made to fulfill the requirements set by the coarse and fine alignment procedures outlined in Chapter III.

CHAPTER V

EXPERIMENTAL VERIFICATION AND RESULTS

The novel automated FTI alignment system is designed and fabricated as delineated in previous chapters to achieve the goal of alignment automation. Design verification of the new closed-loop FTI positioning system for the TAP-NDE is done by initially utilizing the PSD for getting the reflected beam to be close to the required position. This is followed by an automated fine alignment procedure that executes a LABVIEW program for generating 3D waterfalls plotting photodiode voltage as a function of the two GRIN lens angles (relative angular positions with reference to the home position.) The data is captured at various standoff distances to study the capabilities of the new system design. In addition, the repeatability of the system is also checked by repeatedly achieving the same interference intensity at a fixed standoff distance while keeping all other variables constant.

Presently, much effort is focused on developing a non-contact technique effective for monitoring and mapping the thermal profiles of silicon wafers subject to rapid thermal annealing. Therefore, experiments are performed mainly using silicon wafers as the specimens. Moreover, as they are highly reflective, silicon wafers would help attain good object beam intensity close to the reference beam as illustrated in Chapter I. However, results are also captured using a less reflective steel plate to explore the limitation of the design setup.

Experimental Analysis of Coupling of GRIN Lens

The previous mathematical analysis result described in Section 2.1 showed that there exists a coupling between the angles θ_X and θ_Y of the GRIN lens that cannot be separated. However, it has been experimentally established (see Table 1) that with a small change in θ_X , the change in the X-coordinate of the reflected beam in the PSD is

very small as compared to the change of its Y-coordinate. Similarly, with a small change in θ_Y , the change in the Y-coordinate is also very small as compared to the change in X-coordinate. In the case of coarse alignment, the alignment itself is rough and the coupling effect can thus be completely neglected. The fine alignment system uses a LABVIEW program for moving the reflected beam path as shown in Figure 21 of Chapter III. Keeping angle θ_X constant and changing θ_Y , change of X-coordinate itself is in microns for every capture of the voltage output. Therefore, changes of Y-coordinate can be ignored.

Table 1: Coupling of GRIN Lens

θ_X	θ_Y	$\Delta\theta_X$	$\Delta\theta_Y$	V_X	V_Y	ΔV_X	ΔV_Y
0	0	-	-	-3.125	-3.438	-	-
0	35000	0	35000	-1.726	-3.437	1.399	0.001
35000	35000	35000	0	-1.725	-2.037	0.001	1.4

where

θ_X = Angle θ_X of the GRIN lens in terms of the DC servo motor counts of the tip stage controller.

θ_Y = Angle θ_Y of the GRIN lens in terms of the DC servo motor counts of the tilt stage controller.

$\Delta\theta_X$ = Change of angle θ_X of the GRIN lens in terms of the DC servo motor counts of the tip stage controller.

$\Delta\theta_Y$ = Change of angle θ_Y of the GRIN lens in terms of the DC servo motor counts of the tilt stage controller.

V_X = Voltage reading with reference to the X coordinate of the reflected beam in PSD.

V_Y = Voltage reading with reference to the Y coordinate of the reflected beam in PSD.

ΔV_X = Change of voltage reading with reference to the X coordinate of the reflected beam in PSD.

ΔV_Y = Change of voltage reading with reference to the Y coordinate of the reflected beam in PSD.

Target Position for Coarse Alignment

As described, the Target Position is the location in the PSD exactly behind the GRIN lens center as shown in Fig. 16. Since the alignment is coarse in this step, the target position does not need to be calculated with high precision. The voltage readings corresponding to the X and Y coordinates at Position 1 as shown in Fig. 16 are $(V_X, V_Y) = (-1.4 \text{ V}, -5.78 \text{ V})$. The voltage readings corresponding to the X and Y coordinates at Position 2 as shown in Fig. 16 are $(V_X, V_Y) = (-5.82 \text{ V}, -1.40 \text{ V})$. Thus, the voltage readings corresponding to the X and Y coordinates at the target position are $(V_{TX}, V_{TY}) = (-5.82 \text{ V}, -5.78 \text{ V})$. This target position voltage has to be found only once as it is constant and does not depend on the distance between the GRIN lens and the specimen.

Relationship Between GRIN Lens Angles and Fizeau Cavity

The Fizeau Cavity plays a very important role in the alignment of the GRIN lens. By keeping the GRIN lens angles θ_X and θ_Y constant and changing the distance between the GRIN lens and the silicon wafer, reflection of the laser beam from the silicon wafer strikes the GRIN lens at different locations. The diameter of the GRIN lens with its cladding is 4mm. Keeping the angle θ_X (or θ_Y) constant and making a small change in angle θ_Y (or θ_X), the motor counts depend on the distance between the GRIN lens and the silicon wafer for the reflected beam to sweep the entire 4mm diameter as tabulated in Table 2. This information is necessary for calculating errors in the coarse alignment.

The aforementioned LABVIEW program also utilizes this table for optimizing the scanning area of the GRIN lens.

Table 2: Relation between Fizeau Cavity and Motor Count

Approx. Distance Between GRIN Lens & Specimen mm.	Angle change In Terms Of Motor Counts
30	180000
35	160000
40	140000
45	130000
50	115000
60	110000
65	100000
70	90000
75	85000
80	80000
85	78000
90	75000
95	70000
100	65000

The input for Step 7 of the LABVIEW program is given in Table 1. All small increments of the motor in Step 14, 19, 25, 33 and 38 are dependent on the number of loops and the input from Table 2. The LABVIEW program does not need very fine Fizeau cavity measurement. It only needs an approximate calculation with a ± 2.5 mm tolerance.

Coarse Alignment Results

The experiment was done at several different standoff distances between the GRIN lens and the silicon wafer. The experimental procedure as delineated earlier was followed. Results for three different cases are given below:

Case 1: Distance between the GRIN lens and the silicon wafer is approximately 45mm. Voltage readings from the PSD corresponding to the X and Y position of the initial incident light spot (taking the center of the PSD as the origin as explained previously) are $V_{INT} = 2.048V$ and $V_{INT} = 1.719V$ respectively.

Table 3: Coarse Alignment at 45mm Standoff Distance

$\Delta\theta_X$	$\Delta\theta_Y$	V_X	V_Y	ΔV_X	ΔV_Y	$(\Delta V_X / \Delta\theta_X)$ * 10000	$(\Delta V_Y / \Delta\theta_Y)$ * 10000
-20000	-20000	1.194	0.835	0.854	0.884	0.427	0.442
-20000	-20000	0.301	0.141	0.893	0.694	0.4465	0.347
-20000	-20000	-0.626	-0.77	0.927	0.911	0.4635	0.4555
-20000	-20000	-1.406	-1.562	0.78	0.792	0.39	0.396

The values for both $(\Delta V_X / \Delta \theta_X) * 10000$ and $(\Delta V_Y / \Delta \theta_Y) * 10000$ from the Table 3 are found out to be $\approx 0.4V$.

Desired voltage change in X-direction = $VD_X = VT_X - \text{last voltage reading corresponding to X-coordinate} = -5.82 - (-1.406) = -4.414 V$.

Desired voltage change in Y-direction = $VD_Y = VT_Y - \text{last voltage reading corresponding to Y-coordinate} = -5.78 - (-1.562) = -4.218 V$.

The required micrometer motor counts for θ_X to move to desired position = $10000 * VD_X / (\Delta V_X / \Delta \theta_X) = 10000 * (-4.414) / 0.4 = -110350$ counts.

The required micrometer motor counts for θ_Y to move to desired position = $10000 * VD_Y / (\Delta V_Y / \Delta \theta_Y) = 10000 * (-4.218) / 0.4 = -105450$ counts.

It was determined experimentally that -114000 counts for angle θ_X and -103000 counts for angle θ_Y were required for perfect alignment.

Error after coarse alignment in angle $\theta_X = -114000 - (-110350) = -3650$ counts

Error after coarse alignment in angle $\theta_Y = -103000 - (-105450) = 2450$ counts.

It takes approximately 130,000 micrometer motor counts to move 4mm by changing angle θ_X (θ_Y) and keeping angle θ_Y (θ_X) constant when the distance between the GRIN lens and the silicon wafer is 45mm as given in Table 2.

Therefore, the error in angle θ_X in terms of distance = $-3650 * 4 / 130000 = 0.11mm$ and the error in angle θ_Y in terms of distance = $2450 * 4 / 130000 = 0.075mm$

Case 2: Distance between the GRIN lens and the silicon wafer is approximately 65mm. Voltage readings from the PSD corresponding to the X and Y position of the initial incident light spot (taking the center of the PSD as the origin as explained previously) are $V_{INT} = 5.072V$ and $V_{INT} = 3.282V$ respectively.

Table 4: Coarse Alignment at 65mm Standoff Distance

$\Delta\theta_X$	$\Delta\theta_Y$	V_X	V_Y	ΔV_X	ΔV_Y	$(\Delta V_X / \Delta\theta_X)$ * 10000	$(\Delta V_Y / \Delta\theta_Y)$ * 10000
-50000	-40000	2.002	1.094	3.07	2.188	0.614	0.547
-20000	-20000	0.894	0.055	1.108	1.039	0.554	0.5195
-20000	-20000	-0.312	-1.04	1.206	1.095	0.603	0.5475
-20000	-10000	-1.406	-1.562	1.094	0.522	0.547	0.522

The values for both $(\Delta V_X / \Delta\theta_X) * 10000$ and $(\Delta V_Y / \Delta\theta_Y) * 10000$ from Table 4 are found out to be $\approx 0.55V$.

Desired voltage change in X-direction = $VD_X = VT_X - \text{last voltage reading corresponding to X-coordinate} = -5.82 - (-1.406) = -4.414 V$.

Desired voltage change in Y-direction = $VD_Y = VT_Y - \text{last voltage reading corresponding to Y-coordinate} = -5.78 - (-1.562) = -4.218 V$.

The required micrometer motor counts for θ_X direction to move to the desired position = $10000 * VD_X / (\Delta V_X / \Delta\theta_X) = 10000 * (-4.414) / 0.55 = -80250$ counts.

The required micrometer motor counts for θ_Y direction to move to the desired position = $10000 * VD_Y / (\Delta V_Y / \Delta\theta_Y) = 10000 * (-4.218) / 0.55 = -76700$ counts.

Experimentally, it has been found that -83200 counts for angle θ_X and -78600 counts for angle θ_Y were required for perfect alignment.

Error after coarse alignment in angle $\theta_X = -83200 - (-80250) = -2950$ counts

Error after coarse alignment in angle $\theta_Y = -78600 - (-76700) = -1900$ counts.

It takes approximately 100,000 micrometer motor counts to move 4mm by changing angle θ_X and keeping angle θ_Y constant and vice versa when the distance between the GRIN lens and the silicon wafer is 65mm as given in Table 2.

Therefore, the error in angle θ_X in terms of distance = $-2950 * 4 / 100000 = 0.118\text{mm}$ and the error in angle θ_Y in terms of distance = $-1900 * 4 / 100000 = -0.076\text{mm}$

Case 3: Distance between the GRIN lens and the silicon wafer is approximately 100mm
Voltage readings from the PSD corresponding to the X and Y position of the initial incident light spot (taking the center of the PSD as the origin as explained previously) are $V_{INT} = 6.09\text{ V}$ and $V_{INT} = 3.15\text{ V}$ respectively.

Table 5: Coarse Alignment at 100mm Standoff Distance

$\Delta\theta_X$	$\Delta\theta_Y$	V_X	V_Y	ΔV_X	ΔV_Y	$(\Delta V_X / \Delta\theta_X)$ * 10000	$(\Delta V_Y / \Delta\theta_Y)$ * 10000
-50000	-50000	2.243	-0.1	3.847	3.25	0.7694	0.65
-50000	-20000	-0.883	-1.408	3.126	1.308	0.6252	0.654
-20000	-20000	-2.2	-2.656	1.317	1.248	0.6585	0.624

The values for both $(\Delta V_X / \Delta\theta_X) * 10000$ and $(\Delta V_Y / \Delta\theta_Y) * 10000$ from the Table 5 are found out to be $\approx 0.64\text{ V}$.

Desired voltage change in X-direction = $VD_X = VT_X - \text{last voltage reading corresponding to X-coordinate} = -5.82 - (-2.2) = -3.62\text{ V}$.

Desired voltage change in Y-direction = $VD_Y = VT_Y - \text{last voltage reading corresponding to Y-coordinate} = -5.78 - (-2.656) = -3.124\text{ V}$.

The required micrometer motor counts for θ_X direction to move to the desired position = $10000 * VD_X / (\Delta V_X / \Delta\theta_X) = 10000 * (-3.62) / 0.64 = -56600\text{ counts}$.

The required micrometer motor counts for θ_y direction to move to the desired position = $10000 * VD_Y / (\Delta V_Y / \Delta \theta_Y) = 10000 * (-3.124) / 0.64 = -48800$ counts.

Experimentally, it was found that -57200 count for angle θ_x and -48200 counts for angle θ_y were required for perfect alignment.

Error after coarse alignment in angle $\theta_x = -57200 - (-56600) = -600$ counts

Error after coarse alignment in angle $\theta_y = -48200 - (-48800) = 600$ counts.

It takes approximately 65000 micrometer motor counts to move 4mm by changing angle θ_x and keeping angle θ_y constant and vice versa when the distance between the GRIN lens and the silicon wafer is 65mm as given in Table 2.

Therefore, the error in angle θ_x in terms of distance = $-600 * 4 / 65000 = -0.037$ mm and the error in angle θ_y in terms of distance = $600 * 4 / 65000 = 0.037$ mm.

Once coarse alignment has been achieved, it is followed by the fine alignment method detailed below.

Fine Alignment Results - Initial Method

The LABVIEW program was run at different values of the distance between the GRIN lens and the silicon wafer to validate its independency with the Fizeau cavity and to achieve precise results with accuracy. The following results are taken by using the method described in Section 3.3.3 and the path traced by the reflected beam is shown in Fig. 20 using a silicon wafer as the specimen. The data captured using LABVIEW are analyzed in Excel, and 3D surface plots and 2D infringe plots are generated by plotting the photodiode voltage as functions of the two GRIN lens angles (relative angular positions with reference to the home positions).

Case 1: Distance between the GRIN lens and the silicon wafer is approximately 45mm.

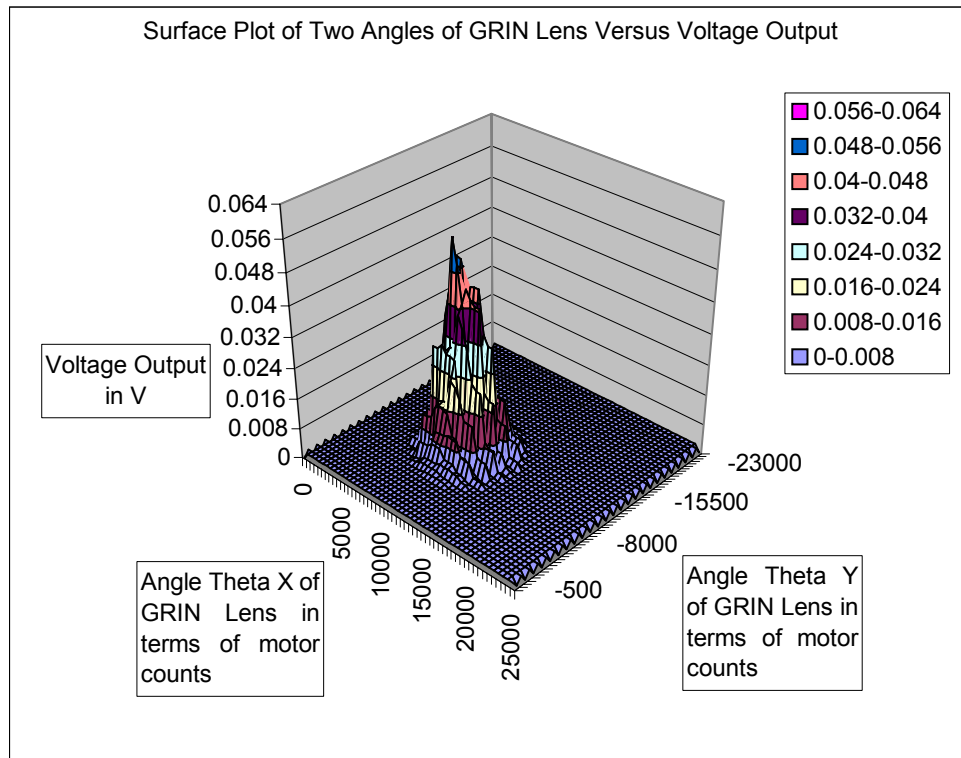


Figure 25: Surface Plot at 45mm Fizeau Cavity

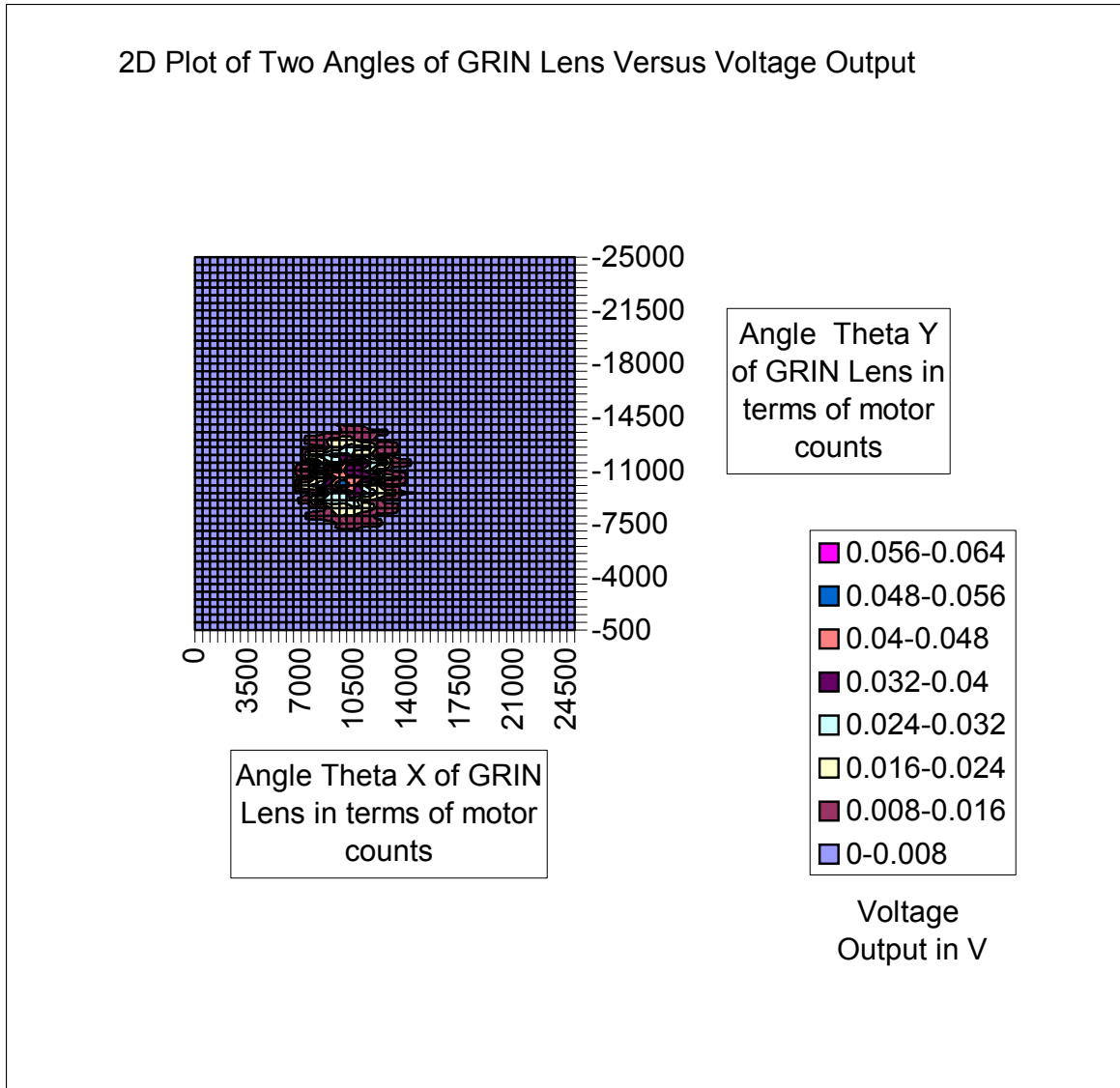


Figure 26: 2D Plot at 45mm Fizeau Cavity

Analysis Result:

Figure 25 shows the 3D surface plot and Figure 26 shows the corresponding infringes pattern at 45mm Fizeau cavity.

Maximum Voltage = 56.046 mV

Motor counts for angle θ_x of GRIN lens at maximum voltage = 9500

Motor counts for angle θ_Y of GRIN lens at maximum voltage = -10000

Therefore, the angles θ_X and θ_Y of GRIN lens is moved to absolute coordinate 9500 and -10000 respectively of the motor counts of tip/tilt stage after the program stopped running for final alignment. This results in perfect alignment of the GRIN lens with respect to the silicon wafer.

Case 2: Distance between the GRIN lens and the silicon wafer is approximately 65mm.

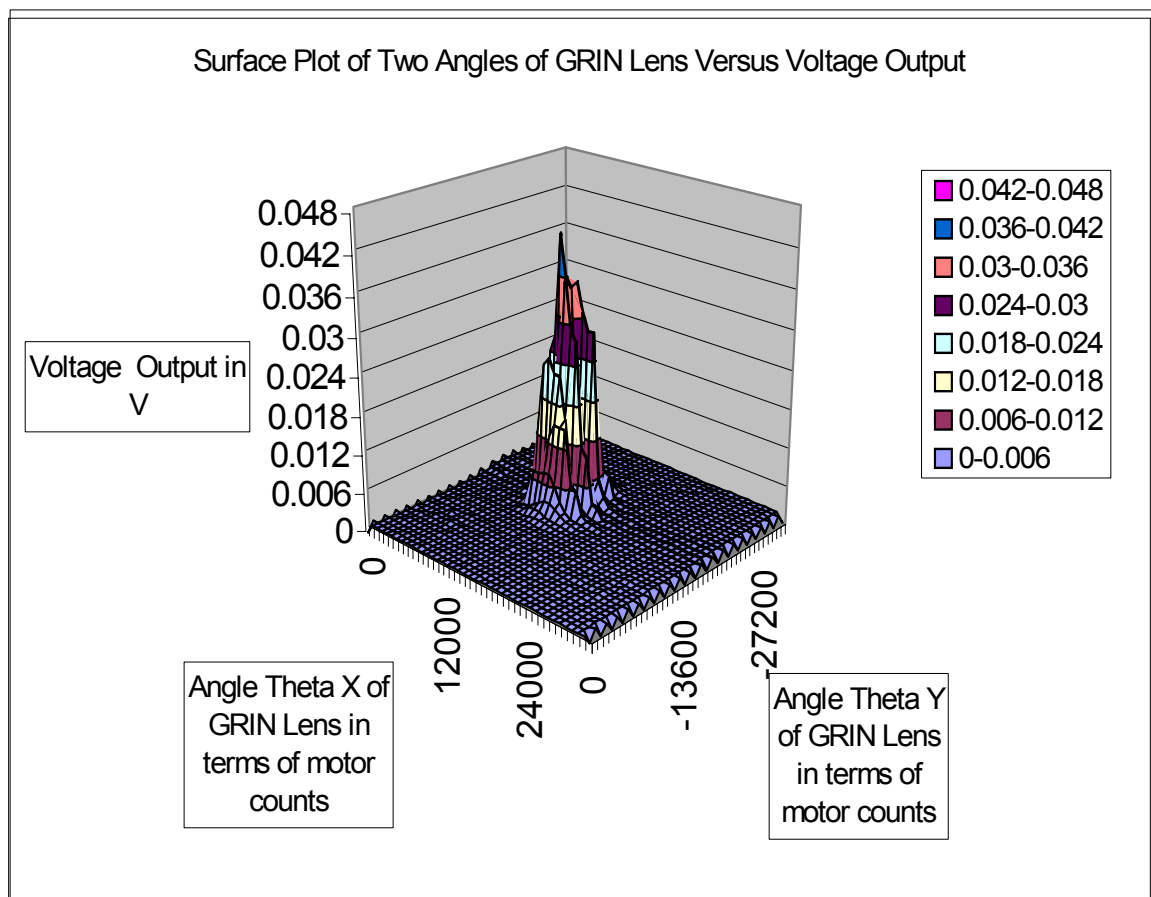


Figure 27: Surface Plot at 65mm Fizeau Cavity

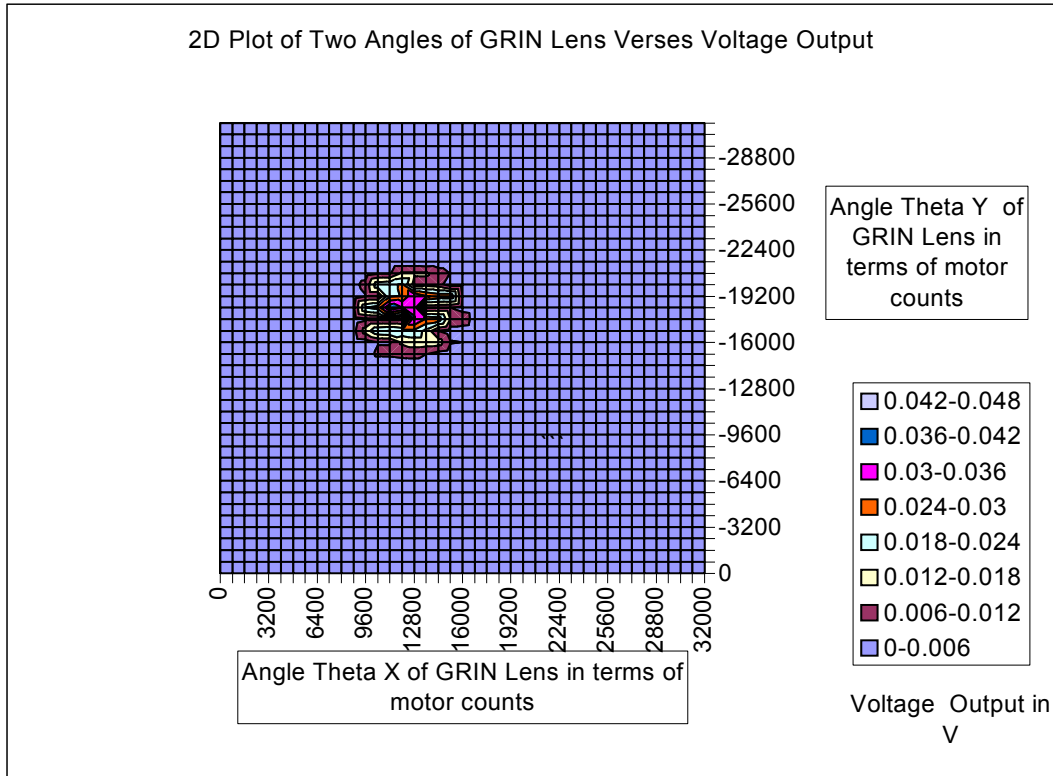


Figure 28: 2D Plot at 65mm Fizeau Cavity

Analysis Result:

Figure 27 shows the 3D surface plot and Figure 28 shows the infringe pattern at 45mm Fizeau cavity.

Maximum Voltage = 42.2247 mV.

Motor counts for angle θ_X of GRIN lens at maximum voltage = 11200

Motor counts for angle θ_Y of GRIN lens at maximum voltage = -18400

Therefore, the angles θ_X and θ_Y of GRIN lens is moved to absolute coordinate 11200 and -18400 respectively of the motor counts of tip/tilt stage after the program stopped running for final alignment. This results in perfect alignment of the GRIN lens with respect to the silicon wafer.

Case 3: Distance between the GRIN lens and the silicon wafer is approximately 100mm.

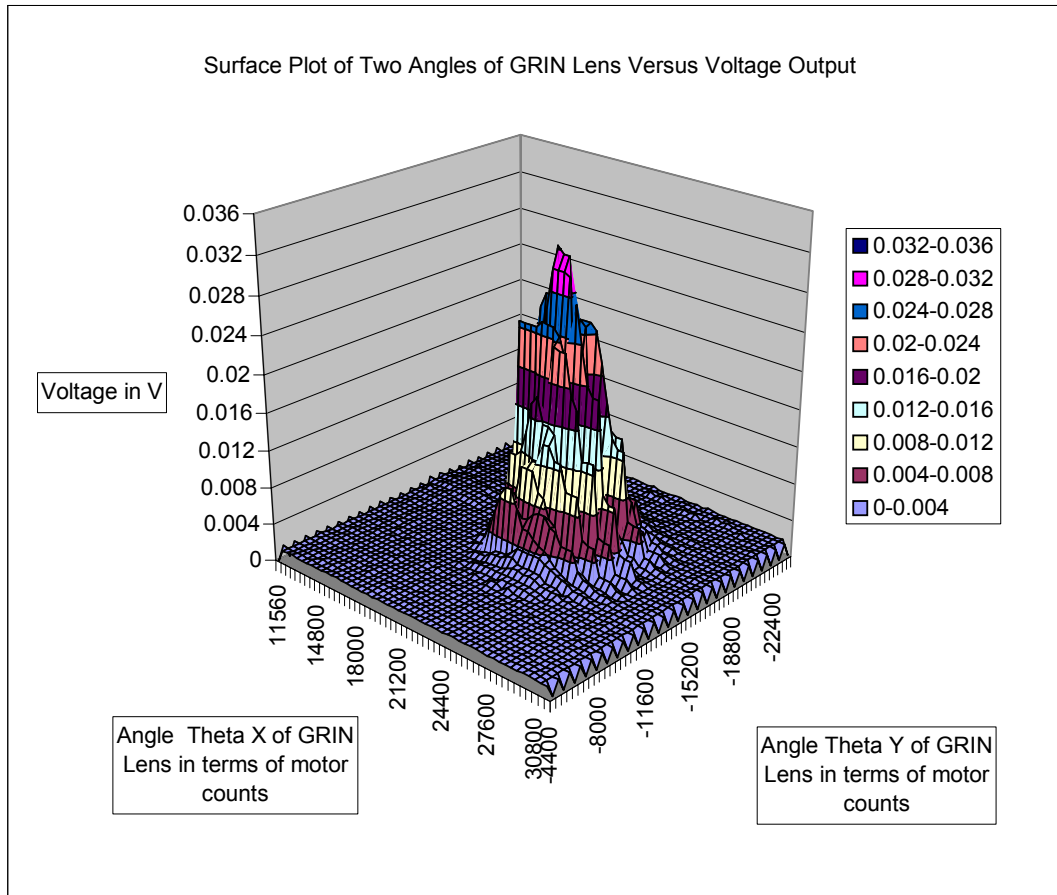


Figure 29: Surface Plot at 100mm Fizeau Cavity

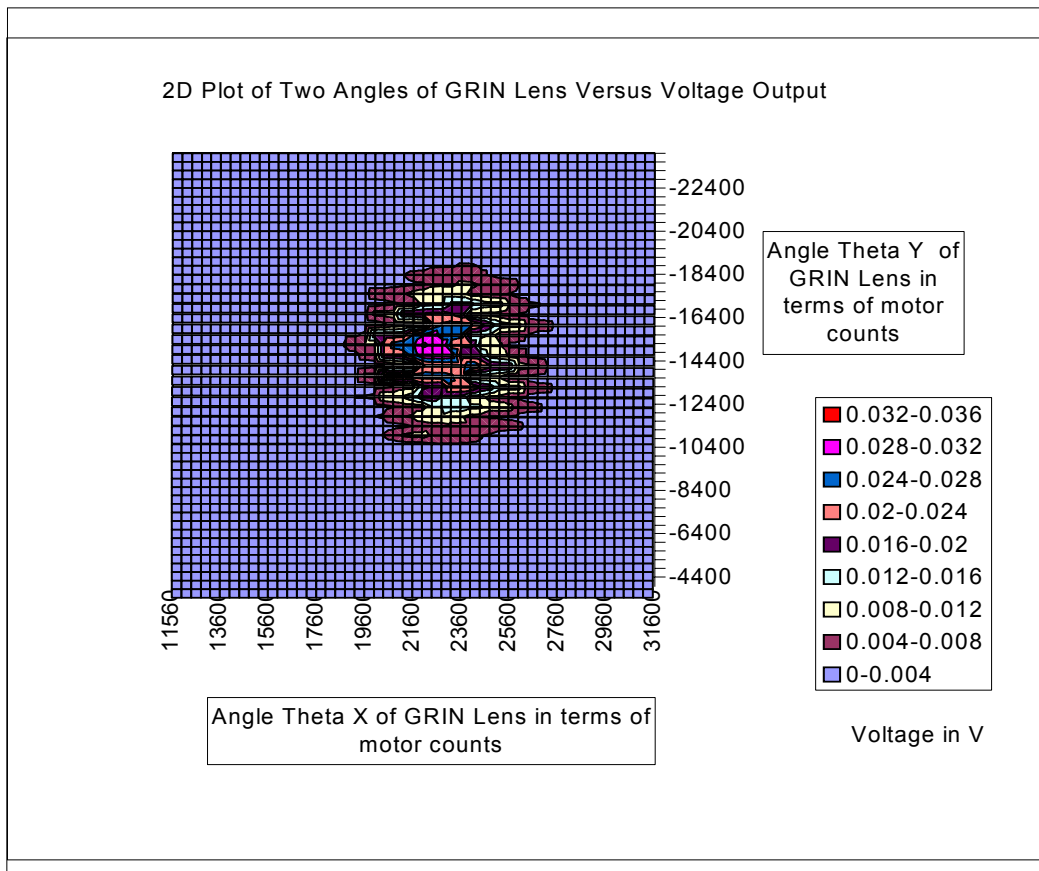


Figure 30: 2D Plot at 100mm Fizeau Cavity

Analysis Result:

Figure 29 shows the 3D surface plot and Figure 30 shows the infringe pattern at 45mm Fizeau cavity

Maximum Voltage = 32.313 mV.

Motor counts for angle θ_x of GRIN lens at maximum voltage = 22000

Motor counts for angle θ_y of GRIN lens at maximum voltage = -15600

Therefore, the angles θ_x and θ_y of GRIN lens is moved to absolute coordinate 22000 and -15600 respectively of the motor counts of tip/tilt stage after the program stopped running

for final alignment. This results in perfect alignment of the GRIN lens with respect to the silicon wafer.

Results for Fine Alignment - Improved Method

The LABVIEW program was further improved to achieve better resolution and scanning path and less execution time as described in Section 3.3.4. The experiment was carried out using a silicon wafer as the specimen. LABVIEW generated 3D waterfall plots and 2D fringe plots by plotting photodiode voltages as functions of the two GRIN lens angles (relative angular positions with reference to the home positions). Studies were done at various standoff distances ranging from 45mm to 200mm. The same program is run several different times at a particular Fizeau cavity, keeping all other variables constant. This was pursued to study the repeatability of the new design system. The capability of the setup was also evaluated using a steel plate as the specimen.

Various Stand-off Distances

As previously discussed, the standoff distance plays a vital role in the alignment of the GRIN lens with the specimen. Thus, one of the biggest challenges of the research is to validate the results for different Fizeau cavity values.

Case 1: Fizeau Cavity: 45mm

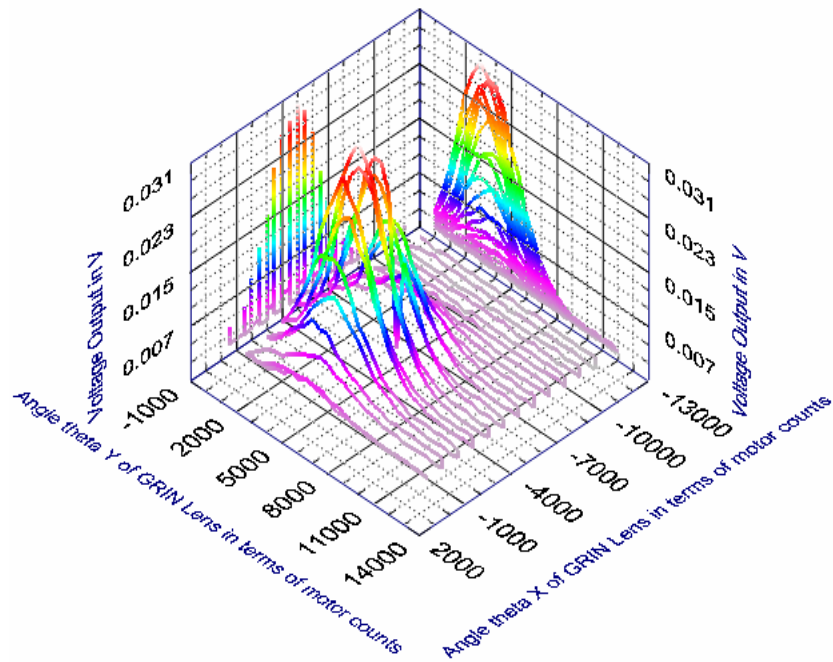


Figure 31: 3D Waterfall Plot at 45mm Standoff

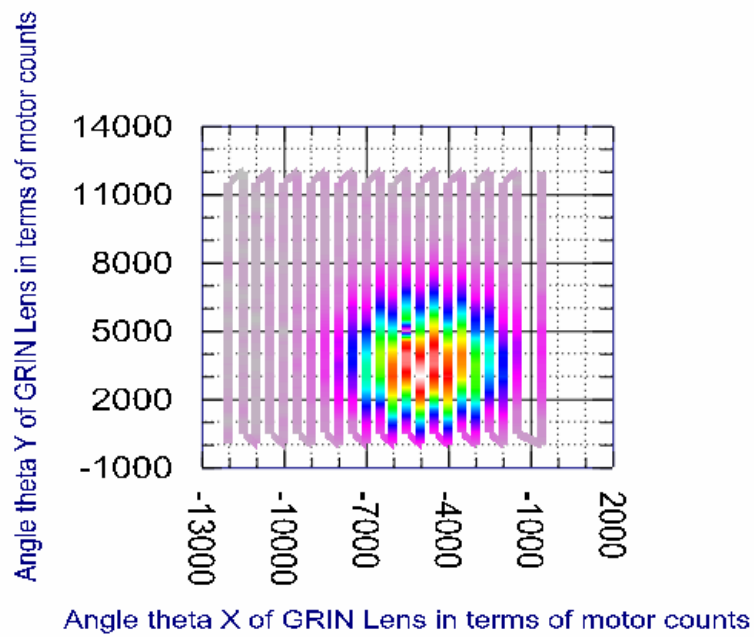


Figure 32: Top View Plot at 45mm Standoff

Case 2: Fizeau Cavity: 65mm

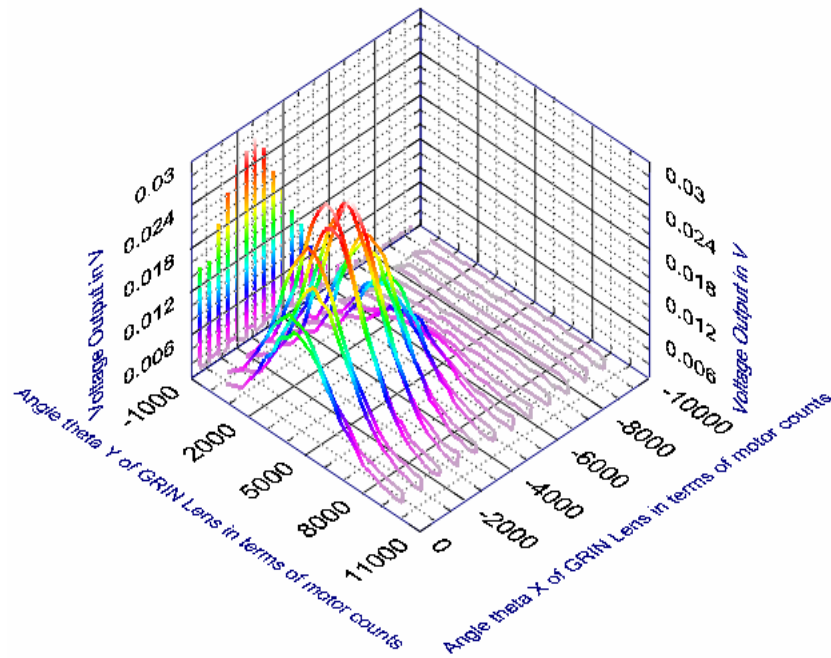


Figure 33: 3D Waterfall Plot at 65mm Standoff

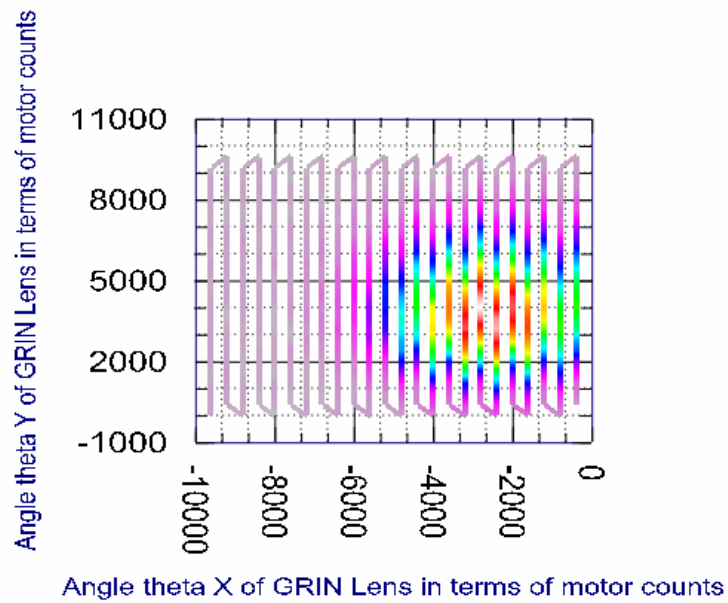


Figure 34: Top View Plot at 65mm Standoff

Case 3: Fizeau Cavity: 90mm

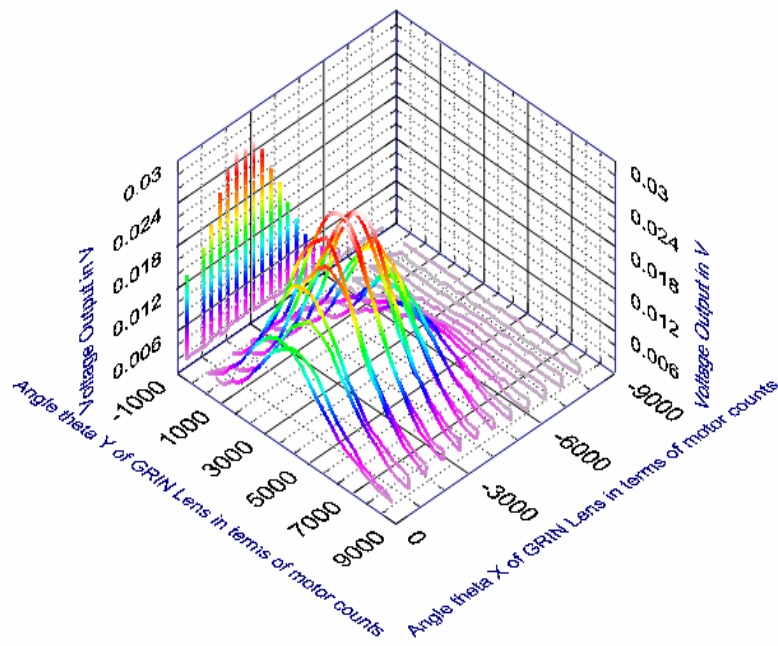


Figure 35: 3D Waterfall Plot at 90mm Standoff

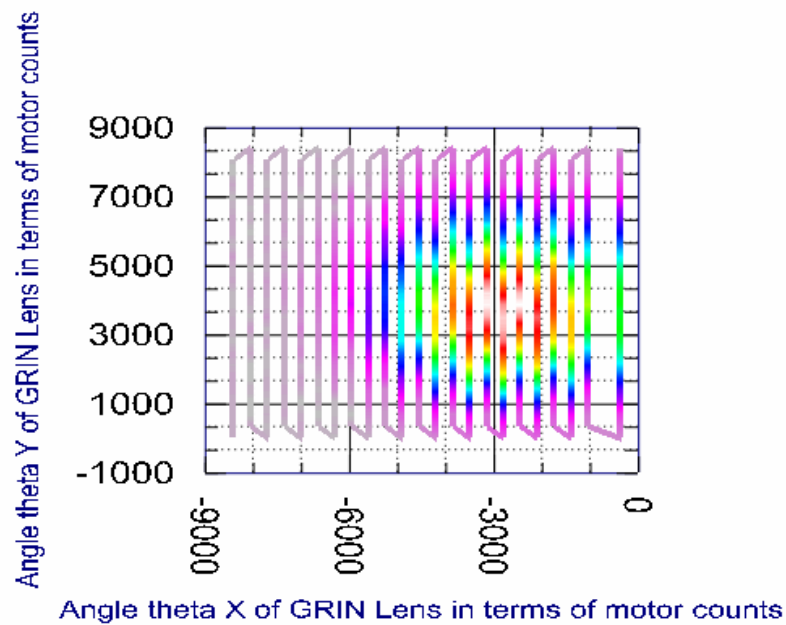


Figure 36: Top View Plot at 90mm Standoff

Case 4: Fizeau Cavity: 110mm

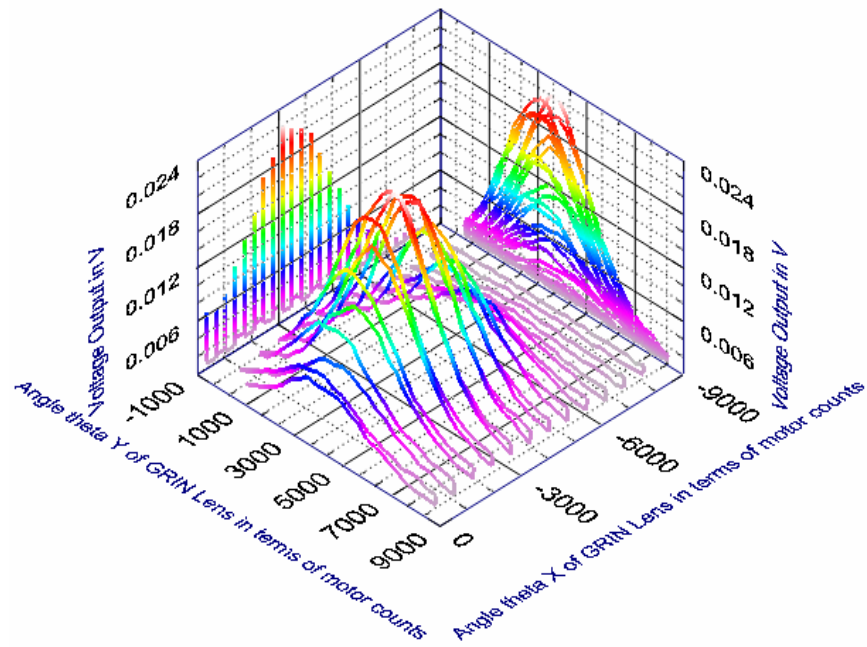


Figure 37: 3D Waterfall Plot at 110mm Standoff

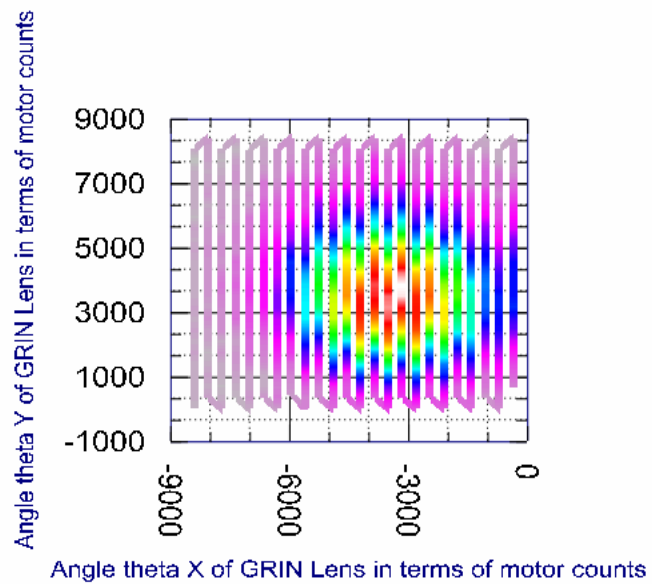


Figure 38: Top View Plot at 110mm Standoff

Case 5: Fizeau Cavity: 130mm

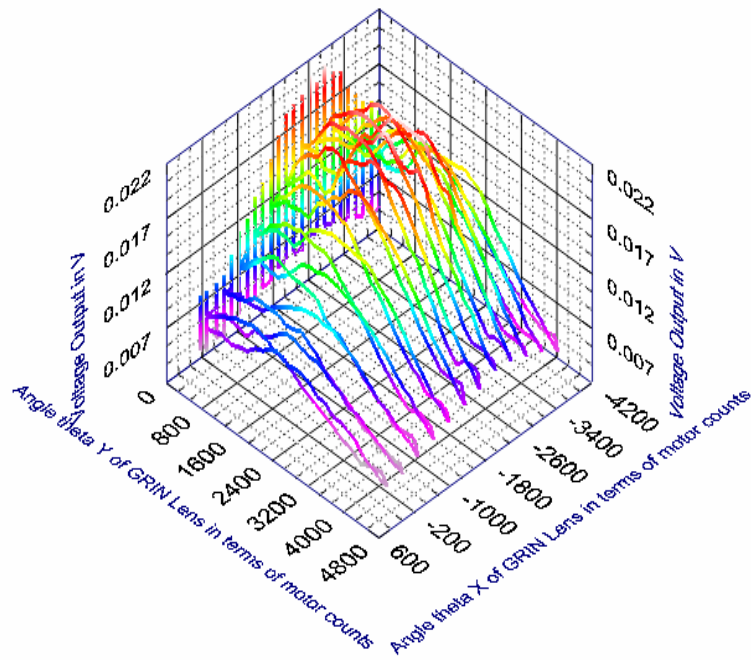


Figure 39: 3D Waterfall Plot at 130mm Standoff

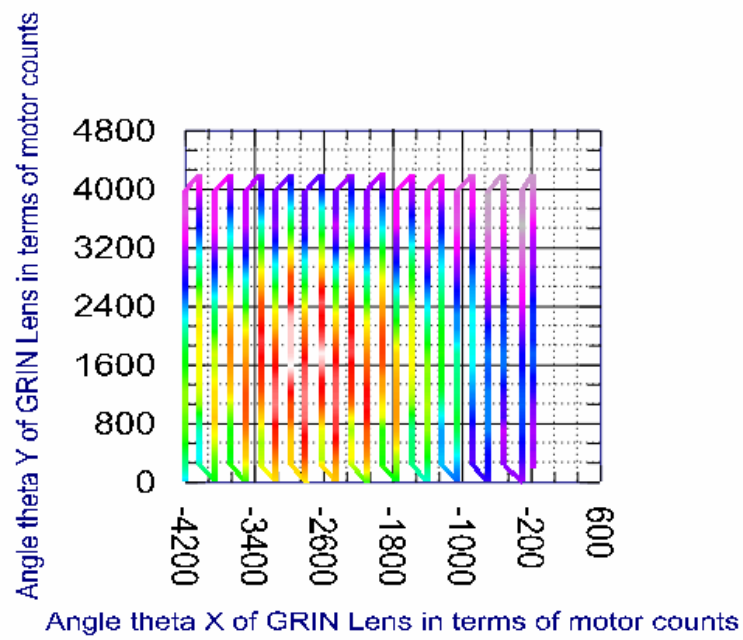


Figure 40: Top View Plot at 130mm Standoff

Case 6: Fizeau Cavity: 140mm

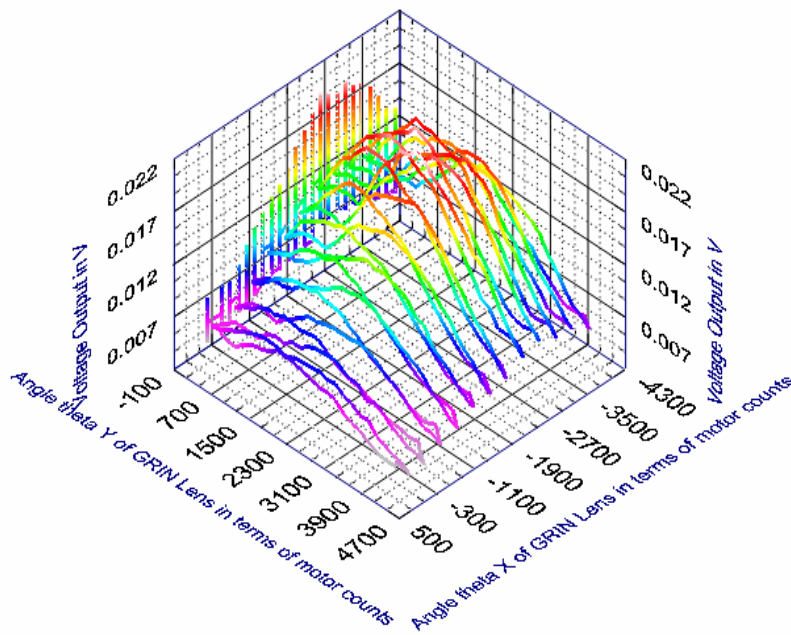


Figure 41: 3D Waterfall Plot at 140mm Standoff

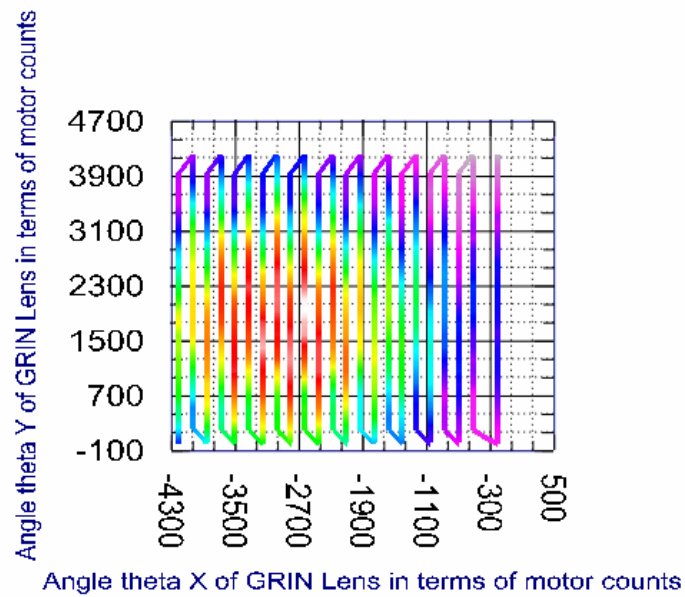


Figure 42: Top View Plot at 140mm Standoff

Case 7: Fizeau Cavity: 160mm

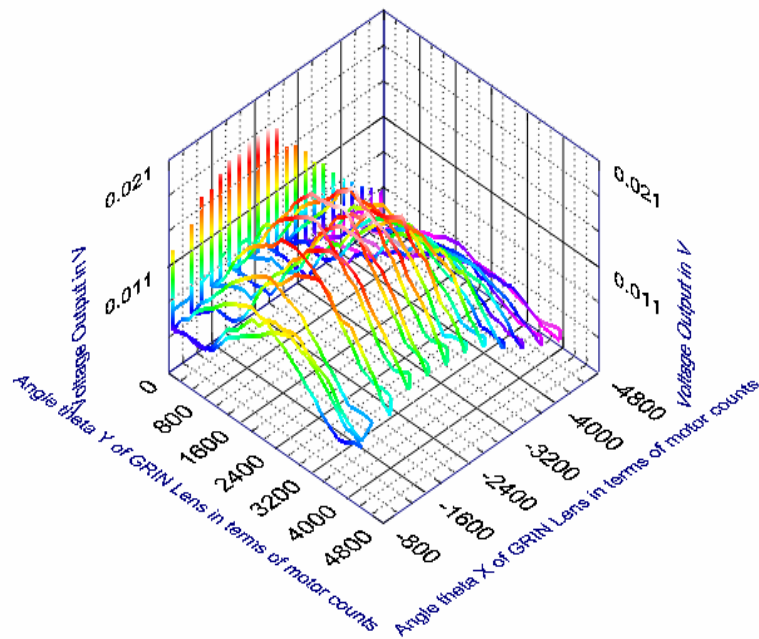


Figure 43: 3D Waterfall Plot at 160mm Standoff

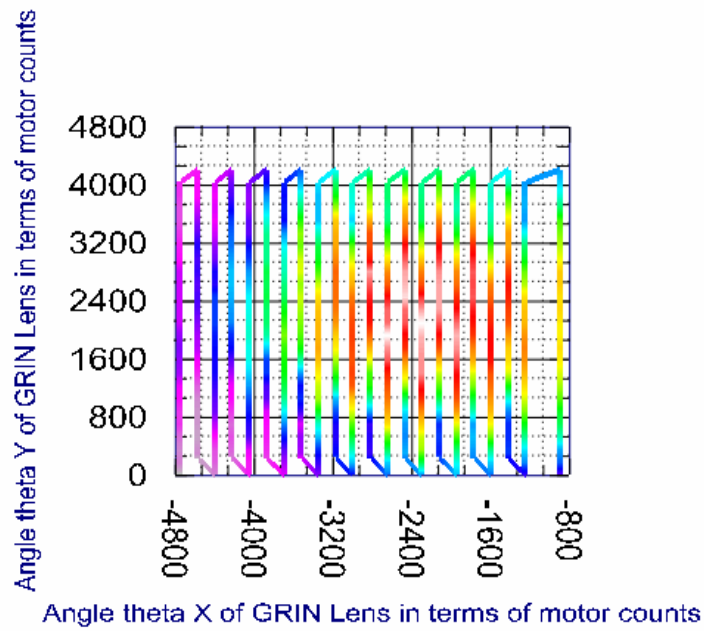


Figure 44: Top View Plot at 160mm Standoff

Case 8: Fizeau Cavity: 180mm

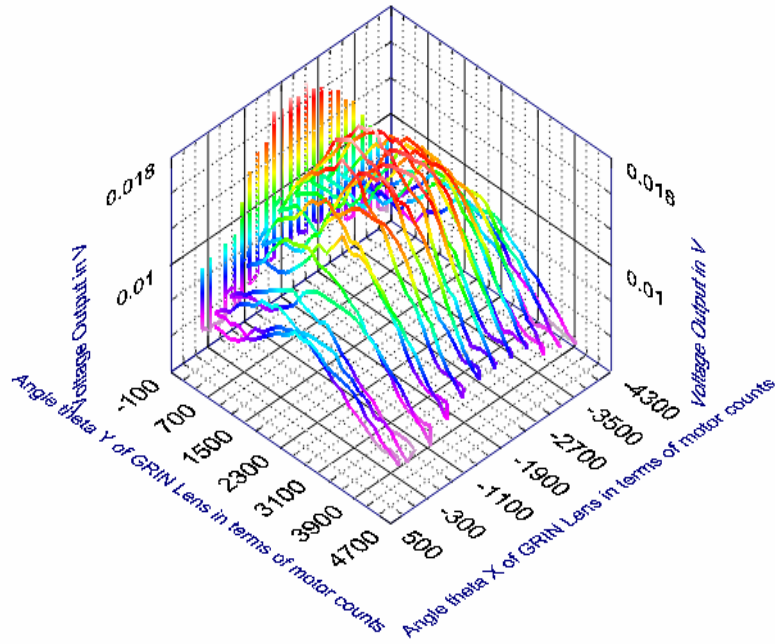


Figure 45: 3D Waterfall Plot at 180mm Standoff

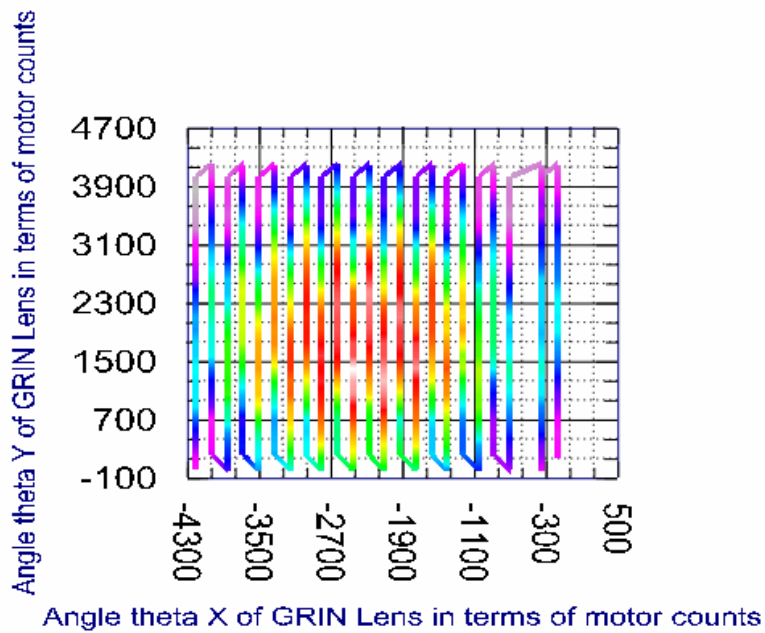


Figure 46: Top View Plot at 180mm Standoff

Case 9: Fizeau Cavity: 200mm

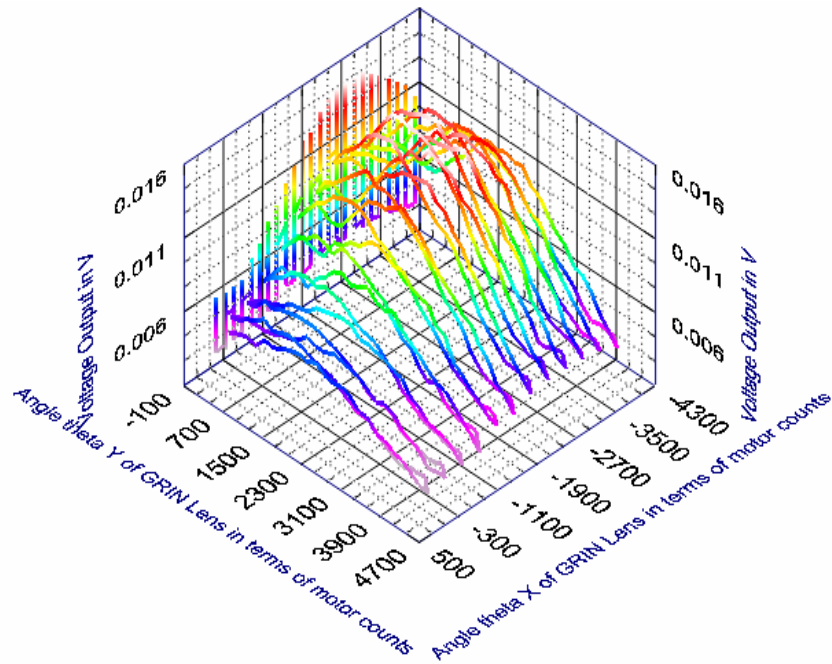


Figure 47: 3D Waterfall Plot at 200mm Standoff

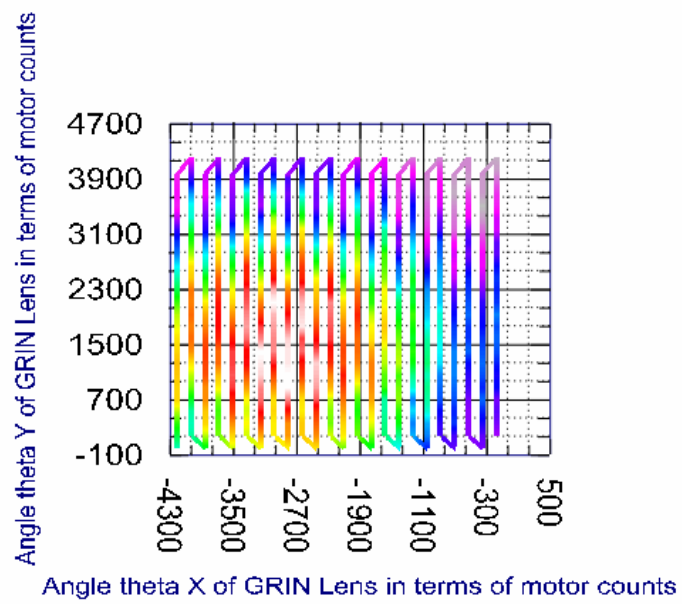


Figure 48: Top View Plot at 200mm Standoff

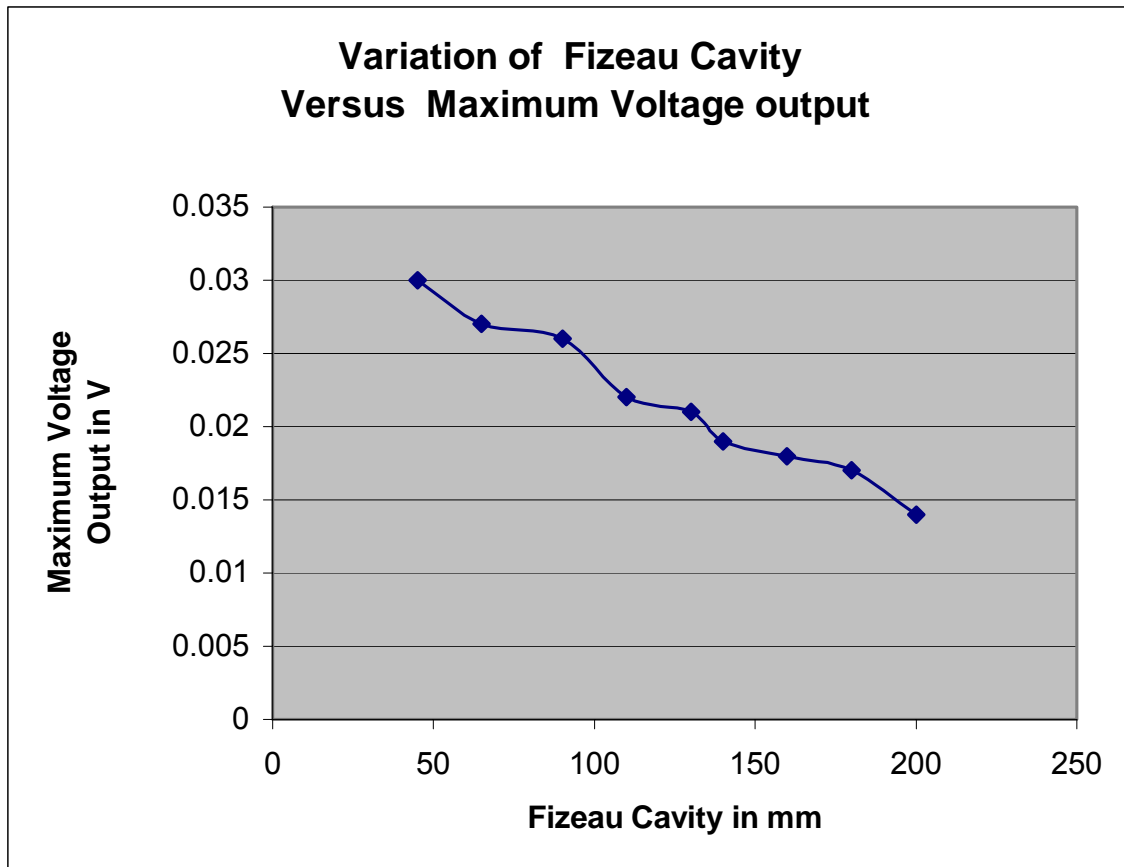
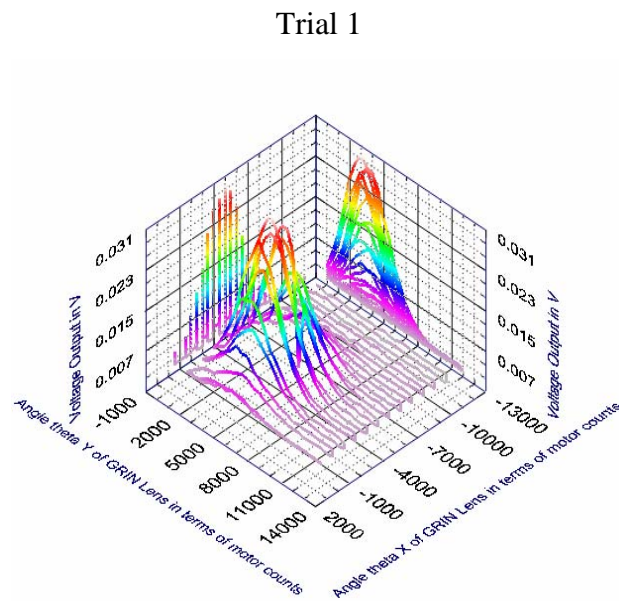


Figure 49: Graph of Fizeau Cavity Versus Maximum Voltage Output in the Photo-Detector

Using the results shown in Figure 31 to Figure 48, a graph was plotted showing the maximum voltage output captured by the LABVIEW program at various standoff distances (Fizeau cavity). This is shown in Figure 49. It can be seen that the maximum voltage drops steadily with increasing Fizeau cavity length as expected. It was found that the output voltage of the photodiode is less than 1.7mV when there is no interference between the reference beam and the object beam and that a voltage reading of more than 2.5mV is good enough to resolve out-of-plane displacement in the specimen. The higher the voltage reading, the better the signal-to-noise ratio as expected.

Repeatability Test

To study the repeatability of the results of the new automated alignment system design, the eight trials were made of the fine alignment LABVIEW program, keeping the stand-off distance at 45mm and using the same equipment and technique for data recording. Plots in Figure 50 to Figure 57 show the output from the LABVIEW program for each trial.



Trial 1

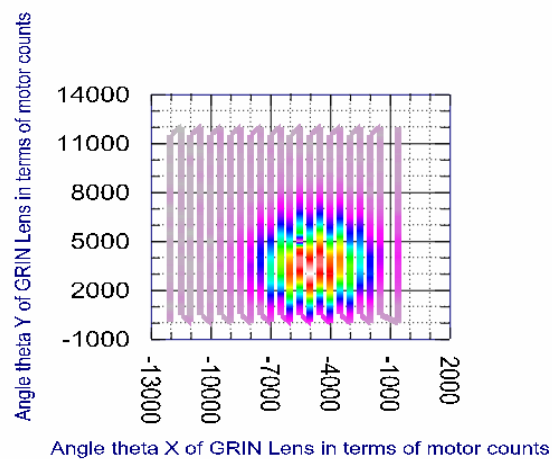
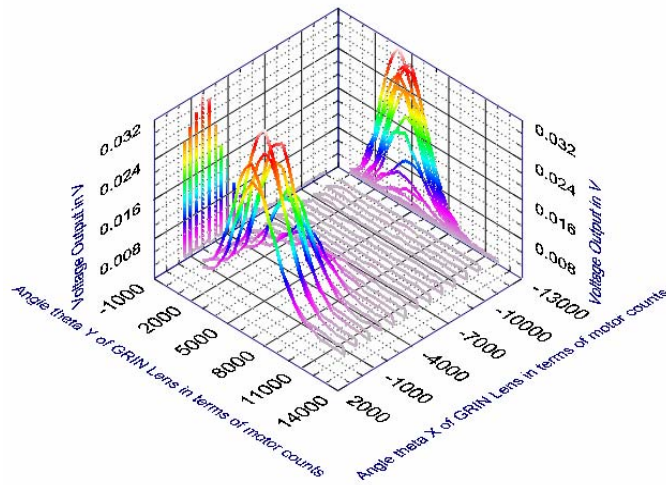


Figure 50: Data Plots for Trial 1; 45mm Fizeau Cavity

Trial 2



Trial 2

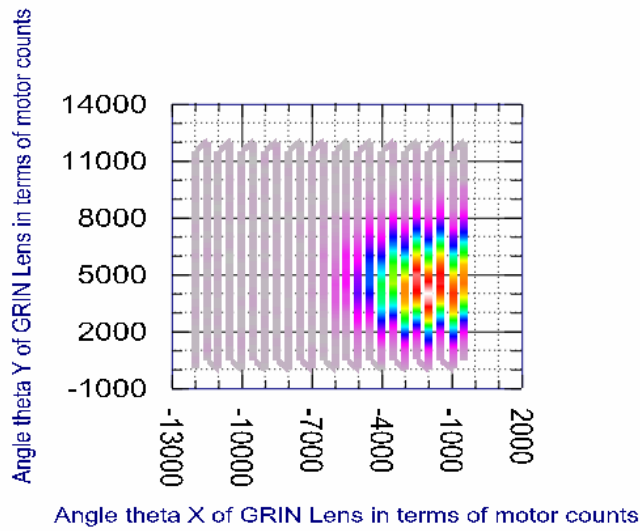
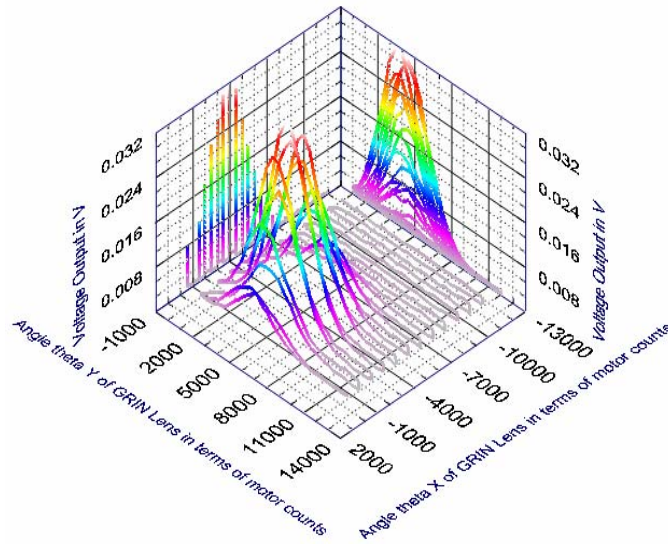


Figure 51: Data Plots for Trial 2; 45mm Fizeau Cavity

Trial 3



Trial 3

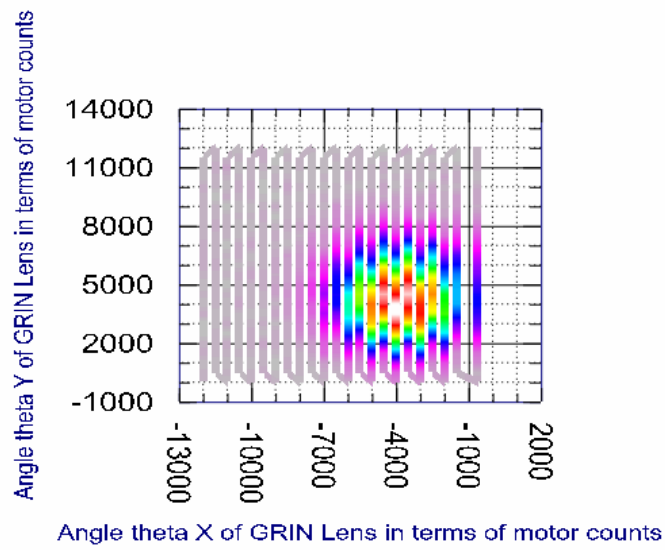
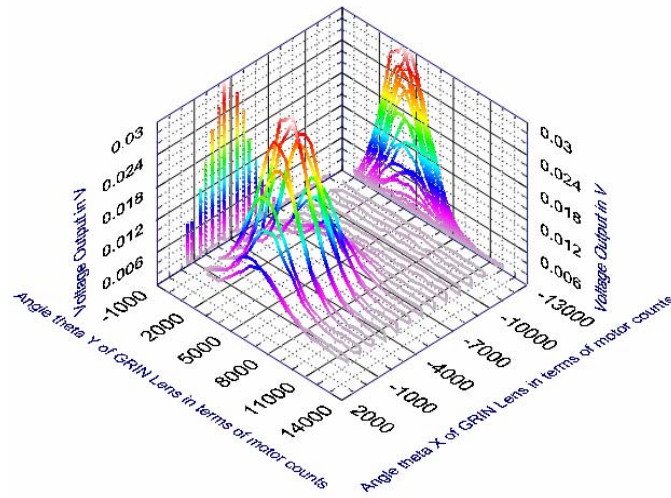


Figure 52: Data Plots for Trial 3; 45mm Fizeau Cavity

Trial 4



Trial 4

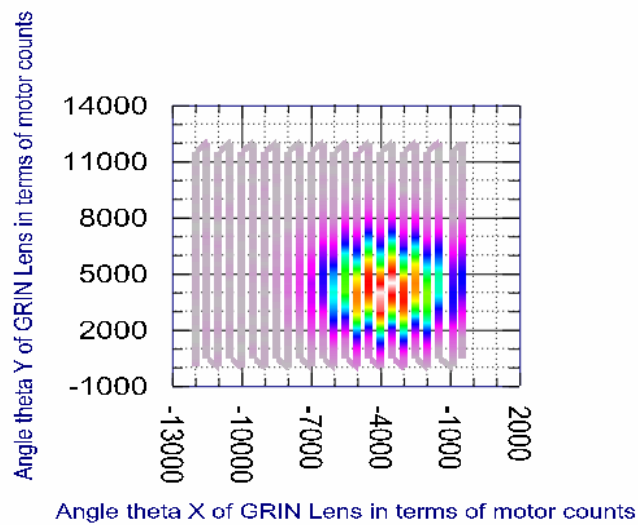
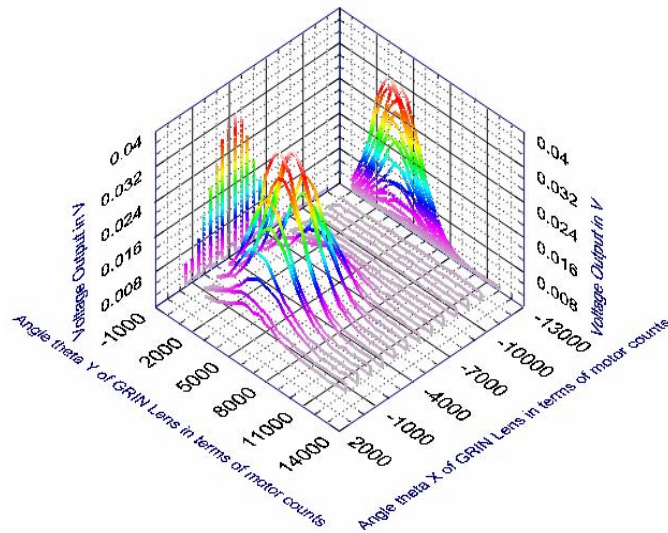


Figure 53: Data Plots for Trial 4; 45mm Fizeau Cavity

Trial 5



Trial 5

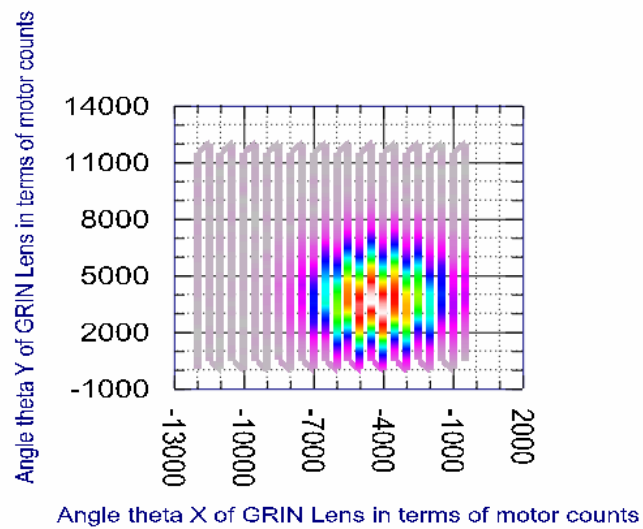
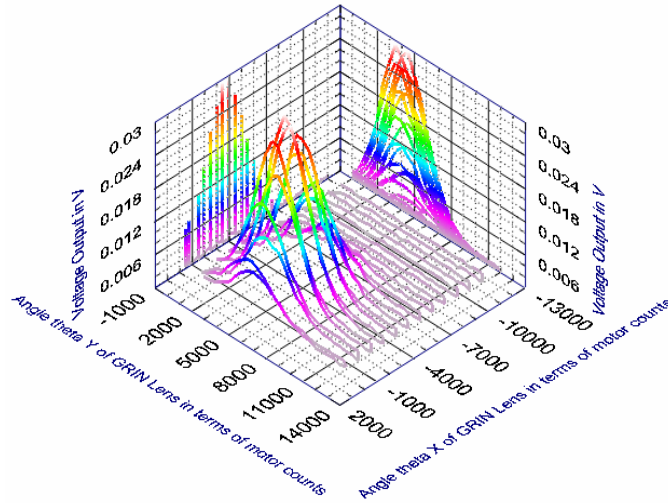


Figure 54: Data Plots for Trial 5; 45mm Fizeau Cavity

Trial 6



Trial 6

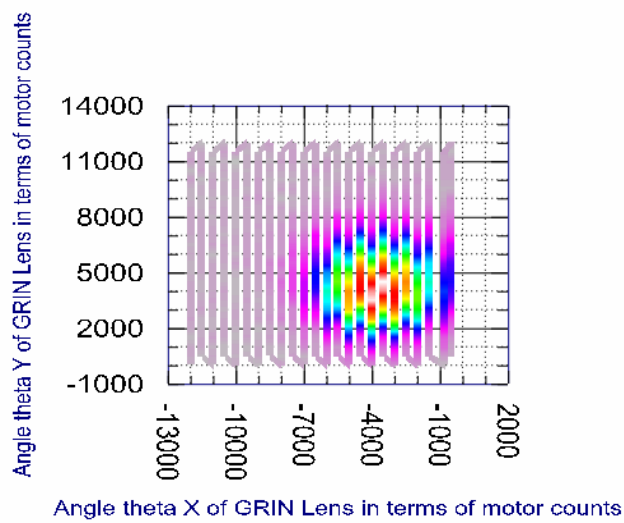
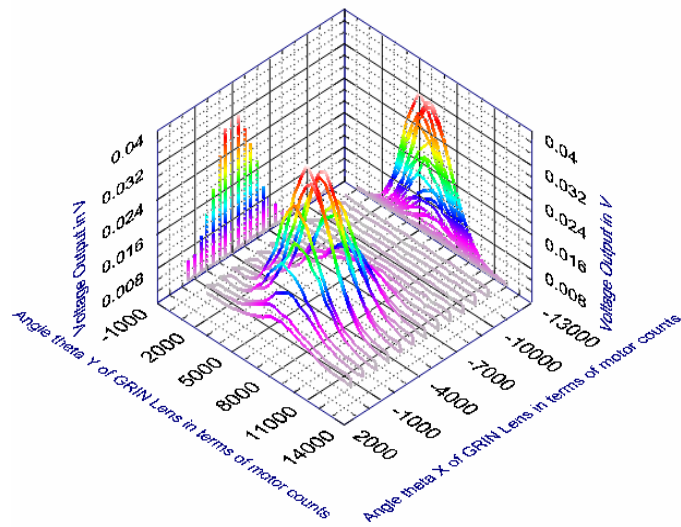


Figure 55: Data Plots for Trial 6; 45mm Fizeau Cavity

Trial 7



Trial 7

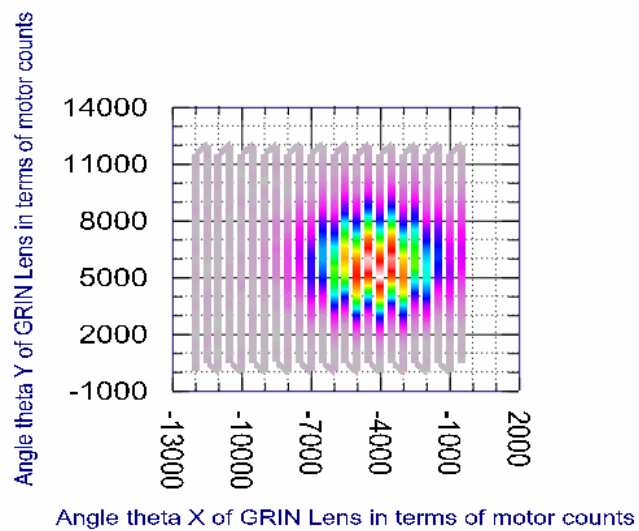
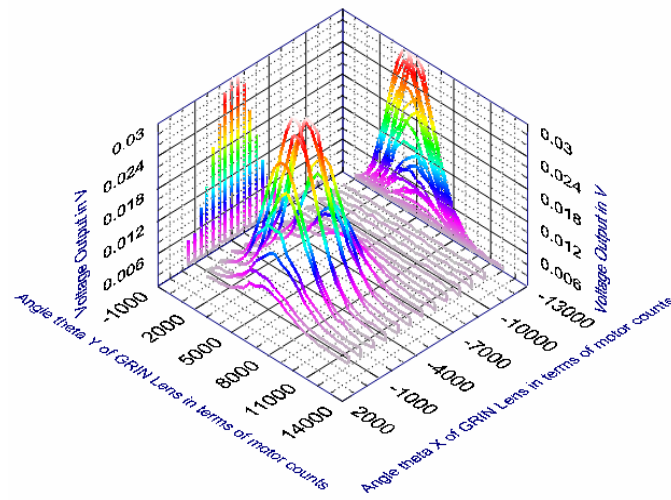


Figure 56: Data Plots for Trial 7; 45mm Fizeau Cavity

Trial 8



Trial 8

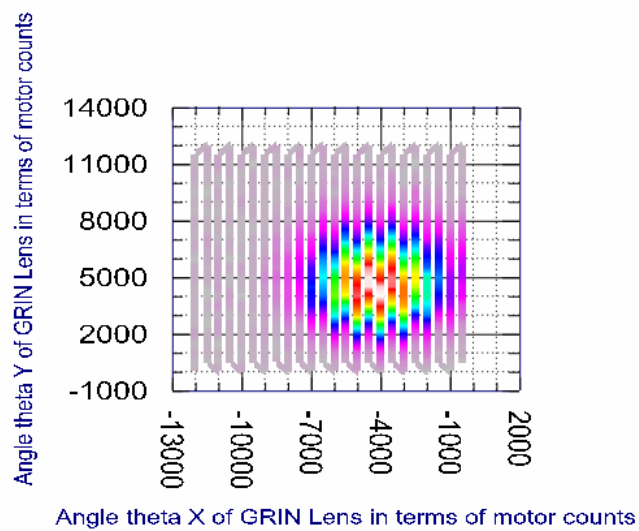


Figure 57: Data Plots for Trial 8; 45mm Fizeau Cavity

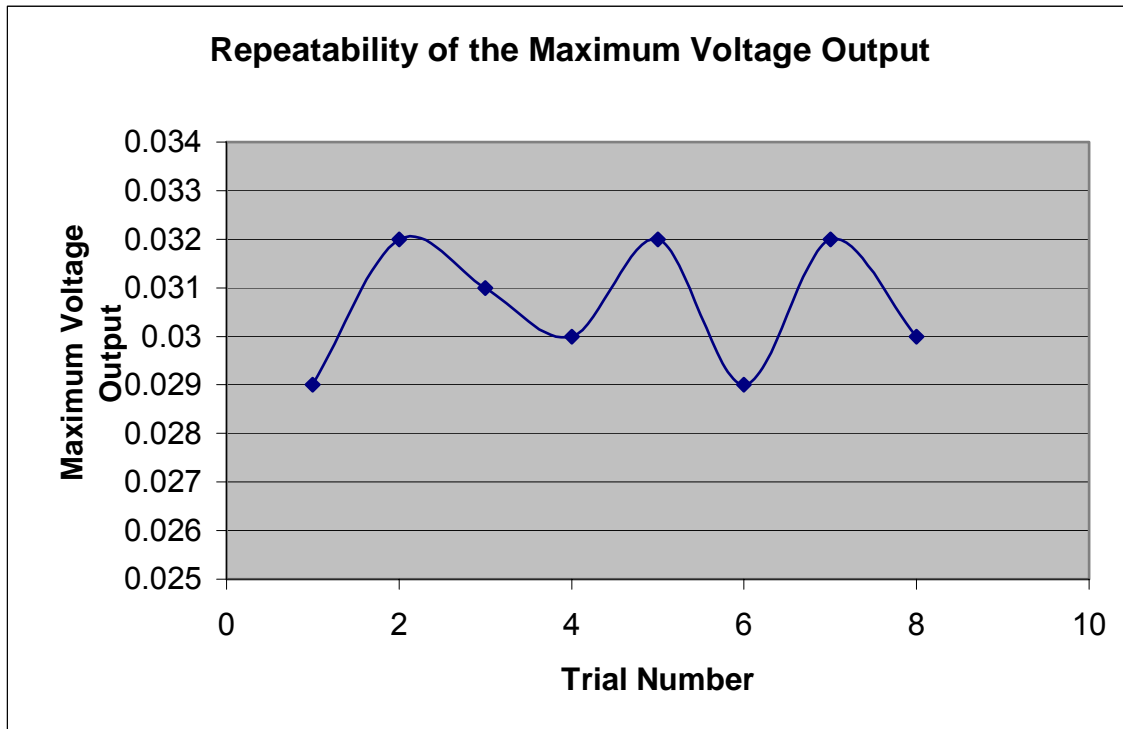


Figure 58: Graph of Maximum Voltage Output Read at the Photo-Detector Versus Trial Number

The repeatability of the new automated design was studied and confirmed by running the fine alignment LABVIEW program eight different times at the same 45mm standoff distance. The maximum voltage output of all the eight program executions are plotted in the Y-axis with the experiment number as the X-axis. It can be seen from Figure 58 that the maximum voltage varies from 29mV to 32mV, which is quite satisfactory as it is difficult to attain such precision with manual alignment.

Design verification was conducted by using a steel plate specimen whose reflectivity is relatively low compared to the highly polished silicon wafers. A maximum voltage output of 3mV was captured by the LABVIEW program as shown in Figure 59, which is considered satisfactory. However, this result clearly shows that materials of poor reflectivity could result in lower output voltages. Thus, the reflectivity of the specimen material is an important parameter for implementation of this kind of alignment system.

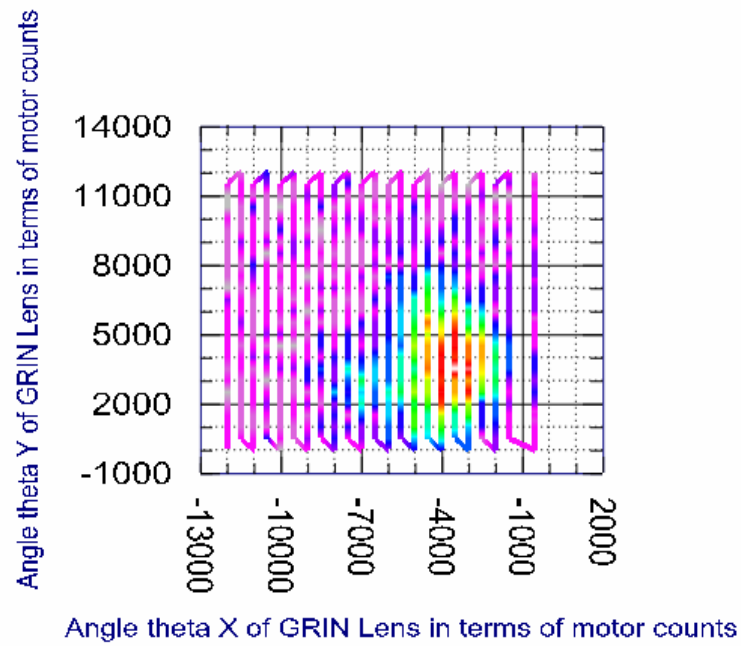
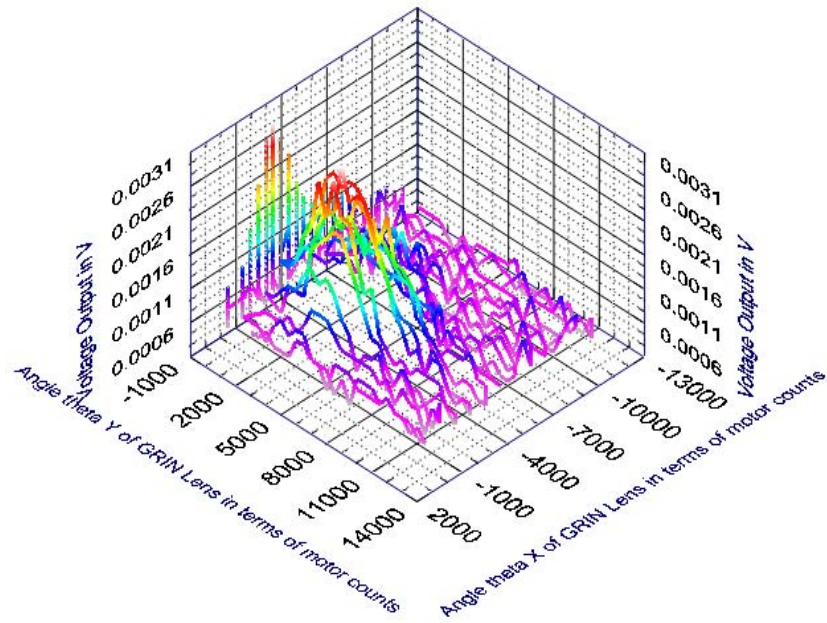


Figure 59: 3D Waterfall and Infringe Plots for Steel Material

Conclusions of Chapter V

The effectiveness of the automated FTI alignment system was evaluated using the current sensors to optimize the level of contrast in the interference pattern. The results for both the coarse and fine alignment were analyzed and the performance of the FTI during various trials with large standoff distances was validated. High precision alignment was achieved by the improved LABVIEW program and can be further enhanced by increasing the number of loops in the program (with a longer execution time). The repeatability of the alignment procedure was also found to be very promising. The proficiency of the automated FTI alignment system applied to specimens other than silicon wafers was also investigated and presented.

CHAPTER VI

CONCLUSIONS AND RECOMMENDATIONS FOR FUTURE WORK

This chapter summarizes the inferences drawn regarding the design, construction and validation of performance of the automated FTI alignment system developed to meet the research objectives of the thesis. A discussion of the applications for which the automated FTI system is appropriate and the impact of the research work is included. Suggestions for future work to improve the overall performance of the alignment system are also made.

Conclusions

In this thesis, the need for automating the alignment of fiber-tip interferometers to achieve optimized interference intensity at various standoff distances between the specimen and the GRIN lens was addressed. The design, construction, and successful implementation of a novel, automated, fiber-tip-interferometer alignment system was presented.

The initial concept of employing a photocell was replaced by the idea of using a highly sensitive and accurate position sensing device for coarse alignment, thus rendering the system more compact and reliable as the tip/tilt angles of the GRIN lens were mapped with the voltage outputs from the PSD. The PSD was able to detect a laser beam spot size of 200 μm in diameter and the voltage outputs were mapped to $\pm 7\text{V}$ along the two orthogonal axes of an active photosensitive area of 22 x 22 mm^2 .

The entire automated alignment procedure of the FTI system is divided into two sequential steps. Alignment starts with a coarse alignment procedure that is fast and relatively inaccurate but results in positioning the GRIN lens close to the desired position.

It takes about 30 sec to run the coarse alignment. A LABVIEW program is executed after the coarse alignment of the GRIN lens. At this position the voltage output captured in the photodiode would be less than 1mV. This LABVIEW program initially sets the GRIN lens at the position where significant voltage output from the photo-detector is achieved. For example, the first highest voltage of 10.22mV was achieved after scanning 170 different angles of the GRIN lens at a 90mm standoff distance. This was followed by the LABVIEW program that generates voltage output at 576 points in a very small micrometer square area and the maximum voltage output of 26mV was found for the 90mm standoff distance. Thus, the alignment procedure is accurate, precise and in the range of nanometers. The system can be made finer and more precise by simply increasing the number of loops executed within the program. The alignment requires only approximate measurement (within a $\pm 2.5\text{mm}$ tolerance) of the distance between the GRIN lens and the silicon wafer specimen. The total execution time of the LABVIEW program for fine alignment was 2 minutes and 35 seconds. Larger the numbers of loops would require a longer execution time.

Experimental alignment results were recorded at nine different standoff distances between the GRIN lens and the silicon wafer. The voltage output from the photodiode was found to be directly proportional to the interference between the object beam and the reference beam inside the GRIN lens. Experimentally, an average voltage output of 2.5mV was found to be satisfactory for sensing surface propagating waves. Therefore, an average voltage output of 14mV at a 200mm standoff distance would definitely be considered suitable as the input for subsequent data analysis and feature extraction using wavelets and instantaneous frequency. Thus, the adaptability of the PSD and LABVIEW program to both large and small standoff distances between the GRIN lens and the silicon wafer was validated. In addition, the feasibility of the design was also demonstrated.

Both the coarse and fine alignment methods are closed-loop with controlled feedback, allowing computational errors to be either reduced or eliminated. All results were quantified, thus resulting in a robust interferometer alignment system independent of the skills of the operator.

However, the primary limitation of the designed automated FTI alignment system was found to be the reflectivity of the specimen under observation. A good reflective surface like that of a silicon wafer gives better results compared to materials having poor reflectivity. However, the voltage output achieved with a steel plate that was of intermediate reflectivity was 3 mV, which was still satisfactory. Despite this limitation, the design is still capable of many significant applications. The GRIN lens alignment can be achieved from a remote location sufficiently away from the physical setup. Thus, it is very useful for various industrial applications where close-in positioning of the FTI is not possible. In summary, the innovative automated aligning system is a much more precise, compact, reliable and accurate method of sensing dynamic out-of-plane displacement for the TAP-NDE technology.

Impact

With the innovation of the automated alignment system, the TAP-NDE technology is getting new directions. Till now capabilities of the TAP-NDE were restricted to the research laboratory environment. But with this compact, reliable and accurate alignment system, this lab tool can be moved to various industrial applications involving material characterization, defect detection, or other applications.

This automated system will have great impact on the semiconductor manufacturing industry. Such industry requires very high level of cleanliness and this automated detection system can maintain their working environment contamination-free. Moreover, its capability of optimizing the level of contrast for the interferometer at large standoff distances will have great significance in measuring the temperature distribution in silicon wafers undergoing thermal annealing where the wafer temperature could easily reach 1000⁰C. Thus, the automated FTI alignment system will have great impact on future non-destructive techniques in both research and industrial applications.

Future Work

Now that the functionality of the design has been experimentally demonstrated, as well as validated, the next logical step is to modify the system to achieve better results. There are many areas that can be improved upon to enhance the automated FTI system. The biggest single problem is the execution time of the LABVIEW program. In order to reduce the execution time of the system in achieving the desired alignment, another algorithm should be introduced that can locate the desired angles of the GRIN lens in fewer steps with the same level of, or better, precision. Also, the present PSD should be replaced with a PSD with a hole, to improve the compactness of the whole FTI system. This would greatly improve and simplify the coarse alignment procedure.

This automated FTI alignment system targets the alignment of only a flat specimen such as a silicon wafer. Thus, for specimens such as cylindrical pipes, a different, but similar, alignment approach would be desired. These improvements would allow the automated system to become a truly compact, versatile and adaptable tool for aligning the GRIN lens for optimizing the level of FTI output and interferometric contrast.

REFERENCES

- [1] E. Hecht, "*Optics*," Third Edition, Reading, MA, Addison Wesley Longman, Inc., pp. 398-403, 1998.
- [2] N. A. Schumacher, "Fiber tip interferometry for non-contact ultrasonic NDE," M.S. thesis, Department of Mechanical Engineering, Texas A&M University, College Station, Aug 1990.
- [3] J. Monchalin, "Optical detection of ultrasound at a distance by laser interferometry," *11th World Conference on Nondestructive Testing, American Society of NDT*, Columbus, OH, pp. 1017-1024, 1985.
- [4] C. A. Sciammarella, M. A. Asmadshani, and B. Subbaraman, "Holographic interferometry measurement of ultrasonic vibration amplitudes," in *Proc. 1986 Spring Meeting, Society for Experimental Mechanics*, New Orleans, LA, pp. 707-710, June 1986.
- [5] C. A. Calder, and C. A. Wilcox, "Non-contact material testing using laser energy deposition and interferometry," *International Conference on Experimental Mechanics, Stress Analysis, 6th, Materials Evaluation*, Munich, Germany, pp. 86-91, January 1980.
- [6] B. B. Djordjevic and R. E. Green, "High speed capture of acoustic emission and ultrasonic transients as detected with optical laser beam probes," in *Proc. of the Ultrasonic Conference*, Grav, Austria, pp. 82-87, 1979.
- [7] R. E. Green, "Some Innovation Techniques for Nondestructive Evaluation of Materials," in *Proc. Conference Novel NDE Methods for Materials*, Dallas, TX, 15-17 Feb. 1982, *The Metallurgical Society/AIME*, pp. 131-139, 1983.
- [8] G. Birnbaum and G. S. White, "Laser techniques in NDE," Vol 7 in R S Sharpe (ed), in *Research Technique in NDT*, London: Academic Press, pp. 260-365, 1984.
- [9] C. H. Palmer, "Optical probing of acoustic emission waves," in *Proc. 23rd Conference Non-Destructive Evaluation of Materials*, Raquette Lake, NY, pp. 347-378, August 1976, New York Plenum Press.

- [10] W. K. Lee, and C. C. Davis, "Laser interferometric studies of laser-induced surface heating and deformation," *IEEE, Journal of Quantum Electronics*, QE-22 (4): pp. 569-573, April 1986.
- [11] A. Aharoni, and K. M. Jassby, "Monitoring surface properties of solids by laser based SAW time-of-flight measurements," *IEEE Trans. on Ultrasonic Ferroelectrics and Frequency Control*, UFFC-33 (3): pp. 250-256, May 1986.
- [12] R. E. Green, "Ultrasonic materials characterization," *Ultrasonic International 85*, Butterworth Scientific Ltd., pp. 11-16, 1985.
- [13] J. A. Gilbert, C. P. Burger, J. A. Smith, B. R. Peters, , T. D. Dudderar, "The detection and evaluation of ultrasonic waves using single mode optical fiber interferometry", *International Congress on Experimental Mechanics, 6th*, Portland, OR, pp. 441-448, June 6-10, 1988.
- [14] R. O. Cook and C. W. Hamm, "Fiber optic lever displacement transducer," *Application Optics*, 18(19): pp. 3230-3241, October 1979.
- [15] B. Culshaw, "Fiber optics sensing techniques," *Res. Rech. in NDT*, London: Academic Press, pp. 191-215, 1984.
- [16] B. J. Hogan, "Fiber optic sensing techniques," *Design News*, 3(1): 62-63, 1972.
- [17] J. C. Wade, P. S. Zerwekh, R. O. Claus, "Detection of acoustic emission in composites by optical fiber interferometry." in *Proc. of the 1981 IEEE Ultrasonic Symposium*, Chicago, IL, pp. 87-96, October 1981.
- [18] S. Uwaha, N. Shibata, J. Tsujiuchi, "Flexible coherent optical probe for vibrational measurements." *Optical Communications*, 23(3): pp. 407-409, 1977.
- [19] C. S. Suh, G. A. Rabroker, R. Chona, and C.P. Burger, "Thermal-acoustic-photonics for non-contact temperature measurement in silicon wafer processing." in *Proc. of SPIE*, Vol. 3783, pp.184-193, 1999.
- [20] V. Vedantham, A. Thummalapalli, B. Yang, and C. S. Suh, "Non-contact laser ultrasonic inspection for cryogenically introduced interlayer defects in epoxy-based composites," *Proc. of IMECE2002 ASME International Mechanical Engineering Congress and Exposition*, San Diego, CA, pp. 19-25 Nov 2002.

- [21] Burger, C. P., Schumacher, N. A., Duffer, C. E., and Knab, T.D., “ Fiber-Optics Techniques for Generating and Detecting Ultrasonic Waves for Quantitative NDE,” *Optics and Lasers in Engineering*, Vol. 19, pp.121-140, 1993.
- [22] K. Kishimoto, Inoue, Hirotsugu, M. Hamada, , T. Shibuya, “Time frequency analysis of dispersive waves by means of wavelet transform, *Journal of Applied Mechanics*, pp. 841-846, 1995.
- [23] C. K. Chui, *An introduction to wavelets*, San Diego, CA, Academic Press, 1992.
- [24] T. D. Dudderar, C. P. Burger, and J. A. Gilbert, “Fiber optic sensing for ultrasonic NDE,” *Journal of Nondestructive Evaluation*, 6(3), pp. 135-146, 1987.
- [25] J. A. Smith, Thermal acoustic-photonics for the generation and detection of ultrasonic waves”, M.S. thesis, Department of Mechanical Engineering, Texas A&M University, College Station, pp. 28-53, Dec 1987.
- [26] C. P. Burger, J. A. Smith, , T. D. Dudderar, J. A. Gilbert, and B. R. Peters, “The use of fiber optic interferometry to sense ultrasonic waves”, *ISA Transactions*, 28(2), pp. 51-55 , 1989.
- [27] B. R. Peters, J. A. Gilbert, and T. D. Dudderar, “The use of fiber-optics for TAP-NDE,” in *Proc. 1989 SEM Spring Conference on Experimental Mechanics*, Cambridge, MA., Society for Experimental Mechanics, pp. 794-798, May 1989.
- [28] H. J. Woltring, “Single and dual-axis lateral photo-detectors of rectangular shape,” *IEEE Transactions on Electronic Device*, vol. ED-22, pp. 581-586, 1975.
- [29] C. Narayan, A. B. Buckman, Busch-Visniac, “Position detection of multiple light beams using phase detection”, *IEEE Transactions on Instrumentation And Measurement*, Vol. 43, No.6, pp. 1688-1694, Dec 1994.

APPENDIX A

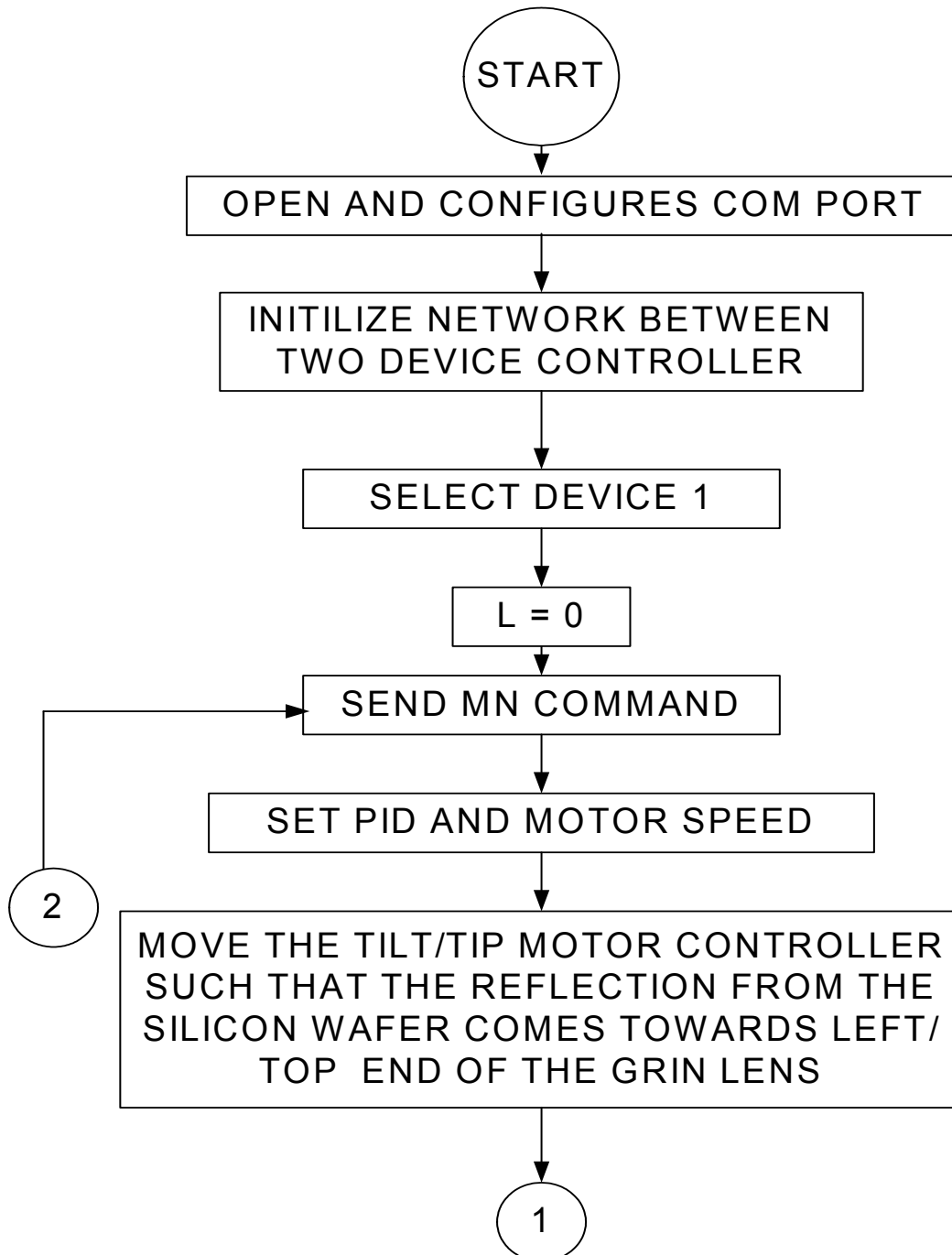
CIRCUIT DIAGRAM FOR PSD

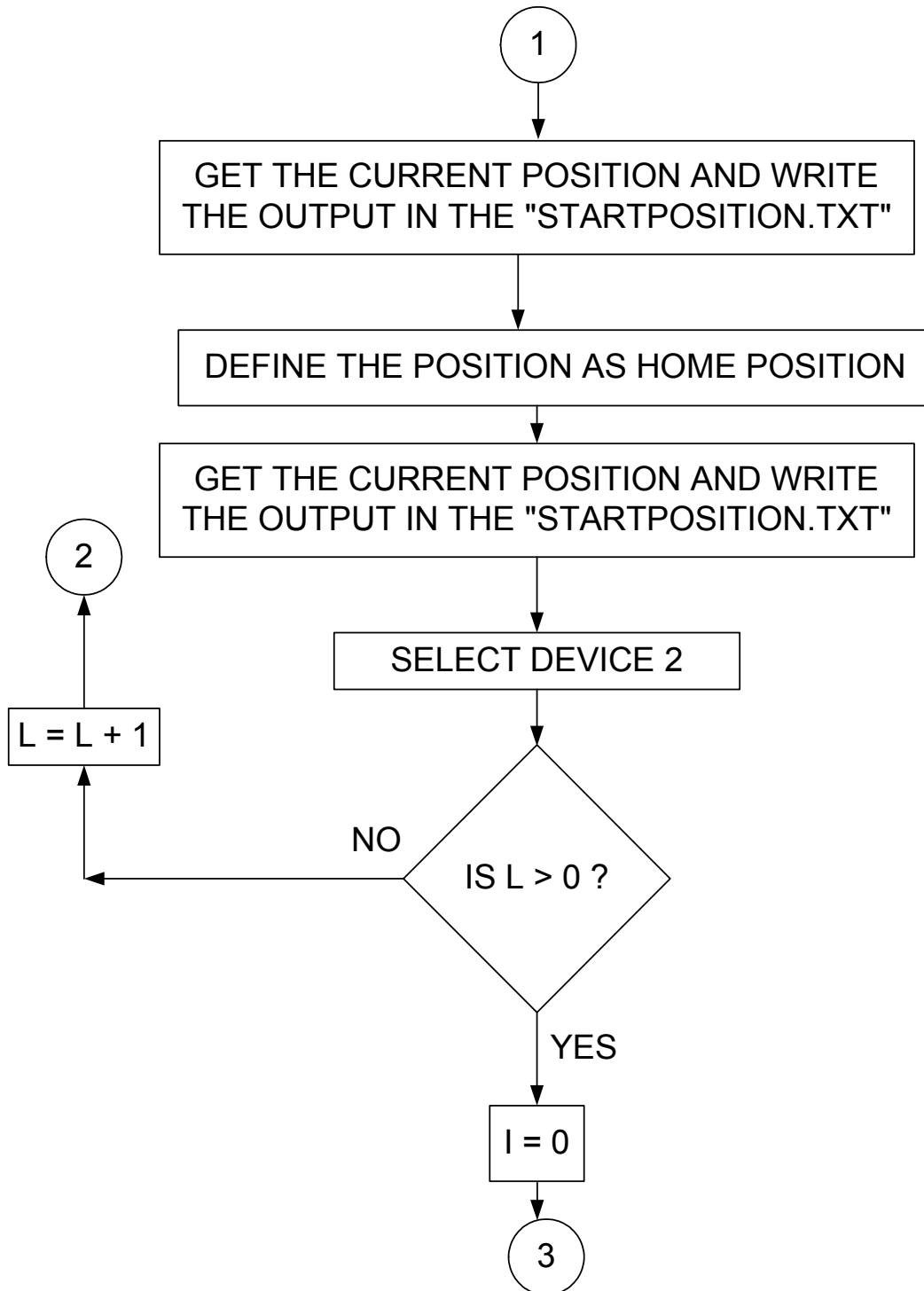
The appendix presents the wiring and circuit diagram of the 2-dimensional position sensitive detectors, 2-D PSD and the driving board C4674. The wiring leads should be as short as possible because longer leads are more susceptible to noise. The table below shows the relation between the through-hole numbers in C4674 and the output pin number of the 2-D PSD.

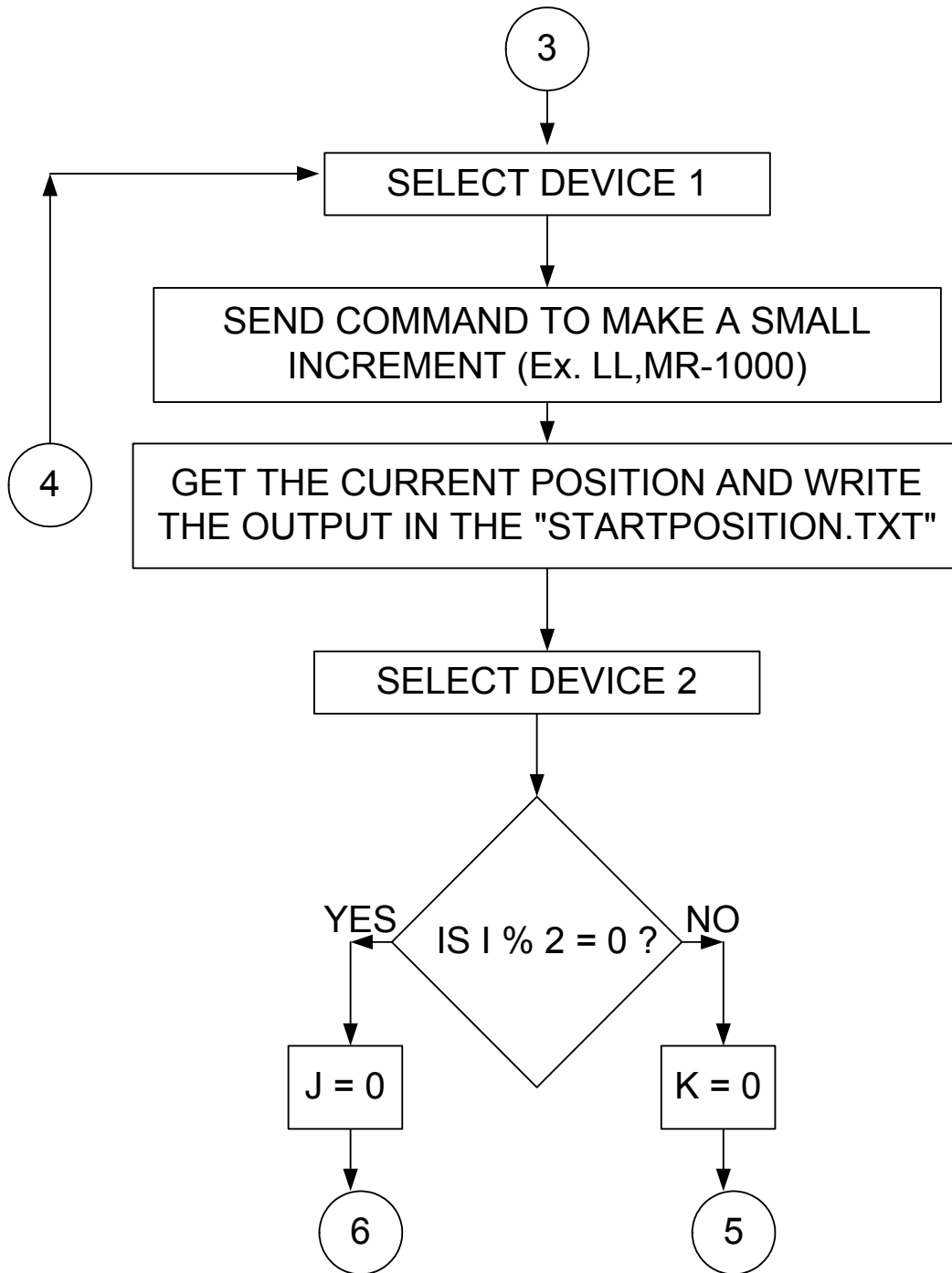
Table 6 : Wiring Connections of 2D-PSD and C4674

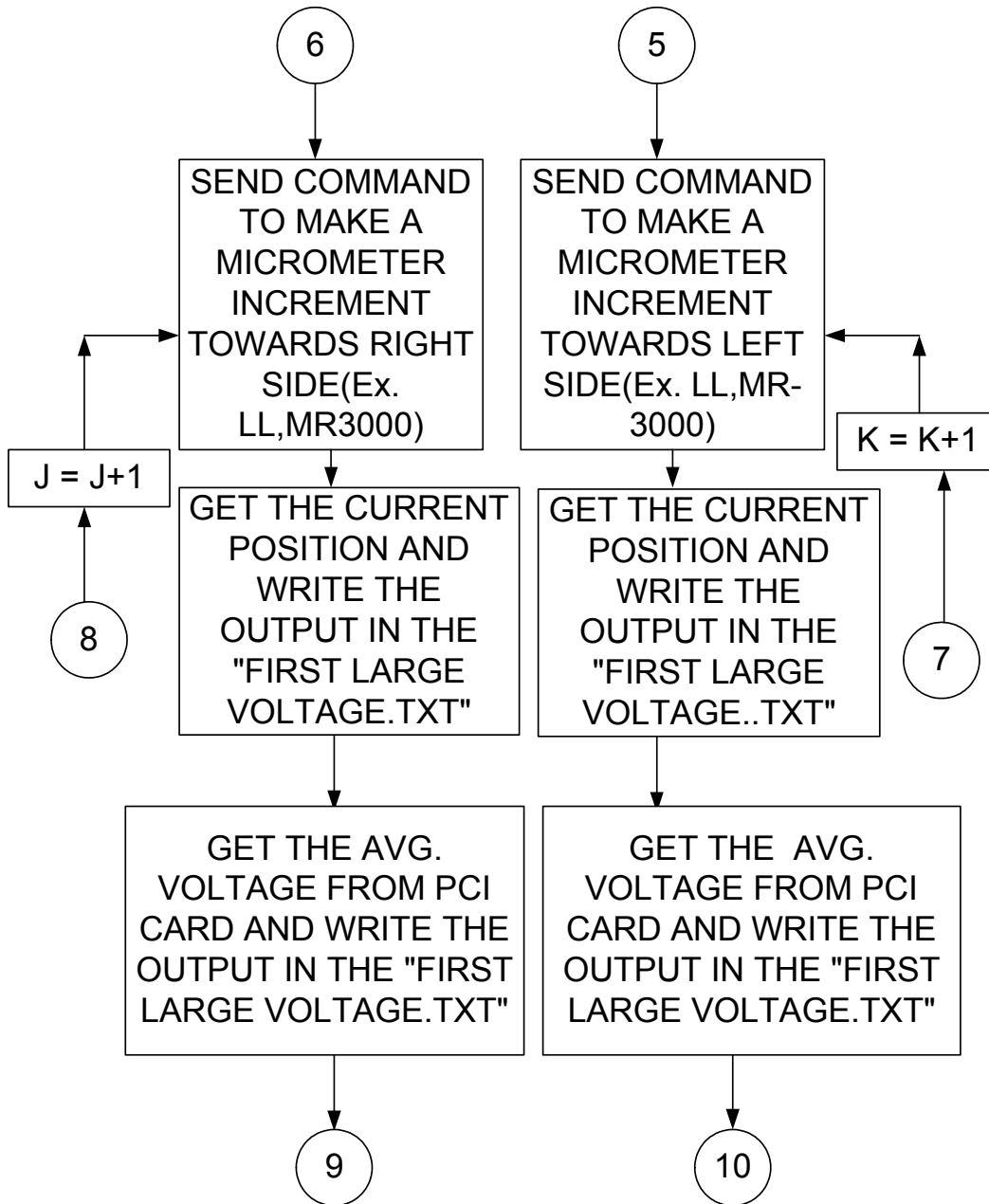
Through holes No. for external connection in C4674	Output pin number of 2-D PSD
1 (GND)	
2 (Y2)	4
3 (X2)	3
4 (V _R)	5
5 (Y1)	2
6 (X1)	1
7 (GND)	

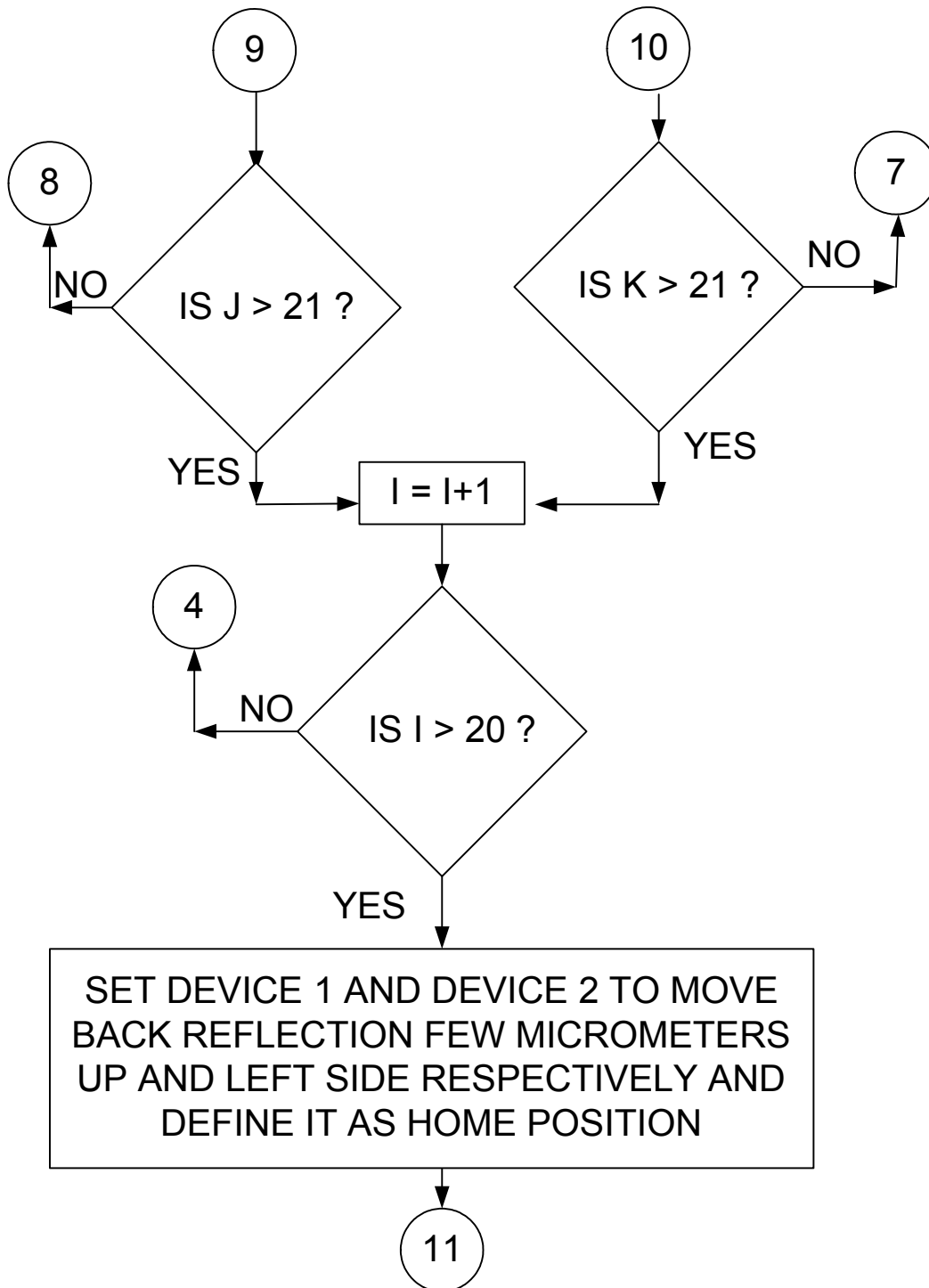
APPENDIX B

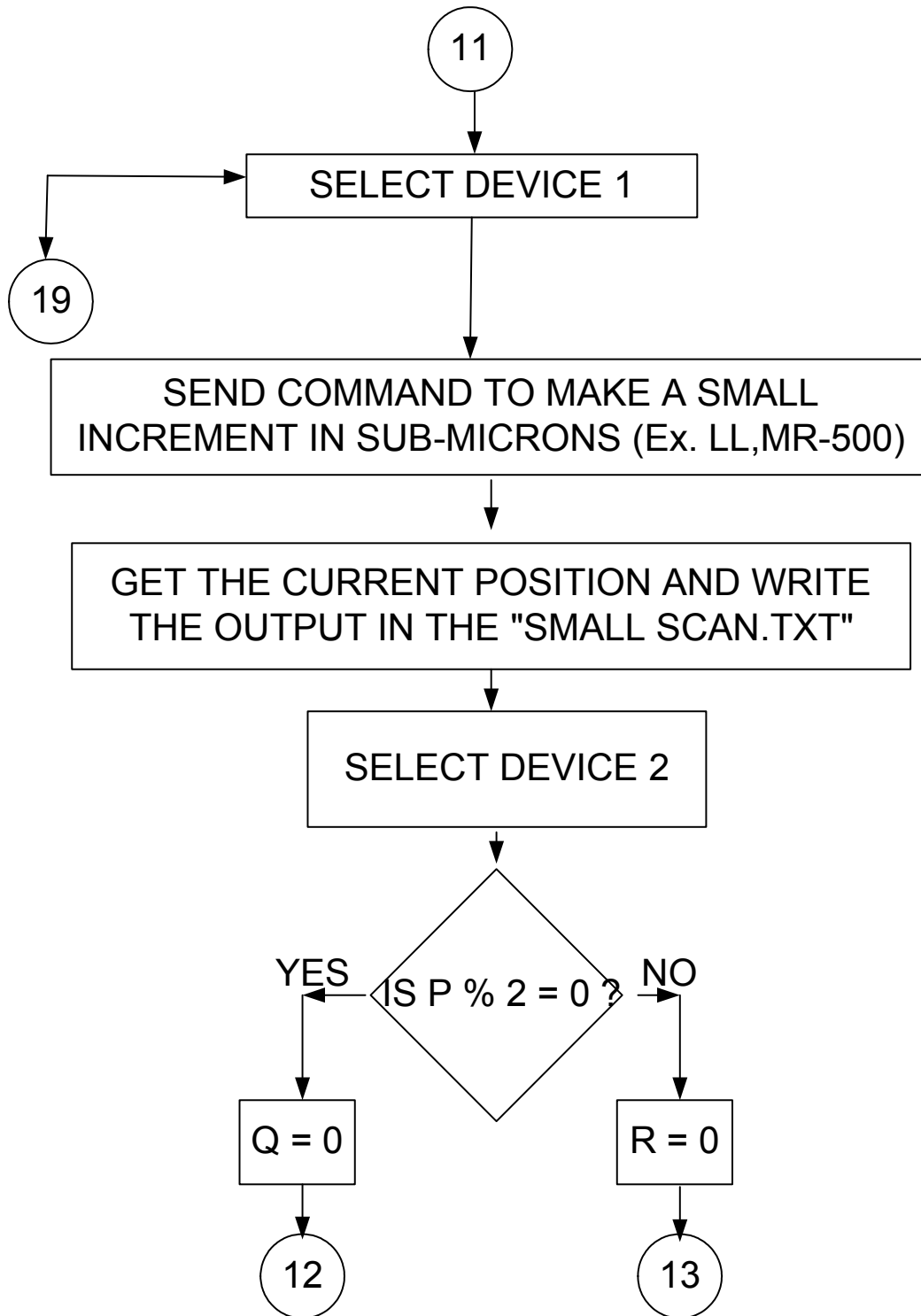
FLOW DIAGRAM FOR LABVIEW PROGRAM USED IN FINE
ALIGNMENT SYSTEM

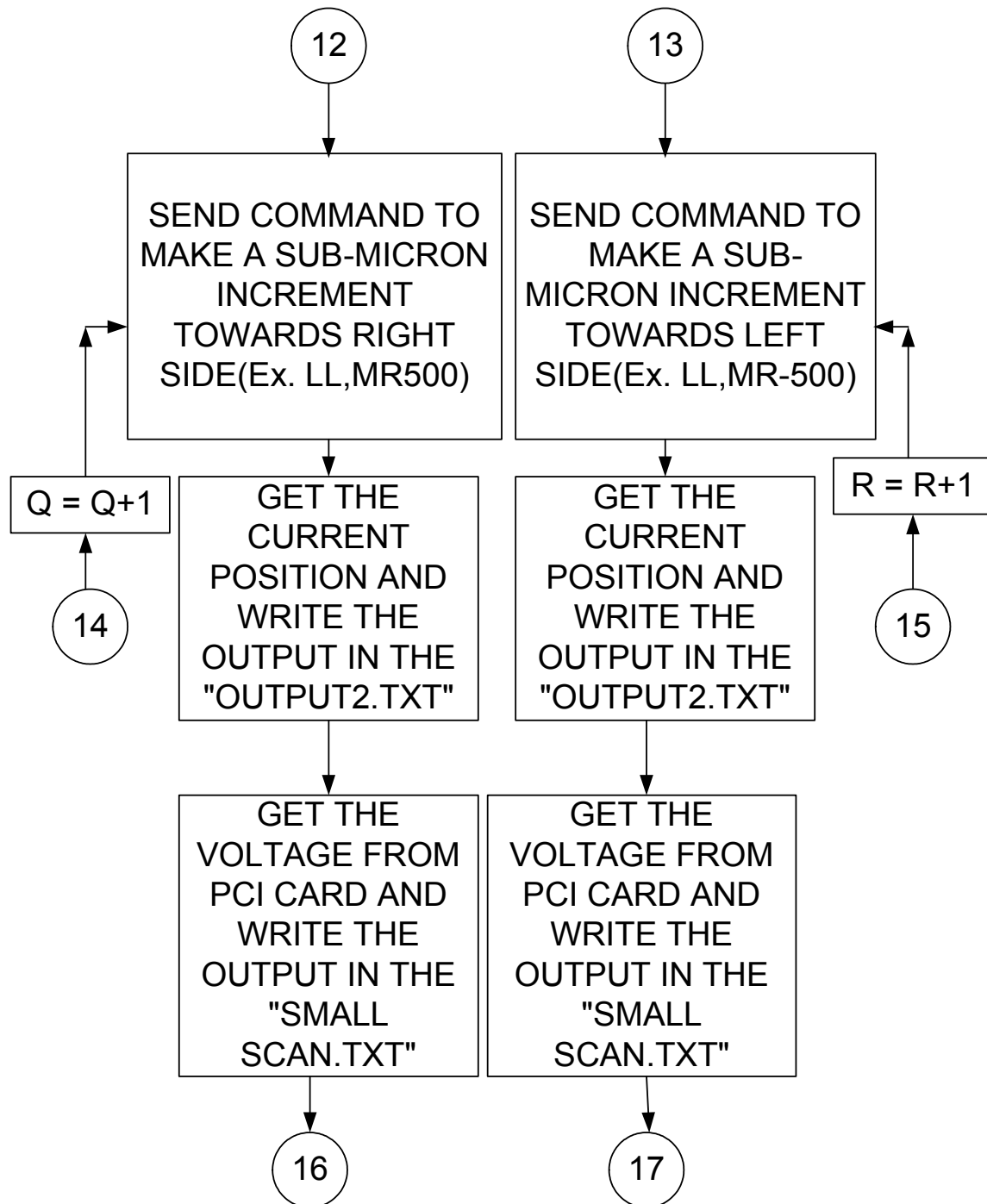


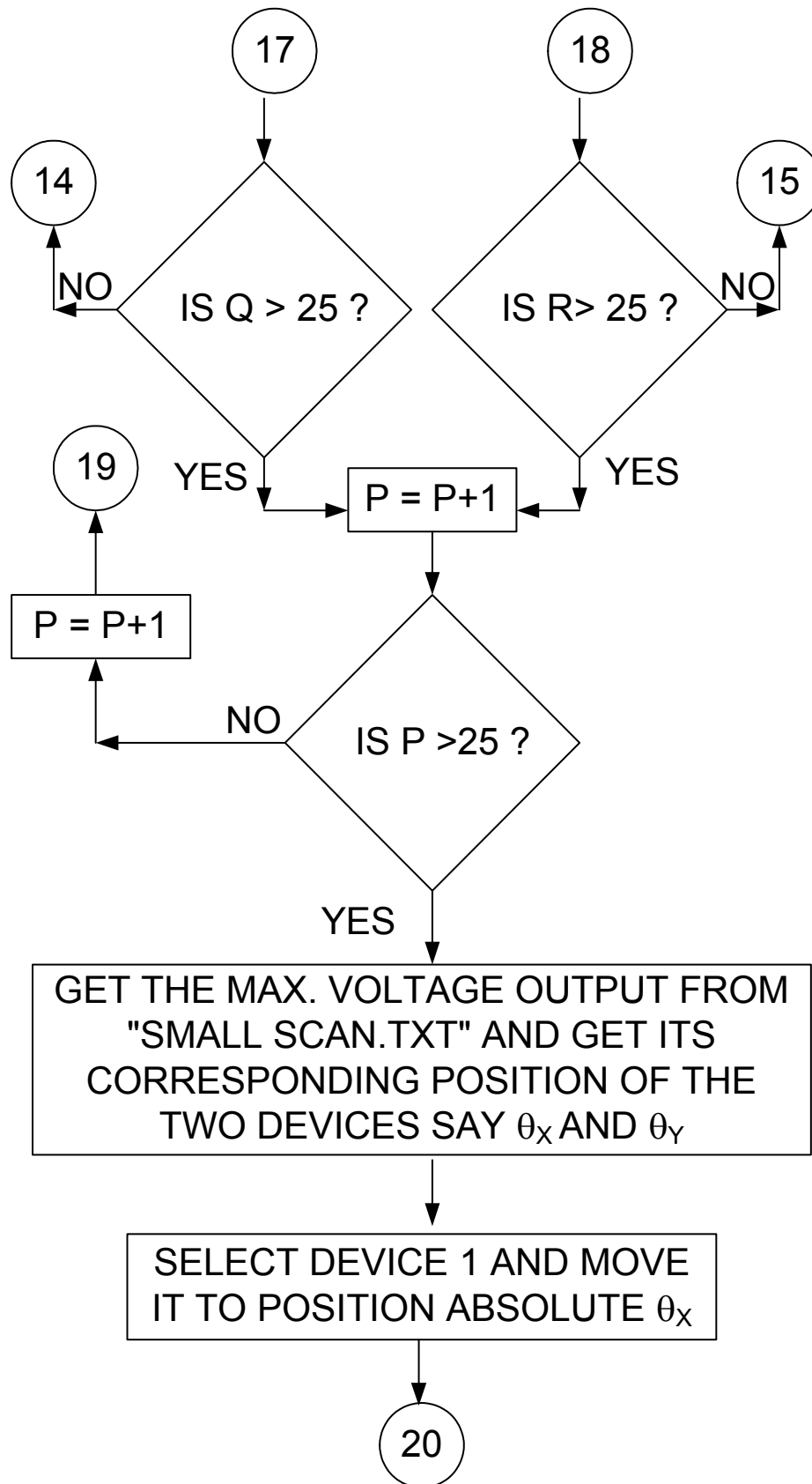


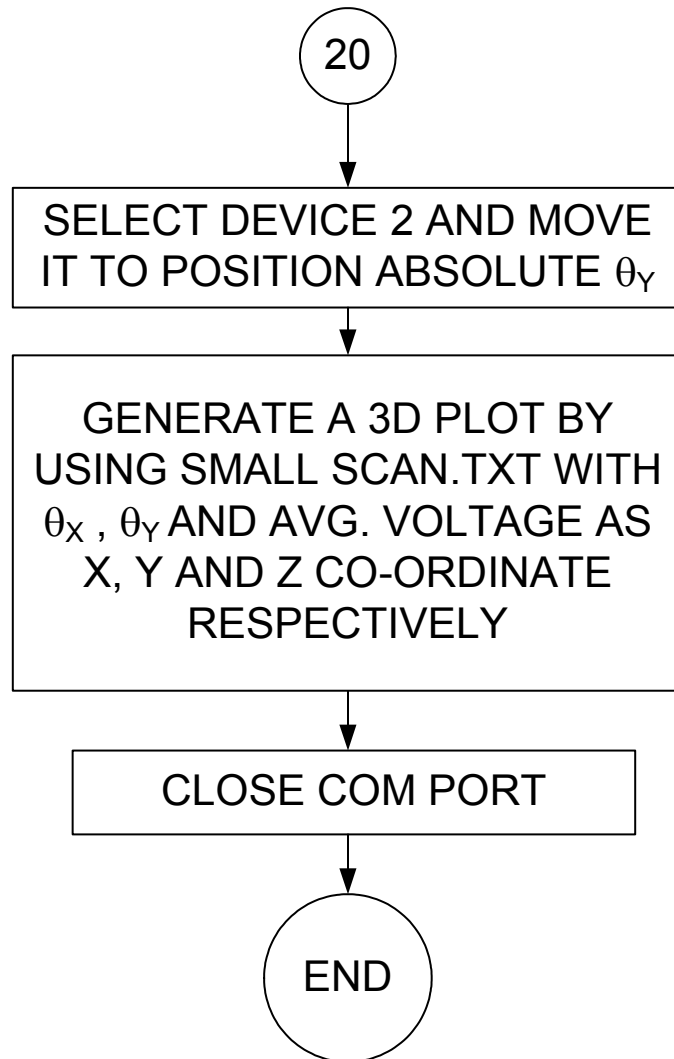












VITA

Mahesh Jalan was born on October 2, 1974 in Sambalpur, Orissa, India. He did his undergraduate study at National Institute of Technology, Surathkal, India. He worked as a section engineer for Bajaj Auto Limited from July 1997 to November 1999 in the Maintenance Department of the Motorcycle Division. He then worked as a consultant in the Product Engineering CAD department of Tata Technologies, Pune, from December 1999 to July 2001. Mahesh Jalan joined Texas A&M University in August 2001 and has since been pursuing his Master of Science degree in the Mechanical Engineering Department.

Mahesh Jalan's permanent address is:

C/o Mr. Mansukh Jalan
Gaiety Talkies Road,
Sambalpur, Orissa
India – 768001.

And his e-mail address is:

m_jalan@tamu.edu